

SUPERRADIANCE: AN ESSAY ON THE THEORY OF COLLECTIVE SPONTANEOUS EMISSION

M. GROSS and S. HAROCHE

Laboratoire de Physique de l'Ecole Normale Supérieure, Paris, France



NORTH-HOLLAND PUBLISHING COMPANY - AMSTERDAM

SUPERRADIANCE: AN ESSAY ON THE THEORY OF COLLECTIVE SPONTANEOUS EMISSION

M. GROSS and S. HAROCHE

Laboratoire de Physique de l'Ecole Normale Supérieure, Paris, France

Received September 1982

Contents:

1. Introduction. Motivation of this essay	303	5.1. Simple evaluation of superradiance delay and delay fluctuations	327
2. Qualitative description of superradiance in small volumes. The "Dicke model"	307	5.2. Fluctuation-less trajectories: The quasi-classical "probability packets"	328
2.1. Description of the atomic system	307	5.3. The initial quantum stage of superradiance	331
2.2. Basic hypothesis concerning the atom-field coupling and the system evolution	307	5.4. The superradiance density matrix as a linear superposition of quasi-classical probabilities	332
2.3. The symmetrical superradiant states	308	5.5. Physical discussion: The quantum fluctuations of the small sample superradiant system	333
2.4. Qualitative description of the N -atom spontaneous emission	310	6. Large sample superradiance	335
2.5. Connexion with the dipole-dipole correlation build-up	310	6.1. General considerations concerning propagation and diffraction effects in a large superradiant sample: The pencil-shaped sample case	335
2.6. Case of two-atom superradiance	311	6.2. Superradiance equations in the one-dimensional propagation approximation	338
3. Superradiance equations for a system of N two-level atoms	313	6.3. Simple analysis of large sample superradiance evolution in the one-dimensional propagation model	344
3.1. The atom + field system Hamiltonian	314	6.4. Numerical solution of three-dimensional large sample superradiance equation (pencil-shaped case)	356
3.2. The Schrödinger approach: Superradiance master equation for the atomic system density matrix	315	6.5. Superradiance equations taking into account competing effects: Doppler shifts, spontaneous emission in off-axis directions or on other transitions	365
3.3. The Heisenberg approach: The Bloch-Maxwell equations for the quantum mechanical field and atomic operators	317	7. Discussion of the "slow variation-approximations": The various regimes of superradiance	366
4. Superradiance in small volumes revisited: Competition between superradiance and Van der Waals dephasing	320	7.1. Validity of the Schrödinger picture: The break-down of the Born-Markov approximation	367
4.1. The superradiant master equation in the small volume case	320	7.2. Validity of the Heisenberg picture: The break-down of the slow varying envelope approximation	370
4.2. Van der Waals dephasing of the symmetrical superradiant states	322	7.3. The various regimes of large sample superradiance	371
4.3. Small symmetrical superradiant samples. Frequency chirping effects of superradiant emission	323	8. Superradiance in multilevel systems, light beating and polarization effects	373
5. Quantitative analysis of the symmetrical superradiant evolution. A first approach to quantum fluctuations in superradiance	325		

Single orders for this issue

PHYSICS REPORTS (Review Section of Physics Letters) 93, No. 5 (1982) 301-396.

Copies of this issue may be obtained at the price given below. All orders should be sent directly to the Publisher. Orders must be accompanied by check.

Single issue price Dfl. 51.00, postage included

8.1. Description of multilevel systems with various types of initial preparation	373	9.1. First example: Case of two independent degenerate transitions with the same polarization and different matrix elements	386
8.2. New physical effects in multilevel superradiance	376	9.2. Second example: Degenerate transitions with identical polarizations sharing a common lower level	388
8.3. Superradiance equations generalized to multilevel systems	376	9.3. Third example: Degenerate transitions with orthogonal polarizations sharing a common lower level	389
8.4. Statistics of initial condition for the classical trajectories	378	9.4. Conclusion: Relation with the limited superradiance phenomenon in a two-level atom small sample system	392
8.5. First example: Beats radiated by a mixture of two isotopes	379	10. Conclusion	393
8.6. Second example: Polarization fluctuations in superradiance	384	References	394
9. Limited superradiance	385		

Abstract:

This essay presents a theoretical description of the superradiance phenomenon, in which both the quantal and the classical aspects are discussed. Starting from the simple two-level atom-small sample Dicke model, we successively introduce various complications inherent to a realistic superradiance experiment: effects of Van der Waals interaction between the atoms, propagation and diffraction of the electromagnetic field in the sample and finally the effects related to atomic level degeneracy or near degeneracy. We recall how to calculate the field radiated by a superradiant system in a single experiment and how to determine, for a series of identically prepared superradiant samples, the large shot to shot fluctuations of the emitted light properties. The presentation tries to unify various points of view and formalisms developed in previous works and to introduce simply and progressively the basic physical concepts relevant to the superradiance phenomenon.

1. Introduction. Motivation of this essay

In “ordinary” fluorescence experiments, a gas of atoms (or molecules) initially prepared in the upper level of an electronic transition decays by spontaneous emission of light towards lower states according to a process in which the atoms (or molecules) of the sample can be considered as interacting *independently* from each other with the radiation field. The emission, obeying an exponential law, takes a characteristic time τ_{sp} equal to the reciprocal of the radiative decay rate Γ of the initially excited level and the radiation pattern of the atomic sample is essentially isotropic (see fig. 1a). These features are

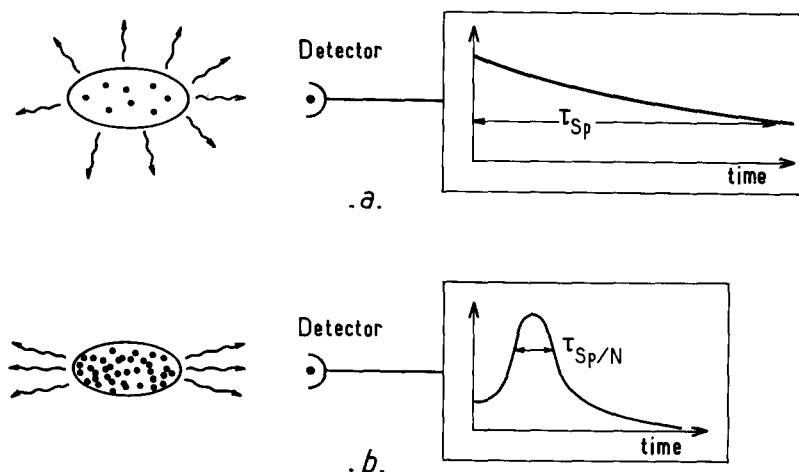


Fig. 1. Comparison between the general characteristics of ordinary fluorescence and superradiance experiments. (a) Ordinary spontaneous emission is essentially isotropic with an exponentially decaying intensity (time constant τ_{sp}). (b) Superradiance is anisotropic with an emission occurring in a short burst of duration $\sim \tau_{sp}/N$.

generally observed on *dilute* atomic systems and are notably altered when the number of radiators in the sample becomes large enough. The collection of atoms (or molecules) then starts to radiate spontaneously *much faster and stronger* than the emission of independent atoms, in a well defined direction depending upon the geometry of the sample. This phenomenon, known as *superradiance* or *superfluorescence*, is due to a spontaneous phase-locking of the atomic dipoles throughout the medium, which radiate a field whose intensity becomes proportional to the square of the number N of radiators. The energy of the atomic system is then radiatively damped in a short radiation burst, within a time of the order of τ_{sp}/N (see fig. 1b).

This collective emission phenomenon has been the subject of an extremely large number of theoretical papers since the pioneering article of Dicke [1] which described for the first time this effect in the context of spontaneous emission study [2–51]. It has also been extensively studied experimentally [52–71] during the last ten years, after the development of pulsed dye-laser systems has made it easy to excite in a very short time a collection of atoms in a well defined electronic level. In the simplest case, a superradiant experiment is realized according to the scheme of fig. 2, on an atomic system essentially exhibiting a “three-level structure”: a pulsed laser beam, resonant with the transition $f \rightarrow e$, initially excites all the atoms (or molecules) in level e , thus producing at time $t = 0$ a total population inversion (but no optical dipole) on the transition $e \rightarrow g$. The subsequent superradiant emission which occurs at the frequency ω_0 of this transition is detected either directly (by measuring the radiated field with a detector) or indirectly [60, 69, 71] by monitoring the fast radiative population transfer from level e to g . Superradiant emission has been studied in this way in the optical [52], infrared [53–66], far infrared [67, 68] and millimeter wave [69, 70, 71] domains.

One of the interests in superradiance study lies in its close connexion with the physics of laser emission. A superradiant medium is indeed nothing but a mirrorless laser pumped in a percussional way at time $t=0$. The superradiant phase-locking of the dipoles belonging to different atoms thus exhibits a strong relationship with the ordering process by which the atoms in a laser amplifier acquire a common phase and start emitting coherently. In some respect, the superradiant phenomenon appears somewhat simpler since one can neglect the pumping and relaxation mechanisms which are important in laser operation and consider only the evolution of atoms exclusively coupled to their own radiation field. In spite of this deceptive simplicity, the phenomenon remains however, as we will see, rather intricate and difficult to analyse in details. In fact, the phenomenon of superradiance has certainly attracted the attention of theorists because of the striking contrast between the simplicity with which the phenomenon can be defined and the complexity of its detailed analysis which involves several of the concepts of quantum electrodynamics, many body problem and non-linear optics.

The superradiant emission is a cooperative process involving in a collective mode all the atoms of the sample. In this collective mode, an “order” appears in the system which can be defined by the build up of correlation between the dipoles belonging to different atoms. This correlation is quite reminiscent of

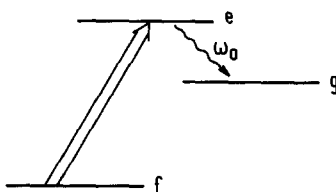


Fig. 2. Typical level scheme for a superradiance experiment: the atomic inversion on transition $e \rightarrow g$ is realized by optical pumping from state f on transition $f \rightarrow e$. Double arrow: pumping transition; wavy line: superradiant transition at frequency ω_0 .

the spin–spin correlation appearing for example in a ferromagnetic sample. This dipole “ordering” evolves from a total disorder at time $t = 0$ since at that time there is no optical dipole at all in the medium. When the emission starts, the quantum fluctuations of the electromagnetic field of the vacuum act on independent atoms. From this action, the dipole–dipole correlations eventually emerge through a kind of symmetry breaking phenomenon. From this short description, it clearly appears that superradiance presents a double quantum and classical aspect. At its early stage, near time $t = 0$, it is genuinely quantum mechanical since the system evolution starts on vacuum field “noise”; at a later stage, when the dipole–dipole correlations have appeared, it becomes “classical” since the subsequent emission is due to the radiation of an ordered array of dipoles analogous to classical antennae radiating in phase throughout the medium. This classical stage itself presents some fluctuations reflecting the random nature of the noise which has triggered the system evolution and – as ferromagnetism for example – superradiance is a “macroscopic phenomenon” retaining throughout its evolution some of the quantum fluctuation character of its initial phase.

In our view, the connexion between the quantum mechanical and classical aspects of superradiance, in the context of a many body situation involving a collection of two-level atoms and photons, is the basic question one has to understand in order to deeply grasp the phenomenon. Unfortunately, or fortunately depending upon the point of view, this problem is to some extent obscured by another intrinsic feature of superradiance: the emitted field propagates along an initially inverted medium, exhibiting strong non-linear behaviour. This is the “non-linear propagation and diffraction” aspect of the phenomenon, giving rise to effects well known in the context of light pulse propagation problems: due to inhomogeneous stimulated emission and reabsorption processes throughout the sample, the emitted radiation undergoes strong reshaping, ringings, frequency chirping effects which can be understood only by numerical computation of complicated non-linear evolution equations. These propagation effects tend – to some extent – to reduce the strong interatomic correlation order which is the key aspect of superradiance and considerably complicate the description of the phenomenon.

Having to cope with this situation, most articles on superradiance fall in one of the two following categories: those which emphasize the basic aspects – atomic correlation, symmetry and fluctuation in two-level atomic systems – and neglect or underestimate the propagation aspect [1, 9, 13, 28] and those which, on the other hand, try to grasp by numerical computation the complexity of the real problem and necessarily lose some of the simplicity of the basic phenomena [17, 30, 34, 40].

Another kind of complication – or enrichment – comes from the fact that, in most cases, the superradiant emission does not simply involve two non-degenerate levels e and g , but rather atomic transition connecting degenerate or nearly degenerate sub-levels. Superradiance then results from the competition between the emission of field components having slightly different frequencies or different polarizations. This competition might – depending upon the situation – lead to light beating effects (superradiance beats), to polarization fluctuation effects or even to quenching of superradiance resulting from negative interference between the light components emitted on degenerate transitions (subradiance or limited superradiance).

All these effects are of course lost in a model describing the atom as two-level systems. Since the two-level atom problem, already difficult to analyse in details, has retained most of the attention, only recently have articles been devoted to these very interesting multilevel aspects of superradiance [44–51] which have been observed in numerous experiments [53, 58, 62, 63].

In this essay, our goal is to present a synthetic view of superradiance in which the various aspects quoted above are fully taken into account within a unified frame. In this way, we hope to make the connexion between various presentations of superradiance and to bring some unity in a field in which

different points of view have often emphasized complementary aspects of the same physical reality. More precisely, the outline of this review will be as follows: In section 2, we introduce some important notations and basic ideas about superradiance. We qualitatively introduce the concepts of atomic permutational symmetry and dipole-dipole correlation which are basic in the description of the phenomenon and we apply them to analyse the simple case of two-atom superradiant emission. In section 3, we derive after many other authors the equations describing the evolution of a superradiant two-level atomic system, both in the Schrödinger and in the Heisenberg points of view. These equations are applied in section 4 to describe the case of a small sample two-level atom superradiant system (whose linear size is smaller than the emission wavelength). The main interest of this case is to be exempt of the complication due to propagation. On the other hand, the superradiant behaviour is then in competition with dipole-dipole dephasing due to Van der Waals interaction between atoms. We analyse in details this effect and describe simple – though not very realistic – situations where “pure superradiance” free of perturbation due to propagation and Van der Waals dephasing can occur. In section 5, we analyse in details the evolution of the system in this simple ideal case and present an analytical solution of the superradiant equation which clearly exhibits the main features of the phenomenon. In section 6, we gradually introduce – still in the two-level atom case – the complications inherent to the large sample problem (propagation in one, then in three dimensions), we briefly analyse the differences with the simple superradiance model of section 5 and we discuss some of the computational problems still open to describe a realistic superradiance situation. In section 7, we conclude the study of the two-level atom superradiance by discussing the validity of the various approximations made to solve the equations. This discussion will lead us to the definition of various “regimes of superradiance” according to the number N of atoms involved and to the size of the sample. In sections 8 and 9, we discuss at last some of the multilevel effects in superradiance. In section 8, the superradiance equations are generalized to include the description of superradiance beats and polarization fluctuation effects. In section 9, we focus the discussion on the problem of negative interference between degenerate superradiant transitions, leading to the phenomenon of subradiance. At last, in section 10, we present some concluding remarks and mention some related problems not discussed in details in this review.

Let us mention that this essay is not intended to present a complete review of former superradiance studies. We give of course in the references the papers in which the results obtained in this essay have been derived for the first time, without trying to present an exhaustive reference list, which would be difficult concerning a research field in which so many articles have been published. Being exclusively devoted to a theoretical discussion, this review does not include the description of recent experiments performed on this subject. Neither does it try to compare in details the theoretical predictions to experimental observations (this comparison can be found in other reviews [72, 73, 74, 88]). The absence of direct reference to any specific experimental situation will allow us to simplify somewhat the theoretical frame and to avoid the detailed description of some of the features of a realistic superradiance experiment which would complicate the discussion, such as the effect of atomic motion (Doppler effect), atomic collision and relaxation processes, existence of other atomic levels not directly concerned with the superradiant transition and so on. We will rather concentrate on the very essence of the superradiance phenomenon, namely the “pure” interaction with the radiation field of a collection of motionless atoms initially prepared in the upper level of an atomic transition.

These limitations will prevent us discussing in detail some features important to an experimental situation such as the notion of “superradiance threshold” for example. Superradiance does indeed present a threshold corresponding to a minimum number of initially inverted atoms because the

dipole-dipole phase locking is in competition with dephasing effects such as spontaneous emission on other transitions, Doppler dephasing, atomic collisions and so on. Neglecting these “spurious effects” amounts to assuming that superradiant emission does always prevail, or equivalently that the “threshold” occurs for as few atoms as one wishes. In fact, all the “realistic” features quoted above can be added to the theoretical frame presented in this paper at the expense of slight complications of the equations, as will be briefly discussed at the end of section 6.

2. Qualitative description of superradiance in small volumes. The “Dicke model” [1]

In this section we present a description of superradiance in a very simple case. We qualitatively analyse the emission of an ensemble of atoms in a volume small compared to the emission wavelength. This is the situation discussed by Dicke in his original paper and we follow here the main steps of his arguments. This qualitative approach will allow us to introduce important concepts and notations and to point out some problems discussed in the next sections.

2.1. Description of the atomic system

We consider an ensemble of N two-level identical atoms, identified by the subscripts $1, 2, \dots, i, \dots, N$. The upper and lower states of each atom are called $|e\rangle$ and $|g\rangle$ respectively and are separated by an energy interval $\hbar\omega_0$ ($\lambda_0 = 2\pi c/\omega_0$ is the wavelength of the superradiant transition). After many other authors [2, 4, 11, 14], we introduce the raising and lowering off-diagonal operators D_i^\pm defined as:

$$D_i^+ = |e\rangle\langle g| ; \quad D_i^- = |g\rangle\langle e| \quad (2.1)$$

and the diagonal operator D_i^3 :

$$D_i^3 = \frac{1}{2}[|e\rangle\langle e| - |g\rangle\langle g|] . \quad (2.2)$$

The D_i^\pm and D_i^3 operators act only in the i th atom subspace and obey the well-known commutation rules:

$$[D_i^3, D_j^\pm] = \pm \delta_{ij} D_i^\pm ; \quad [D_i^+, D_j^-] = 2\delta_{ij} D_i^3 . \quad (2.3)$$

These operators can be used to define the electric dipole operator of the i th atom:

$$\mathcal{D}_{ai} = (D_i^+ + D_i^-) d \boldsymbol{\epsilon}_a . \quad (2.4)$$

In this equation, $\boldsymbol{\epsilon}_a$ and d are respectively the normalized vector defining the polarization of the $|e\rangle \rightarrow |g\rangle$ transition and the electric dipole matrix element of the transition (assumed to be real without loss of generality, with a convenient choice of the eigenstates $|e\rangle$ and $|g\rangle$ phases).

2.2. Basic hypothesis concerning the atom-field coupling and the system evolution

We assume that all atoms are prepared at time $t = 0$ in the upper level $|e\rangle$ so that the state of the

atomic system at that time is:

$$|\psi(0)\rangle = |e, e, e \dots e\rangle. \quad (2.5)$$

We suppose that all the atoms are motionless and located within a volume whose linear dimensions are small compared to λ . We also assume that the subsequent evolution of the system is only due to the coupling of the atoms to the radiation field (i.e. we neglect all other causes of evolution such as atomic collisions and relaxation mechanisms) and we make the basic assumption that this *coupling is symmetrical with respect to the exchange of any two atoms in the system*. This very important hypothesis might at first sight naturally follow from the fact that the atoms are supposed to be confined in a volume small compared to λ : the emission or absorption of a photon of wavelength λ cannot – according to the Heisenberg uncertainty – be assigned to a specific atom in the sample and the indiscernability of the atoms with respect to the emission or absorption process seems to imply directly the above symmetry property. In fact, as shown below in section 4, this symmetry argument is highly questionable and holds only for very specific shapes of the atomic distribution. We will however, in this qualitative section, assume that this important property is satisfied, which will allow us to introduce simple notions of symmetry and atomic correlations which are the very essence of the superradiance phenomenon and which can be generalized, at the expense of some mathematical complications, to describe more realistic superradiant situations.

2.3. The symmetrical superradiant states

Once the above assumptions are made, it is clear that the atomic system evolution must remain restricted to a Hilbert subspace invariant by all atomic permutations. This property naturally follows from the fact that the initial state of the system (eq. (2.5)) is invariant by any exchange of two atoms and that the atom to field coupling is assumed to obey the same property. It is convenient to describe each two-level atom of the ensemble as a fictitious spin 1/2 system with states $|e\rangle$ and $|g\rangle$ being the spins up and down states with respect to an arbitrary direction in an abstract space. In this representation, the D_i^\pm and D_i^3 operators are analogous to Pauli spin matrices. Any N -atom state invariant by atom permutation is isomorphous to a symmetrical superposition of N spin 1/2 states, which is known to be an eigenstate corresponding to the maximum $J = N/2$ value of the angular momentum of an N spin 1/2 system. There are indeed $N+1$ such states, obtained by repeated action of the symmetrical collective deexcitation operator $\sum_i D_i^-$ on the initial state $|\psi(0)\rangle$:

$$|JM\rangle = \sqrt{\frac{(J+M)!}{N!(J-M)!}} \cdot \left(\sum_i D_i^- \right)^{(J-M)} |e, e, e \dots e\rangle \quad (2.6)$$

with $-J \leq M \leq J$.

The $|JM\rangle$ state represents the fully symmetrical state in which $J+M$ atoms are in the upper level $|e\rangle$ and $J-M$ in the lower level $|g\rangle$. It can be expressed formally as resulting from the action of the “symmetrization operator” S on a simple product state as:

$$|JM\rangle = S \left[\underbrace{|e, e \dots e}_{J+M} \quad \underbrace{|g, g \dots g\rangle}_{J-M} \right]. \quad (2.7)$$

Introducing the collective operators:

$$D^\pm = \sum_i D_i^\pm \quad (2.8)$$

$$D_3 = \sum_i D_i^3 \quad (2.9)$$

and

$$D^2 = \frac{1}{2}(D^+D^- + D^-D^+) + D_3^2, \quad (2.10)$$

the $|JM\rangle$ states are of course defined as the eigenstates of D_3 and D^2 with the eigenvalues M and $J(J+1)$:

$$D_3|JM\rangle = M|JM\rangle \quad (2.11)$$

$$D^2|JM\rangle = J(J+1)|JM\rangle \quad (2.12)$$

and they obviously obey the following relation:

$$\langle JM | \sum_i D_i^+ D_i^- | JM \rangle = J + M; \quad \langle JM | \sum_i D_i^- D_i^+ | JM \rangle = J - M \quad (2.13)$$

in which $\sum_i D_i^+ D_i^-$ and $\sum_i D_i^- D_i^+$ respectively appear as the operators representing the number of atoms in the upper and lower state.

The energy of the $|JM\rangle$ state is $M\hbar\omega_0$, with the energy of the half-deexcited system ($M=0$) being taken as origin.

With these definitions, the atomic system evolution simply appears as a cascade emission down a “ladder” of $2J+1=N+1$ equidistant levels, quite analogous to the problem of spontaneous emission of an angular momentum J (see fig. 3).

We proceed to qualitatively analyse this emission in the next subsection.

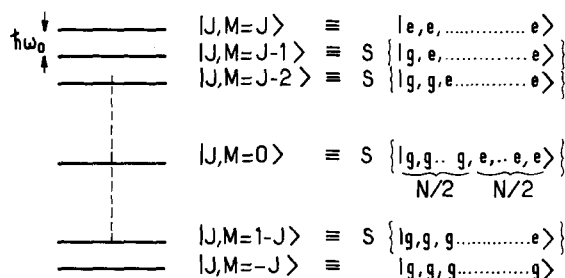


Fig. 3. The “ladder” of $N+1$ symmetrical states $|JM\rangle$: the atomic system starts at time $t=0$ from the $|J, M=J\rangle=|e, e, \dots, e\rangle$ state and cascades down to the $|J, M=-J\rangle=|g, g, \dots, g\rangle$ state. The intermediate state $|J, M\rangle$ is the fully symmetrical state in which $J+M$ atoms are in state $|e\rangle$ and $J-M$ in state $|g\rangle$.

2.4. Qualitative description of the N -atom spontaneous emission

Since the atoms are located in a volume small compared to λ , it is natural to assume that the N radiators behave as a point-like dipole resulting from the sum of the N individual dipoles:

$$\mathcal{D}_a = \sum_i \mathcal{D}_{ai} = d\epsilon_a \sum_i (D_i^+ + D_i^-). \quad (2.14)$$

Recalling that the rate of photon emission for a single atom [75, 96] is:

$$W_1 = \Gamma \langle D_i^+ D_i^- \rangle \quad (2.15)$$

where Γ is the atomic natural linewidth corresponding to the $e \rightarrow g$ transition and $\langle \rangle$ denotes a quantum mechanical average, we quite naturally generalize this expression to get the N -atom point-like system radiation rate:

$$W_N = \Gamma \langle D^+ D^- \rangle. \quad (2.16)$$

For a $|JM\rangle$ state, the expectation value of eq. (2.16) is very easy to perform, since the D^\pm operators are analogous to the transverse components J_\pm of an angular momentum $J = N/2$. One immediately gets:

$$W_N = \Gamma(J + M)(J - M + 1) \quad (2.17)$$

which shows that the rate of photon emission by the atomic system increases from a value equal to $2J\Gamma = N\Gamma$ for $M = J$ (fully excited state) to a value equal to $J(J + 1)\Gamma = \frac{1}{2}N(\frac{1}{2}N + 1)\Gamma$ for $M = 0$ (half-deexcited atom system). As a result, we understand that the rate of photon emission strongly increases when the system cascades down the ladder of $|JM\rangle$ states and loses energy with a maximum rate of emission proportional to N^2 obtained for $M = 0$. Eventually, when the system ends up in the $M = -J$ level, the rate of photon emission vanishes and the emission ends.

2.5. Connexion with the dipole-dipole correlation build-up

The strong increase of the $\langle (\sum_i D_i^+) (\sum_j D_j^-) \rangle$ product as the system cascades down the ladder of $|JM\rangle$ states is directly related to the appearance of correlation between the dipoles of different atoms. In a symmetrical state, the expectation value of any $D_i^+ D_j^-$ product with $i \neq j$ does not depend upon the i, j couple so that one can indeed write:

$$\left\langle \left(\sum_i D_i^+ \right) \left(\sum_j D_j^- \right) \right\rangle = N(N - 1) \langle D_i^+ D_j^- \rangle + \sum_i \langle D_i^+ D_i^- \rangle \quad (2.18)$$

which, according to equations (2.13) and (2.17), yields in a $|JM\rangle$ state:

$$\langle JM | D_i^+ D_j^- | JM \rangle = \frac{J^2 - M^2}{N(N - 1)}. \quad (2.19)$$

The correlation between two atoms i and j , measured by the $\langle D_i^+ D_j^- \rangle$ quantity, thus increases from zero to a maximum value of the order of $1/4$ when M goes from J to zero and then decreases down to zero when M goes to $-J$.

We can thus summarize the above discussion in the following terms: in this simple model, the superradiant emission is directly related to the *indiscernability* of the atom with respect to photon emission. Due to this indiscernability, the system evolves in a state invariant by atom permutation in which strong correlations build up between the dipoles. These correlations are directly responsible for the appearance of a global radiating dipole proportional to N , i.e. to a radiated intensity proportional to N^2 . Energy conservation then requires that the emission of N photons should occur in a time N times shorter than the spontaneous emission of a single atom.

To conclude this simple study, we will now make more quantitative statements concerning the case of two atoms ($N = 2$).

2.6. Case of two-atom superradiance

We consider here two atoms at a distance much smaller than λ . The $|JM\rangle$ states are in this case restricted to three levels $M = 1, 0, -1$ corresponding respectively to both atoms excited, one atom excited, the other being in the lower level and both atoms deexcited (see fig. 4). Let us call respectively $\Pi_1(t)$, $\Pi_0(t)$, $\Pi_{-1}(t)$ the probabilities of having at time t the system in either of these states, and let us determine the time evolution of these probabilities from simple arguments based on the previous sections considerations.

At time $t = 0$, one has obviously:

$$\Pi_1(0) = 1; \quad \Pi_0(0) = \Pi_{-1}(0) = 0. \quad (2.20)$$

Furthermore, the rate at which the initial state $M = 1$ decays is obviously equal to 2Γ : the first photon is indeed emitted by independent atoms (no initial dipole-dipole correlation), each atom having a probability Γ of emitting it. Hence:

$$d\Pi_1/dt = -2\Gamma\Pi_1. \quad (2.21)$$

Another relation between the Π 's is provided by energy conservation requirement. The average rate of photon emission from states $|J = 1, M = 1\rangle$ and $|J = 1, M = 0\rangle$ are, according to eq. (2.17), equal to 2Γ whereas the rate of photon emission from state $|J = 1, M = -1\rangle$ is zero. Hence, the rate of photon emission at time t is obviously:

$$W_2 = 2\Gamma[\Pi_1 + \Pi_0] \quad (2.22)$$

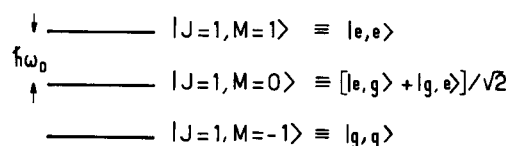


Fig. 4. Energy level diagram of the collective atomic system made of two atoms in fully symmetrical states.

and the average number of excited atoms is:

$$\left\langle \sum_i D_i^+ D_i^- \right\rangle = 2\Pi_1 + \Pi_0. \quad (2.23)$$

Energy conservation requires that the decrease in atomic excitation should at any time be compensated by the increase of the photon number so that:

$$\frac{d}{dt} \left\langle \sum_i D_i^+ D_i^- \right\rangle = -W_2 \quad (2.24)$$

which, according to eqs. (2.22) and (2.23), can be written as:

$$2 d\Pi_1/dt + d\Pi_0/dt = -2\Gamma[\Pi_1 + \Pi_0]. \quad (2.25)$$

Equations (2.21) and (2.25) can be readily integrated to yield:

$$\Pi_1(t) = e^{-2\Gamma t} \quad (2.26)$$

and

$$\Pi_0(t) = 2\Gamma t e^{-2\Gamma t} \quad (2.27)$$

$\Pi_{-1}(t)$ being obtained by conservation of the total probability:

$$\Pi_{-1}(t) = 1 - \Pi_0(t) - \Pi_1(t) = 1 - e^{-2\Gamma t}(1 + 2\Gamma t). \quad (2.28)$$

Once the evolution of the Π 's is known, it is easy to compute the photon emission rate from eq. (2.22):

$$W_2(t) = 2\Gamma e^{-2\Gamma t} [1 + 2\Gamma t]. \quad (2.29)$$

It is instructive to compare this rate to the one obtained by assuming that the two atoms emit independently:

$$W_2^{(\text{ind})}(t) = 2\Gamma e^{-\Gamma t}. \quad (2.30)$$

$W_2^{(\text{ind})}(t)$ corresponds for example to the total rate of photon emission by two atoms located at a large distance r_{12} from each other ($r_{12} \gg \lambda$). We have plotted on fig. 5 in solid line the function $W_2(t)$ and in dashed line $W_2^{(\text{ind})}(t)$. The two rates are – as expected – equal at time $t = 0$ since at that time the two atoms are not correlated to each other. As time evolves, $W_2(t)$ becomes larger than $W_2^{(\text{ind})}(t)$, exhibiting the basic superradiant effect. (Of course, since the *total* radiated energy is equal in both cases, the superradiant rate eventually becomes smaller than the independent atom one.) The difference between $W_2(t)$ and $W_2^{(\text{ind})}(t)$ is not very spectacular in the case of $N = 2$ atom superradiant emission. The superradiant behaviour exhibiting an N^2 intensity dependance (instead of an N -one for independent atom emission) is of course much more dramatic for larger N values.

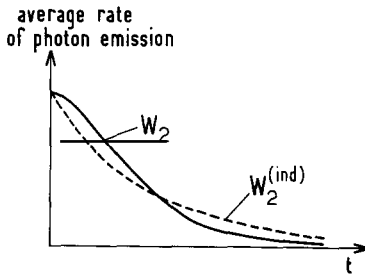


Fig. 5. Time dependence of the average rate W_2 of photon emission for two-atom superradiance (solid line) compared to the emission rate $W_2^{(\text{ind})}$ of independent atoms (dashed line).

Obviously, the discussion of this section, which was intended as a simple introduction to the subject of superradiance, has raised more questions than it has solved. The small sample case is indeed not very realistic. Even if we assume that the atoms are in a volume small compared to λ , we have given no convincing argument for the fact that the atom to field coupling should be invariant by atom permutation. And even if this is true, we have not given yet a quantitative description of the system evolution for $N > 2$ (the simple energy conservation argument of section 2.5 is obviously not sufficient for larger systems). In order to answer these questions, it is necessary to start by deriving the equations which, in quantum electrodynamics, describe the evolution of an assembly of atoms coupled to the radiation field.

3. Superradiance equations for a system of N two-level atoms

Two different points of view can be used to describe superradiance. The first one, developed in the original paper of Dicke [1] and recalled in the previous section, considers it as the phenomenon of collective spontaneous emission by the full quantum system made of the N two-level atoms initially in their excited state. The second point of view [17] rather sees superradiance as the transient amplification of photon noise by an extended atomic medium described at each space point by its time dependent polarization and population inversion. The first approach quite naturally makes use of the Schrödinger picture of Quantum Mechanics, which gives a complete description of the state of the system itself. The second approach, on the other hand, adopts the Heisenberg picture which focuses on the direct study of a small number of observables (field, atomic polarization and populations) and disregards the quantum state of the atomic system.

Of course, if correctly derived, both points of view are fully quantum mechanical in the sense that they are both based on the general principles of Quantum Electrodynamics. But the Heisenberg picture is much closer to a semi-classical analysis, since the equations directly obtained in this point of view are formally identical to the Bloch–Maxwell equations of the atom–field classical theory. This picture emphasizes field amplification and stimulated emission by some atoms of the field emitted by others, which are notions that can be given a clear classical interpretation. The Schrödinger approach, on the other hand, seems at first sight more genuinely quantum mechanical, since it deals only with spontaneous emission of a collective system and appears as the N -atom extension of the Wigner–Weisskopf theory [76] of single atom radiative decay.

This difference in points of view has not always been understood as purely semantical and has sometimes led to the idea that the word “superradiance” might represent in fact two distinct

phenomena, the collective spontaneous emission effect being called “Dicke superradiance” and being opposed to the “Laser superradiance” observed in a transient optical amplifier. In order to clarify this point and to stress the fact that both pictures describe the same physical effect, we analyse in this essay superradiance in the two points of view. In this section, we recall the equations which describe superradiance in the Schrödinger and in the Heisenberg representations. These equations have been of course derived previously by numerous authors. We feel however that it is interesting to recall here the way they are derived, not only to be able to show later the complete equivalence of the two approaches, but also in order to analyse precisely the kind of approximations one has to make to solve these equations. These approximations will be discussed in detail in section 7. The reader who is already acquainted with the problem of superradiance can proceed directly to eqs. (3.18), (3.29) and (3.30) and skip the remainder of this section.

3.1. The atom + field system Hamiltonian

Having introduced in subsection 2.1 the notations relative to the atomic system, we have now to define similarly the radiation field quantities. The electric field operator \mathbf{E} is described in terms of superposition of creation and annihilation operators $a_{k\epsilon}^+$ and $a_{k\epsilon}$ (acting on the mode of the field with wave-vector \mathbf{k} and polarization ϵ). In the same way as we have separated the atomic dipole in two parts, it is convenient also to divide \mathbf{E} in its positive and negative frequency parts E^+ and E^- defined as:

$$\mathbf{E}^+(\mathbf{r}) = -i \sum_{k,\epsilon} \mathcal{E}_{k\epsilon} a_{k\epsilon} e^{i\mathbf{k}\cdot\mathbf{r}} \quad (3.1)$$

$$\mathbf{E}^-(\mathbf{r}) = i \sum_{k,\epsilon} \mathcal{E}_{k\epsilon} a_{k\epsilon}^+ e^{-i\mathbf{k}\cdot\mathbf{r}} \quad (3.2)$$

where

$$\mathcal{E}_{k\epsilon} = \sqrt{\frac{\hbar ck}{2\epsilon_0 \mathcal{V}}} \epsilon \quad (3.3)$$

is the “electric field per photon” (\mathcal{V} is an arbitrary quantization volume, much larger than the atomic sample). The field polarization and wave-vectors \mathbf{k} obey the transversality condition

$$\epsilon \cdot \mathbf{k} = 0 \quad (3.4)$$

and the $a_{k\epsilon}$ and $a_{k\epsilon}^+$ obey the standard commutation relation:

$$[a_{k\epsilon}, a_{k'\epsilon'}^+] = \delta_{kk'} \delta_{\epsilon\epsilon'} . \quad (3.5)$$

The evolution of the “atom + field system” is ruled by the Hamiltonian:

$$H = H_{\text{at}} + H_{\text{rad}} + V \quad (3.6)$$

where:

$$H_{\text{at}} = \hbar\omega_0 \sum_i D_i^3 \quad (3.7)$$

$$H_{\text{rad}} = \sum_{k\epsilon} \hbar\omega_k (a_{k\epsilon}^+ a_{k\epsilon} + \frac{1}{2}) \quad (3.8)$$

$$V = - \sum_i (\mathbf{E}^+(\mathbf{r}_i) + \mathbf{E}^-(\mathbf{r}_i)) \cdot \mathcal{D}_{ai} \quad (3.9)$$

are the atomic, field and atom-field interaction Hamiltonians respectively. The interaction term is expressed in the electric dipole approximation which amounts to neglecting the difference between the electron and the center of mass location in each atom. Note also that writing the interaction in the form of eq. (3.9) amounts to choosing a gauge in which *all the effects* of the coupling of atoms to the electromagnetic field (including the electrostatic interaction between atoms) is included in a single term (the $\mathbf{E} \cdot \mathcal{D}$ one). This is the big advantage of this representation over the $\mathbf{A} \cdot \mathbf{p} + \mathbf{A}^2$ atom-field coupling description, to which one should add to describe the electrostatic effects, a $1/r_{ij}^3$ potential energy contribution. A complete discussion of this problem can be found in ref. [77] and its relevance to the problem of superradiance has been discussed by Friedberg and Hartman [21] (see section 4).

3.2. The Schrödinger approach: Superradiance master equation for the atomic system density matrix

In the Schrödinger picture, the atom + field system is described by its density matrix $\Phi(t)$, which obeys the evolution equation:

$$i\hbar d\Phi/dt = [H, \Phi]. \quad (3.10)$$

Transforming into the interaction representation, eq. (3.10) becomes:

$$i\hbar d\tilde{\Phi}/dt = [\tilde{V}, \tilde{\Phi}] \quad (3.11)$$

with

$$\tilde{\Phi} = \exp\{i[H_{\text{at}} + H_{\text{rad}}]t/\hbar\} \Phi \exp\{-i[H_{\text{at}} + H_{\text{rad}}]t/\hbar\} \quad (3.12)$$

and a similar definition for \tilde{V} .

In general, we are interested in atomic observables, which depend only on the atomic density operator $\tilde{\rho}$ defined by tracing $\tilde{\Phi}$ over field variables:

$$\tilde{\rho}(t) = \text{Tr}_{\text{rad}} \tilde{\Phi}(t). \quad (3.13)$$

By straightforward integration and iteration, eqs. (3.11) and (3.13) lead to the following exact integro-differential evolution equation for $\tilde{\rho}$:

$$\frac{d\tilde{\rho}}{dt} = -\frac{1}{\hbar^2} \text{Tr}_{\text{rad}} \int_0^t d\tau [\tilde{V}(t), [\tilde{V}(t-\tau), \tilde{\Phi}(t-\tau)]] \quad (3.14)$$

which has to be solved with the initial condition at $t=0$:

$$\tilde{\Phi}(0) = \Phi(0) = |0\rangle_{\text{rad}}\langle 0| \otimes \tilde{\rho}(0) = |0\rangle_{\text{rad}}\langle 0| \otimes \left\{ \prod_i |\epsilon\rangle_i \langle \epsilon| \right\} \quad (3.15)$$

representing the field in its vacuum state with all the atoms in the upper level.

In spite of its deceptively simple appearance, eq. (3.14) is a formidably complicated expression, since it contains a summation over all field modes and atoms. Furthermore, the evolution of $\tilde{\rho}$ at time t depends on the whole previous history of the atom + field system described by $\tilde{\Phi}(t - \tau)$. In order to solve this equation and to express simply the evolution of the atomic system, one performs an approximation known as the Born–Markov [4, 11, 37] one. It consists in neglecting the build-up of correlation between the atoms and the field (Born) and in considering the atom–field correlation time as being negligibly short compared to the evolution time of the atomic system (Markov). Practically, one makes the Born approximation by replacing $\tilde{\Phi}(t - \tau)$ by $\tilde{\rho}(t - \tau) \otimes |0\rangle_{\text{rad}}\langle 0|$ in eq. (3.14), and the Markov approximation by replacing at the same time $\tilde{\rho}(t - \tau)$ by $\tilde{\rho}(t)$. Consistently, one can then also replace the upper limit of the integral by infinity and one finally gets the following evolution equation:

$$\left[\frac{d\tilde{\rho}}{dt} \right]_{\text{Born-Markov}} = -\frac{1}{\hbar^2} \text{Tr} \int_0^{+\infty} d\tau [\tilde{V}(t) [\tilde{V}(t - \tau), \tilde{\rho}(t) \otimes |0\rangle_{\text{RR}}\langle 0|]]. \quad (3.16)$$

Coming back to $\rho(t)$ by the transformation:

$$\rho(t) = \exp\{-iH_{\text{at}}t/\hbar\} \tilde{\rho}(t) \exp\{iH_{\text{at}}t/\hbar\} \quad (3.17)$$

and replacing V by its expansion over the field modes (eqs. (3.1), (3.2) and (3.9)) one gets after a straightforward calculation the following *superradiance master equation*:

$$\begin{aligned} \frac{d\rho}{dt} = & \frac{1}{i\hbar} \left[\sum_j H_j, \rho \right] - \frac{cd^2}{16\varepsilon_0\pi^3\hbar} \int_0^{+\infty} d\tau \int_0^{+\infty} k^3 dk \int d\Omega (\boldsymbol{\varepsilon} \cdot \boldsymbol{\varepsilon}_a)^2 \sum_{ij} \exp\{ik(\mathbf{r}_i - \mathbf{r}_j) - ick\tau\} \\ & \times \{D_i \exp\{-iH_j\tau/\hbar\} D_j \exp\{iH_i\tau/\hbar\} \rho - \exp\{-iH_j\tau/\hbar\} D_j \exp\{iH_i\tau/\hbar\} \rho D_i\} \\ & + \text{hermitian conjugate of the integral.} \end{aligned} \quad (3.18)$$

In this equation, the integration is performed over the time and over the field mode frequency ck and direction (Ω). The integration over Ω involves of course implicitly the summation over the transverse field polarization $\boldsymbol{\varepsilon}$. Projected along the eigenstates $|\alpha\rangle$, $|\beta\rangle$ of the collective atomic system, this equation appears as a differential linear equation:

$$\frac{d\rho_{\alpha\alpha'}}{dt} = -i(E_\alpha - E_{\alpha'}) \rho_{\alpha\alpha'} + \sum_{\beta\beta'} R_{\alpha\alpha',\beta\beta'} \rho_{\beta\beta'} \quad (3.19)$$

with time independent coefficients $R_{\alpha\alpha',\beta\beta'}$ resulting from a summation over all couples of atoms and from the integrations over k , Ω and τ described above.

The integration over Ω and $\boldsymbol{\varepsilon}$ yields the diffraction type function:

$$\begin{aligned} F_{ij}(kr_{ij}) = & \int (d\Omega) (\boldsymbol{\varepsilon} \cdot \boldsymbol{\varepsilon}_a)^2 \exp\{ik(\mathbf{r}_i - \mathbf{r}_j)\} \\ = & 4\pi \left[1 - \frac{(\boldsymbol{\varepsilon}_a \cdot \mathbf{r}_{ij})^2}{r_{ij}^2} \right] \frac{\sin kr_{ij}}{kr_{ij}} + 4\pi \left[1 - 3 \frac{(\boldsymbol{\varepsilon}_a \cdot \mathbf{r}_{ij})^2}{r_{ij}^2} \right] \left[\frac{\cos kr_{ij}}{(kr_{ij})^2} - \frac{\sin kr_{ij}}{(kr_{ij})^3} \right] \end{aligned} \quad (3.20)$$

whose “width” in k space is of the order of $1/r_{ij}$. The integration over k in eq. (3.18) then introduces “time-correlation” functions $G_{ij}(\tau)$ of the form:

$$G_{ij}(\tau) = \int k^3 F_{ij}(kr_{ij}) e^{-ik\tau} dk \quad (3.21)$$

which appear as the Fourier transform of the product of the field mode distribution function (k^3) by the atom-distribution diffraction function $F_{ij}(kr_{ij})$. The $G_{ij}(\tau)$ ’s are thus convolution products of a function of τ having a typical width of the order of $1/\omega_0 = \lambda/c$ (Fourier transform of k^3) by another function of τ with a width of the order of r_{ij}/c [Fourier transform of $F_{ij}(kr_{ij})$]. Since the $G_{ij}(\tau)$ ’s act as integration kernels in eq. (3.18), their width obviously represents the correlation time (memory time) of the superradiant process. This correlation time is thus equal to the shorter of l/c and λ/c , where l is the typical size of the atomic medium (i.e. a typical value for r_{ij}):

$$\tau_c = \inf(\lambda/c, l/c). \quad (3.22)$$

The Born–Markov approximation, which amounts to considering τ_c as infinitely short, has thus the physical effect of neglecting retardation in the superradiant coupling between atoms [97].

This approximation is quite generally assumed in describing the evolution of a “small” system (here the N two-level atoms) coupled to a “big” reservoir (here the electromagnetic field modes) which has a broad continuum of energy levels and whose evolution is not too much modified by its coupling to the small system. The same approximation is of course made in the case of single-atom spontaneous emission. It is then known as the Wigner–Weisskopf one [76] and is justified by the fact that the optical period λ/c (which is the correlation time in that case) is extremely short as compared to the natural radiative life time $1/\Gamma$ (the ratio between these two times being of the order of the cube of the fine structure constant). In the case of superradiance with $N \gg 1$, the radiative lifetime of the system is shortened by a ratio of the order of N whereas the correlation time τ_c becomes larger than the optical period for samples bigger than the optical wavelength λ . It is thus obvious that for some critical N value, the Born–Markov approximation will break down. This problem is studied in section 7.

The general master equation (3.18) has been used under this form or an equivalent one by many authors [4, 39]. To explicitly compute the $R_{\alpha\alpha',\beta\beta'}$ requires the precise knowledge of the atom distribution in space. Let us note in general that these coefficients have a real and an imaginary part. The real part describes the irreversible radiative damping of the atomic system, i.e. the very essence of the superradiance phenomenon. The imaginary contribution has been sometimes described as a “collective Lamb-shift”. It does indeed reduce, in the case $N = 1$, to the ordinary Lamb-shift term and appears in general as the integral over field modes of a dispersion-like function reminiscent of a radiative shift. It can in fact be shown (see sections 4 and 6 below) that this dispersive imaginary term more fundamentally describes the electrostatic dipole–dipole interaction between the atoms [98] (in the case of a volume small compared to λ) and the effects connected to the propagation of the electromagnetic field throughout the medium (if the sample is large compared to λ).

3.3. The Heisenberg approach: The Bloch–Maxwell equations for the quantum mechanical field and atomic operators

The density matrix ρ contains in fact a tremendous amount of information. It has in general 2^{2N} different matrix elements! Only in some special cases, does it reduce to a much smaller space, spanned

by only $N + 1$ so-called symmetrical states (see section 4). Beyond these special cases, the price to pay for studying superradiance in the Schrödinger picture is exorbitant, since one has to determine a huge mathematical object (the density matrix) which gives in principle the clue for the evaluation of any atomic observable (all the dipole correlations up to N th order!) whereas we are in general interested in the radiated field which only depends upon a very small number of atom–atom correlations. It is then much more economical to turn to the Heisenberg approach which directly focuses on the observables of interest and does not try to describe extensively the atom + field system. Instead of defining a global density operator for the whole system, we introduce local atomic polarization and population inversion operators $P(\mathbf{r})$ and $\mathcal{N}(\mathbf{r})$ by the definitions:

$$\mathcal{N}(\mathbf{r}) = \sum_i \delta_\epsilon(\mathbf{r} - \mathbf{r}_i) [D_i^3] \quad (3.23)$$

$$P^\pm(\mathbf{r}) = d\epsilon_a \sum_i \delta_\epsilon(\mathbf{r} - \mathbf{r}_i) D_i^\pm. \quad (3.24)$$

In these expressions, the δ_ϵ functions are “coarse-grained” δ distributions with a support extending over dimensions ϵ large compared to an atom size and small compared to the emitted wavelength. (The procedure thus used to define a macroscopic atomic polarization is similar to the one developed for deriving the macroscopic Maxwell equation in a dielectric medium [78].)

The evolution equation for \mathcal{N} , P and $E(\mathbf{r})$ are given by the Heisenberg equations:

$$\frac{dX}{dt} = \frac{1}{i\hbar} [X, H]$$

with X being \mathcal{N} , P or E and H the Hamiltonian of the system (eq. (3.6)). After straightforward calculations, one gets for the motion of \mathcal{N} and P :

$$\frac{\partial \mathcal{N}(\mathbf{r}, t)}{\partial t} = \frac{i}{\hbar} [\mathbf{E}^+(\mathbf{r}, t) + \mathbf{E}^-(\mathbf{r}, t)] [\mathbf{P}^+(\mathbf{r}, t) - \mathbf{P}^-(\mathbf{r}, t)] \quad (3.25)$$

$$\frac{\partial \mathbf{P}^+(\mathbf{r}, t)}{\partial t} = i\omega_0 \mathbf{P}^+(\mathbf{r}, t) + 2i \frac{d^2}{\hbar} \epsilon_a \{ \epsilon_a \cdot [\mathbf{E}^+(\mathbf{r}, t) + \mathbf{E}^-(\mathbf{r}, t)] \} \mathcal{N}(\mathbf{r}, t). \quad (3.26)$$

As for the field evolution, it is expressed by iterating twice the derivation with respect to t :

$$\frac{\partial^2 E^+(\mathbf{r}, t)}{\partial t^2} - c^2 \nabla \times \nabla E^+(\mathbf{r}, t) = -\frac{1}{\epsilon_0} \frac{\partial^2 P^-(\mathbf{r}, t)}{\partial t^2}. \quad (3.27)$$

These equations are known as the Bloch–Maxwell equations [30]. They describe the self-consistent evolution of the atomic system in its own radiation field. They look formally identical to the equations one would have derived similarly in the frame of semi-classical theory [79, 17] with the major difference that \mathcal{N} and P on one side and E^+ and E^- on the other side are here non-commuting operators. This non-commuting character, which contains the quantum fluctuations of the system, is obviously essential

to understand the early evolution of the superradiant system (classical equations with the initial conditions $E = P = 0$ would merely not start and the atoms would stay for ever in their upper level).

A remark is here in order concerning the ordering of the operators in eqs. (3.25) and (3.26). It is clear that the E^+, E^- operators on the one hand and P^+, P^- and \mathcal{N} on the other hand commute with each other at equal time since they refer to two different systems at time $t = 0$ and since they can be deduced from their $t = 0$ value by the same $e^{iHt/\hbar}$ unitary transformation. As a result, the ordering of E^\pm and P^\pm , or E^\pm and \mathcal{N} in eqs. (3.25) and (3.26) can be chosen arbitrarily, according to convenience. This is no longer the case if, as is often done, one divides the field into a vacuum and a radiated contribution: the solution of the inhomogeneous Maxwell equation (3.27) can indeed be written as:

$$\mathbf{E} = \mathbf{E}^{\text{vac}} + \mathbf{E}^{\text{rad}} \quad (3.28)$$

where \mathbf{E}^{vac} is the solution of the homogeneous equation (with $P = 0$) corresponding to the vacuum field, and \mathbf{E}^{rad} is the radiated field, proportional to the atomic dipoles. It is important to notice that \mathbf{E}^{vac} and \mathbf{E}^{rad} separately do not commute with P or \mathcal{N} at equal times. As a result, when this division is made, the ordering of E and P has to be chosen one for all and not modified during calculation. It is convenient to choose the normal ordering which consists in each product in placing E^+ at the right and E^- at the left [97]. With this choice, all expectation values corresponding to the vacuum field part vanish and the system evolution can be described only with the radiated part contribution. Equations (3.25) and (3.26) with normal ordering become:

$$\left\{ \begin{array}{l} \frac{\partial \mathcal{N}}{\partial t} = \frac{i}{\hbar} \mathbf{E}^{-\text{rad}} [\mathbf{P}^+ - \mathbf{P}^-] + \frac{i}{\hbar} [\mathbf{P}^+ - \mathbf{P}^-] \cdot \mathbf{E}^{+\text{rad}} \\ \frac{\partial \mathbf{P}^+}{\partial t} = i\omega_0 \mathbf{P}^+ + 2i \frac{d^2}{\hbar} \boldsymbol{\epsilon}_a \cdot \{ \boldsymbol{\epsilon}_a (\mathbf{E}^{-\text{rad}} \mathcal{N} + \mathcal{N} \mathbf{E}^{+\text{rad}}) \}. \end{array} \right. \quad (3.29)$$

Equations (3.18) on the one hand and (3.27), (3.29), (3.30) on the other hand are the starting points for the description of superradiance in the Schrödinger or in the Heisenberg picture. Each has its advantage and drawbacks. The first one takes the form of a very simple linear set of first-order differential equations for a very complex quantity (the density matrix ρ). The second ones are complicated equations coupling in a non-linear way very simple quantities, namely the operators actually measured in a superradiance experiment. The Heisenberg equations seem at first sight to have a more general validity since we have not had to perform any approximation of the Born–Markov type in order to derive them. The Bloch–Maxwell equations describe indeed a finite memory time process, since the derivatives of $P(\mathbf{r})$ and $\mathcal{N}(\mathbf{r})$ at time t depend upon the field at the same time, which through the second-order propagation equation (3.27) is dependent upon the values of the atomic polarization at former times. We will see however that in order to be able to numerically solve these equations, it is necessary to assume that the field and the polarization can be described as the product of complex exponentials (oscillating in time and space at the frequency and the wavelength associated to the atomic transition) by “slow varying” envelopes changing over much larger characteristic intervals. We will see that this factorization amounts in fact to performing a kind of Born–Markov approximation. A complete discussion comparing the domains of validity of the Schrödinger and Heisenberg approaches is presented in section 7.

4. Superradiance in small volumes revisited: Competition between superradiance and Van der Waals dephasing

As a first application of the superradiance equation, we come back in this section to the case of atoms confined in a volume small compared to the radiated wavelength $\lambda_0 = 2\pi/k_0$, a situation that we have already qualitatively considered in section 2. At first sight, this problem appears to be very easy to describe in the Schrödinger picture. Since all atoms are very close to each other, it seems legitimate to merely replace by one the dephasing factors $\exp\{ik(r_i - r_j)\}$ in the master equation (3.18). This equation then should take a symmetrical form and the evolution it describes should be restricted to the symmetrical states introduced in section 2, leading to a “perfect case” of “symmetrical” superradiance. Unfortunately, this analysis is in general incorrect, as first pointed out by Friedberg, Hartman and Manassah [19]. The sum over k in eq. (3.18) extends indeed over all k values (and not only around $k_0 = 2\pi/\lambda_0$) and there is an infinite number of k values for which $\exp(ikr_{ij}) \neq 1$. These k values contribute to a very important imaginary part in the master equation which describes the dipole–dipole Van der Waals coupling between the atom ($\sim 1/r_{ij}^3$). For a sample made of many atoms, this coupling is in general non-invariant by atom permutation. As a result, the system evolution is no longer restricted to the maximum-correlated-symmetrical states and does not follow in general the perfect “symmetrical” superradiant behaviour. In this section, which follows closely the point of view of refs. [4, 23], we analyse the effect of this Van der Waals interaction and we discuss some special situations where – in spite of the Van der Waals force – the symmetrical superradiant behaviour is preserved.

4.1. The superradiant master equation in the small volume case

In eq. (3.18), we perform the angular integration over Ω which introduces the diffraction functions $F_{ij}(kr_{ij})$ and we separate $\exp(-iH_j\tau/\hbar) D_j \exp(iH_j\tau/\hbar)$ in its positive and negative frequency parts using the relation:

$$\exp(-iH_j\tau/\hbar) D_j \exp(iH_j\tau/\hbar) = \exp(ick_0\tau) D_j^- + \exp(-ick_0\tau) D_j^+ \quad (k_0 = \omega_0/c). \quad (4.1)$$

The integration over τ then introduces the $\delta(k - k_0)$ and $\text{PP}[1/(k - k_0)]$ distributions according to:

$$\int_0^{+\infty} c d\tau \exp\{-ic(k \mp k_0)\tau\} = \pi\delta(k_0 \mp k) \pm i \text{PP} \frac{1}{k_0 \mp k}. \quad (4.2)$$

The master equation then becomes:

$$\begin{aligned} \frac{d\rho}{dt} &= \frac{1}{i\hbar} \left[\sum_j H_j, \rho \right] - \frac{d^2}{16\epsilon_0\pi^3\hbar} \sum_{i,j} \int_0^{+\infty} k^3 F_{ij}(kr_{ij}) \left[\pi\delta(k_0 - k) + i \text{PP} \frac{1}{k_0 - k} \right] [D_i D_j^- \rho - D_j^- \rho D_i] dk \\ &\quad - \frac{d^2}{16\epsilon_0\pi^3\hbar} \sum_{i,j} \int_0^{+\infty} k^3 F_{ij}(kr_{ij}) \left[\pi\delta(k_0 + k) - i \text{PP} \frac{1}{k_0 + k} \right] [D_i D_j^+ \rho - D_j^+ \rho D_i] dk \\ &\quad + \text{hermitian conjugate of the integrals.} \end{aligned} \quad (4.3)$$

Let us now consider in turn the real and imaginary parts of this equation.

4.1.1. The real part of the master equation: the symmetrical damping term

The real part of the integral in eq. (4.3) corresponds to the term with $\delta(k_0 - k)$, i.e. describes the coupling with resonant photons ($k_0 = k$). [$\delta(k_0 + k)$ does not contribute since k is integrated from zero to infinity.] The presence of the $\delta(k_0 - k)$ distribution implies that $F_{ij}(kr_{ij})$ has to be evaluated for $k = k_0$. In a small volume ($k_0 r_{ij} \ll 1$), $F_{ij}(k_0 r_{ij})$ can be replaced by $8\pi/3$ for all r_{ij} 's. When this replacement is performed, the integration over k merely yields k_0^3 and the real part of the integral reduces to:

$$\left(\frac{d\rho}{dt}\right)_{\text{real}} = -\frac{\Gamma}{2} \sum_{i,j} [D_i^+ D_j^-, \rho]_+ + \Gamma \sum_{i,j} D_j^- \rho D_i^+ \quad (4.4)$$

with:

$$\Gamma = k_0^3 d^2 / (3\pi\epsilon_0\hbar) \quad (4.5)$$

being the single atom spontaneous emission rate on the e → g transition.

To get eq. (4.4), we have taken into account the hermitian conjugate of the terms written in eq. (4.3) and replaced products as $D_i D_j^-$ by $D_i^+ D_j^-$. This replacement corresponds to a *secular approximation*, which amounts to assuming that terms like $D_i^- D_j^-$, which couple matrix elements of ρ evolving at frequencies differing by $2\omega_0$ have a negligible effect on the system evolution whose characteristic evolution time is much longer than $1/\omega_0$. This approximation is perfectly consistent with the Born–Markov one, where it has been assumed that the evolution of the system occurs over characteristic times much longer than the correlation time λ/c .

Eq. (4.4) can be expressed under a more compact form by introducing the collective operators D^+ , D^- (see eq. (2.8)).

One has:

$$\left(\frac{d\rho}{dt}\right)_{\text{real}} = -\frac{\Gamma}{2} [D^+ D^-, \rho]_+ + \Gamma D^- \rho D^+. \quad (4.6)$$

This equation, derived by many authors [4, 9, 23], describes a totally symmetrical *damping* process in which the system, starting at time $t = 0$ from the symmetrical state $|e, e, e \dots e\rangle$, evolves in the subspace of atomic states invariant by atomic permutations which are nothing but the $|JM\rangle$ states introduced in section 2.

Projected along these states, eq. (4.6) becomes:

$$d\rho_M/dt = -\Gamma(J+M)(J-M+1)\rho_M + \Gamma(J+M+1)(J-M)\rho_{M+1} \quad (4.7)$$

where ρ_M is the probability of finding the system at time t in state $|JM\rangle$ (i.e. the probability that the system has emitted at this time $s = J - M$ photons). As noticed in section 2, this equation describes a process formally identical to the spontaneous emission of an angular momentum $J = N/2$ placed in a magnetic field associated to a Larmor frequency ω_0 . The system, starting from the upper $|JJ\rangle$ level cascades down the ladder of the $|JM\rangle$ levels with transition rates $\Gamma_{M \rightarrow M-1} = \Gamma(J+M)(J-M+1)$ and ends up at time $t = +\infty$ in the $|J-J\rangle = |g, g \dots g\rangle$ totally deexcited state (see fig. 4). The dynamics of this decay process is described in detail in section 5.

4.1.2. The imaginary part of the master equation: the dipole–dipole interaction

The imaginary part of the integrals in eq. (4.3) corresponds to the dispersive $1/(k_0 - k)$ and $1/(k_0 + k)$ terms and thus describes the effects of off-resonant photon processes. Let us distinguish between the $i = j$ and the $i \neq j$ terms. The former ones are associated to $F_{ii}(0) = 1$ terms and are identical to the one obtained in the single atom spontaneous emission master equation for atom i : they merely describe the Lamb-shift of each atom and can be reintegrated in the Hamiltonian part of eq. (4.3) as a renormalization of the free atomic eigenfrequency ω_0 . The $i \neq j$ terms on the other hand are new contributions representing the exchange of virtual transverse photons between atoms i and j . Regrouping the positive and negative frequency parts with their hermitian conjugates and performing the integration over k which amounts to computing a Hilbert transform $\int_{-\infty}^{+\infty} \{k^3 F_{ij}(kr_{ij})/(k_0 - k)\} dk$, one readily obtains, at the limit $kr_{ij} \rightarrow 0$:

$$\left(\frac{d\rho}{dt} \right)_{\text{imag}} = \frac{1}{i\hbar} \left[\sum_{i>j} \Omega_{ij} D_i D_j, \rho \right]_- \quad (4.8)$$

with:

$$\hbar \Omega_{ij} = \frac{d^2}{4\pi\epsilon_0 r_{ij}^3} \left[1 - \frac{3(\boldsymbol{\epsilon}_a \cdot \mathbf{r}_{ij})^2}{r_{ij}^2} \right]. \quad (4.9)$$

One recognizes in eq. (4.9) the electrostatic Van der Waals interaction between the atoms, which has to be added to the free atom Hamiltonian. This interaction, implicit in the electric dipole Hamiltonian of eq. (3.6), cannot be neglected when $r_{ij} < \lambda$, since the Ω_{ij} matrix elements then dominate the real damping rate Γ by a ratio $(\lambda/r_{ij})^3$!

4.2. Van der Waals dephasing of the symmetrical superradiant states

The dipole–dipole interaction generally breaks the permutation symmetry of the atom–field coupling because various atoms in the sample have different close-neighbour environments. This effect has been studied in detail in refs. [19, 20, 21, 23] where it has been shown that the perturbation due to these interactions is analogous to an inhomogeneous dephasing of the dipoles, leading to a loss of dipole–dipole correlation. In other words, the non-symmetrical dipole–dipole coupling connects the highly correlated $|JM\rangle$ states to levels of lower symmetry, corresponding to eigenvalues of the fictitious total angular momentum smaller than J . This considerably complicates the description of superradiance in the Schrödinger picture. Of course, this effect does not occur for $N = 2$, a case in which the dipole–dipole coupling is obviously symmetrical, so that the analysis developed in section 2 for two atoms remains valid even if Van der Waals interaction between the two atoms is taken into account. The simplest case in which such dephasing – or symmetry breaking – effects do occur is the superradiance of three atoms forming a triangle with a base smaller than the other sides. Let us consider as an example the case $r_{12} \ll r_{23}, r_{13}$ (see fig. 6). The coupling $\Omega_{12} \sim r_{12}^{-3}$ is then much stronger than Ω_{13} and Ω_{23} so that, in first approximation the Van der Waals interaction is represented in the $|\text{eeg}\rangle, |\text{ege}\rangle, |\text{gee}\rangle$ subspace by the matrix:

$$\Omega \simeq \begin{bmatrix} 0 & \Omega_{12} & 0 \\ \Omega_{12} & 0 & 0 \\ 0 & 0 & 0 \end{bmatrix} \quad (4.10)$$

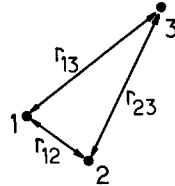


Fig. 6. Simple three atom configurations in which Van der Waals dephasing contributes to destroy the atomic symmetry: atoms 1 and 2 are closer to each other than 1 and 3 (or 2 and 3) so that the Van der Waals interaction is not invariant by permutation of 1 and 3 or 2 and 3.

which admits the eigenstates $|gee\rangle$, $(1/\sqrt{2})[|eeg\rangle + |ege\rangle]$ and $(1/\sqrt{2})[|eeg\rangle - |ege\rangle]$ with eigenvalues 0, $+\Omega_{12}$ and $-\Omega_{12}$ respectively. Let us now assume that at a given time, after having emitted one photon, the system is in the symmetrical state:

$$|\psi\rangle = \frac{1}{\sqrt{3}} [|eeg\rangle + |ege\rangle + |gee\rangle] \quad (4.11)$$

with strong dipole-dipole correlations:

$$\langle \psi | D_1^+ D_2^- | \psi \rangle = \langle \psi | D_2^+ D_3^- | \psi \rangle = \langle \psi | D_3^+ D_1^- | \psi \rangle = \frac{1}{3}. \quad (4.12)$$

Due to the dipole-dipole coupling, $|\psi\rangle$ will evolve at a later time τ into the state:

$$|\psi(\tau)\rangle = \frac{1}{\sqrt{3}} [e^{-i\Omega_{12}\tau} |eeg\rangle + e^{-i\Omega_{12}\tau} |ege\rangle + |gee\rangle] \quad (4.13)$$

in which the dipole-dipole correlations have become:

$$\langle \psi(\tau) | D_1^+ D_2^- | \psi(\tau) \rangle = \frac{1}{3}; \quad \langle \psi(\tau) | D_2^+ D_3^- | \psi(\tau) \rangle = \frac{e^{-i\Omega_{12}\tau}}{\sqrt{3}}; \quad \langle \psi(\tau) | D_3^+ D_1^- | \psi(\tau) \rangle = \frac{e^{i\Omega_{12}\tau}}{3}. \quad (4.14)$$

We have assumed here that $\tau < 1/\Gamma$, so that the radiative decay can be neglected during time τ . The dephasing $\Omega_{12}\tau$ appearing in eq. (4.14) can however be very important during that time since $\Omega_{12} \gg \Gamma$. As a result, the various couples of dipoles are obviously dephased very much before they radiate and the cooperative character of superradiance is considerably weakened. A quantitative analysis of this superradiance quenching effect can be found in ref. [23] for various small sample systems. It is found in ref. [21] that for a small sphere with uniform atom distribution, the dipole-dipole “decohering” effect destroys the superradiant emission when half of the atoms have been deexcited. We analyse in the next subsection some other simple situations where, in spite of these strong Van der Waals interactions, the symmetrical superradiance behaviour is not perturbed.

4.3. Small symmetrical superradiant samples. Frequency chirping effects of superradiance emission

The dephasing effect discussed above does not occur if the Van der Waals interaction Ω is, as the real part of the decay, symmetrical by atom exchange. This implies that all atoms should have an equivalent environment. At least two configurations obeying this requirement do exist [23]. They correspond to the case of a single or double ring of regularly spaced atoms with polarization ϵ_a

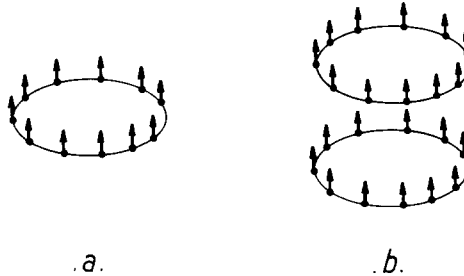


Fig. 7. Two configurations of atoms corresponding to a Van der Waals coupling symmetrical by atom permutation: the single (a) and double (b) ring of atoms whose plane is perpendicular to the polarization vector of the atomic transition.

perpendicular to the ring planes (see fig. 7). In that case, the $|JM\rangle$ states are eigenstates of the symmetrical Ω perturbation and the dipole-dipole Hamiltonian does not “mix” the “eigenstates” of the damping rate equation (4.7). The system decay is then exactly described by this equation. One should note that in that case the various $|JM\rangle$ levels are no longer equidistant since each of them undergoes a different dipole-dipole shift [4, 20]. As a result, the photons emitted successively in the superradiant cascade have different frequencies, resulting in a time-dependent frequency shift of the superradiant emission (frequency chirping effect). It is easy to compute this effect in the case of a superradiant ring of atoms. Due to the $1/r_{ij}^3$ decrease of the dipole-dipole coupling, it is clear that most of the Van der Waals interaction comes from closest neighbour coupling. Calling r the distance between these neighbours, one has:

$$\hbar\Omega \approx \frac{d^2}{4\pi\epsilon_0 r^3} \sum_i D_i D_{i+1}. \quad (4.15)$$

Since the expectation value of any $D_i D_j$ product with $i \neq j$ is the same in a symmetrical $|JM\rangle$ state, one can write:

$$\langle JM | \hbar\Omega | JM \rangle = \frac{d^2}{4\pi\epsilon_0 r^3} \frac{1}{N-1} \sum_{i>j} \langle JM | D_i^+ D_j^- + D_i^- D_j^+ | JM \rangle. \quad (4.16)$$

One can replace the sum of $D_i^+ D_j^-$ products in eq. (4.16) by $D^+ D^- + D^- D^+ - \sum_i D_i^2$ whose eigenvalues are $2(J^2 - M^2)$. Thus:

$$\langle JM | \hbar\Omega | JM \rangle = \frac{d^2}{4\pi\epsilon_0 r^3} \frac{J^2 - M^2}{J - \frac{1}{2}}. \quad (4.17)$$

Eq. (4.17) shows that the various $|JM\rangle$ states undergo a positive shift depending on the value M^2 (see fig. 8). The frequency shift $\delta\omega_s$ of the s th photon in the cascade ($s = J - M$) is obtained by differentiating eq. (4.17) with respect to M . One gets:

$$\hbar \delta\omega_s \approx -\frac{d^2}{4\pi\epsilon_0 r^3} \left[1 - \frac{2s}{N} \right]. \quad (4.18)$$

The first photons of the superradiance emission appear to be red-shifted (by a maximum amount

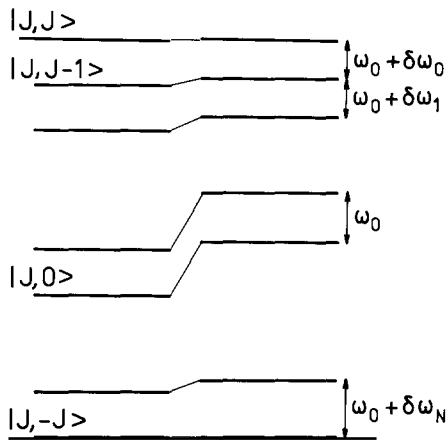


Fig. 8. Energy diagram of the $|JM\rangle$ states for a symmetrical ring of atoms. The left column represents the equidistant levels obtained when the Van der Waals shift is omitted. The right column shows the level shifted by the Van der Waals interaction. The shift is zero for both $M = J$ and $M = -J$ levels and always positive in between. The first photons of the cascade are red-shifted ($\delta\omega_0, \delta\omega_1 < 0$) and the last ones blue-shifted ($\delta\omega_N > 0$).

$-d^2/4\pi\epsilon_0 r^3$) whereas the last ones ($s \sim N$) are blue-shifted by the same amount. At the time of half the energy emission ($s = N/2$), the shift goes through the zero value.

A remark is at this stage in order concerning the *physical reality* of these shifts. It is clear that they are observable only if they are larger than the frequency uncertainty associated to the finite decay time of the superradiant system. In order to measure the frequency chirping, we must place in front of the detectors frequency filters with a bandwidth $\delta\omega_f$ small enough to discriminate the frequencies of successive photons ($\delta\omega_f < d^2/(N^2\Gamma)$), but large enough to be able to discriminate the times of arrivals of these photons ($\delta\omega_f > N^2\Gamma = N^2 d^2 \omega^3 / 3\pi\epsilon_0 \hbar c^3$; one has indeed to observe N photons emitted in a time of the order of $1/N\Gamma$; see sections 2 and 5). The compatibility of these conditions implies that:

$$\frac{N^3 d^2 \omega^3}{3\pi\epsilon_0 \hbar c^3} \ll \frac{d^2}{4\pi\epsilon_0 r^3} \quad (4.19)$$

which can also be expressed as:

$$2\pi Nr \ll \lambda. \quad (4.20)$$

Eq. (4.20) means that the length of the ring has to be smaller than λ , which is precisely the small sample condition! In other words, the frequency chirping is physically real and can – at least in principle – be measured by a set of ideal filters and detectors.

5. Quantitative analysis of the symmetrical superradiant evolution.

A first approach to quantum fluctuations in superradiance

Although it corresponds to a very special case – small sample with regular atomic distribution – which has never been realized in an actual experiment, the symmetrical damping equation (4.7) has been extensively studied and its solution analysed in a large number of papers dealing with super-

radiance [4, 9, 13, 28]. This equation exhibits indeed all the main features of the phenomenon – strong and fast emission, existence of important fluctuations – without being obscured by the intricate diffraction and propagation effects encountered in the large sample superradiant case (see section 6). The symmetrical equation (4.7) describes a very simple model of superradiance which allows us to understand – at least qualitatively – the behaviour of more complex – and more realistic – systems.

The set of linear differential equations (4.7) with the initial condition $\rho_M(0) = \delta_{MJ}$ admits a solution which can be expanded as a series of time varying exponentials whose time-constants are the reciprocals of the eigenvalues of the matrix associated with this set of equations. This formal solution – given in refs. [4, 9] – generalizes for $N > 2$ the exponential solution given in subsection 2.6 for two atoms. Unfortunately, this solution is not of great use to compute the $\rho_M(t)$ probabilities as soon as N is a large absolute number. The contribution of the very fast varying exponentials requires, in order to be computed accurately, that one keeps approximately as many digits in the calculation as the number of atoms. For N larger than a few tens, it is more practical to solve the differential equations numerically, which amounts to dividing the time in a finite number of intervals t_α , and to computing the $\rho_M(t_\alpha)$ step by step. Figure 9 shows the distribution $\rho_M(t_\alpha)$ for various delays t_α as it has been computed in ref. [9] for $N = 200$. This figure shows that $\rho_M(t)$ starts at $t = 0$ from the δ_{MJ} Dirac distribution and spreads out very quickly over a wide range of M values as the system cascades down. At early times, $\rho_M(t)$ has an exponentially decreasing shape. At later times, when the average $\langle M \rangle$ value gets close to zero (point of half emission), $\rho_M(t)$ is a bell-shaped distribution practically covering all M values. At still later times,

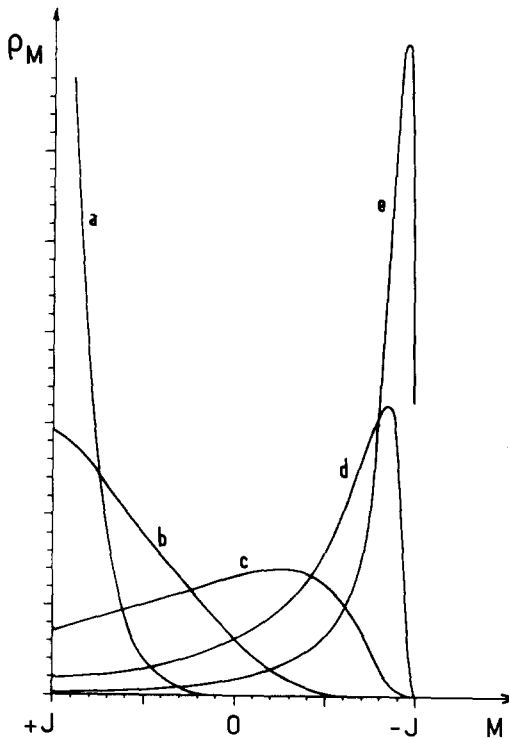


Fig. 9. The $\rho_M(t)$ distribution obtained for $N = 200$ atoms by numerical computation of eq. (4.7) for increasing values of t (from ref. [9]). Curves a, b, c, d, e correspond respectively to $t = 2.65, 3.97, 5.3, 6.62, 7.95$ in units of $(N\Gamma)^{-1}$. Note the evolution of the distribution which is narrow at small time (curve a) broadens to cover the whole range of M values at intermediate times (curves b, c, d) and becomes narrow again at the end (curve e) of the evolution.

towards the end of the cascade, $\rho_M(t)$ gets narrower and ends up as the δ_{M-J} Dirac distribution. These features do not depend upon N , provided it is large enough: for larger N 's, one expects to find the same distribution shapes, the only difference being of course the time scale of the system evolution. Several important characteristics of the emission dynamics (expectation value of the radiated intensity, statistics of photon number fluctuations, etc.) can be determined once the $\rho_M(t)$ are known. For example, the expectation value of the atomic energy is:

$$\langle H_{\text{at}} \rangle = \hbar\omega_0 \langle D^3 \rangle = \hbar\omega_0 \sum_M M \rho_M(t), \quad (5.1)$$

the rate of radiated energy is:

$$I(t) = -\frac{d\langle H_{\text{at}} \rangle}{dt} = -\hbar\omega_0 \sum_M M \frac{d\rho_M}{dt} \quad (5.2)$$

and the atomic energy mean square root deviation:

$$\Delta H_{\text{at}} = \sqrt{\langle H_{\text{at}}^2 \rangle - \langle H_{\text{at}} \rangle^2} = \hbar\omega_0 \left[\sum_M M^2 \rho_M - \left(\sum_M M \rho_M \right)^2 \right]^{1/2}. \quad (5.3)$$

The fact that $\rho_M(t)$ is, in the middle of the emission process, a wide distribution over M values means that the atomic energy then has a large mean square root deviation:

$$\Delta H_{\text{at}}/\langle H_{\text{at}} \rangle \sim 1. \quad (5.4)$$

It equivalently means that a measurement of M – i.e. a measurement of the number $s = J - M$ of emitted photons at a given time – will exhibit large shot to shot fluctuations:

$$\Delta s/\langle s \rangle \sim 1. \quad (5.5)$$

In order to describe exactly the statistics of these fluctuations, it is very convenient to have a *simple tractable* analytical expression for $\rho_M(t)$ and not to have to rely on the results of numerical computation, increasingly difficult to perform when N increases. It is indeed possible to derive such an expression, which is asymptotically exact when N increases towards infinity and which coincides remarkably well with the numerically calculated solution for N as small as a few units. It is the purpose of this section to present this solution [13, 24]. The physical arguments we will develop here will be interesting for the generalization of the theory to large sample superradiance. We will indeed see that $\rho_M(t)$ can be analysed as a linear superposition of probability distributions describing the evolution of the superradiant systems along “classical” fluctuationless trajectories. This analysis is very similar to the one which is used to solve – in the Heisenberg point of view – the problem of large sample superradiance (see section 6).

5.1. Simple evaluation of superradiance delay and delay fluctuations

It is quite simple to give a qualitative description of the cascade emission down the ladder of $|JM\rangle$ states, which accounts for the fluctuations exhibited by the exact solution. The rate of emission of the

s th = $(J - M)$ th photon is:

$$\Gamma_s = \Gamma_{M \rightarrow M-1} = \Gamma(J+M)(J-M+1). \quad (5.6)$$

For s much smaller than N , i.e. for the beginning of the emission, this rate can be “linearized” as

$$\Gamma_s = \Gamma N s \quad (5.7)$$

by replacing in eq. (5.6) $J + M$ by N and $J - M + 1$ by s . Eq. (5.7) means that the first superradiance photon is emitted in an average time $(\Gamma N)^{-1}$, the second in a time $(2\Gamma N)^{-1}$ and so on. Summing all these elementary time intervals, one obtains as an order of magnitude for the overall process duration:

$$\langle t_D \rangle \sim \frac{1}{N\Gamma} \left[1 + \frac{1}{2} + \dots + \frac{1}{N} \right] = \frac{\text{Log } N}{N\Gamma}. \quad (5.8)$$

[Obviously, the last terms of the series are not given accurately by the linearized expression (5.7) but we look here for an order of magnitude.]

There is of course an uncertainty for each of these elementary process durations. Assuming that one can add quadratically these uncertainties, one gets as an order of magnitude for the dispersion of delays:

$$\Delta t_D = \sqrt{\langle t_D^2 \rangle - \langle t_D \rangle^2} \sim \left[1 + \frac{1}{2^2} + \frac{1}{3^2} + \dots \right]^{1/2} \simeq 1.3/N\Gamma. \quad (5.9)$$

The relative delay dispersion $\Delta t_D/\langle t_D \rangle$ is thus of the order of $1/\text{Log } N$, a finite value which will be evaluated more precisely below. The fact that this value is finite – and not negligibly small – means that the time of maximum emission appreciably fluctuates from one realization of the experiment to the next. If instead of measuring the emission delay, we now fix t and measure the size of the signal (number of emitted photons) at that time, it is clear that we should also observe important fluctuations and this justifies that the relative variance $\Delta s/\langle s \rangle$ is large (eq. (5.5)).

5.2. Fluctuation-less trajectories: The quasi-classical “probability packets”

The above analysis has shown that the quantum fluctuations exhibited by the superradiant emission originate from the early stages of the process (first terms in the development of eq. (5.9)), when the uncertainties associated to each emission step are still quite important. After a large absolute number of photons has been emitted, these uncertainties become quite small and add only a negligible contribution to Δt_D . Thus the fluctuations are expected to vanish almost completely if the system starts from a state in which many photons have already been emitted. In order to show this result, let us assume for the time being that, instead of starting from $M = J$, the system is initially prepared in a $|JM_0\rangle$ state, corresponding to a finite number $s_0 = J - M_0$ of emitted photons obeying the condition:

$$1 \ll s_0 \ll N \quad (5.10)$$

and let us consider the subsequent cascade emission from this state down. The new average delay:

$$t_D(s_0) \approx \frac{1}{N\Gamma} \left[\frac{1}{s_0} + \dots + \frac{1}{N} \right] \approx \frac{1}{N\Gamma} \log \frac{N}{s_0} \quad (5.11)$$

is not appreciably modified (since $\log N \gg \log s_0$), whereas the new delay dispersion:

$$\Delta t_D(s_0) = \frac{1}{N\Gamma} \left[\frac{1}{s_0^2} + \dots + \frac{1}{N^2} \right]^{1/2} \approx \frac{1}{N\Gamma} \times \frac{1}{s_0^{1/2}} \quad (5.12)$$

is reduced by a large absolute factor $s_0^{1/2}$. The relative delay dispersion $\Delta t_D/\langle t_D \rangle$ becomes very quickly negligibly small and hence, the relative variances $\Delta s/\langle s \rangle$ and $\Delta H_{\text{at}}/\langle H_{\text{at}} \rangle$ should also remain negligible. This result – shown here by qualitative arguments – can be demonstrated in a more rigorous way [13, 24, 28]. It means that the initial probability distribution, centered at time $t=0$ around $M=M_0$, propagates towards $M=-J$ without undergoing any important spreading. We call such a distribution a “quasi-classical” probability packet by analogy with the wave packets of ordinary wave mechanics. We should however notice that we are dealing here with superposition of positive probabilities (and not of complex amplitudes). These packets are “quasi-classical” because they do not spread and that H_{at} is decorrelated:

$$\langle H_{\text{at}}^2 \rangle \sim \langle H_{\text{at}} \rangle^2 \quad (5.13)$$

which can also be expressed as:

$$\langle (D_3)^2 \rangle \approx \langle D_3 \rangle^2. \quad (5.14)$$

As a consequence of this decorrelation, a measurement of D_3 at any time $t > 0$ will give a well defined fluctuation-less $\langle M(t) \rangle$ value and the probability distribution $\rho_M^{\text{cl}}(s_0, t)$ for the classical packet starting from $M_0 = J - s_0$ at time $t = 0$ can be written as:

$$\rho_M^{\text{cl}}(s_0, t) = \delta[M - \langle M(t) \rangle]. \quad (5.15)$$

In other words, the time evolution of such a quasi-classical probability packet is completely determined when one knows the motion $\langle M(t) \rangle$ of its center. This motion can be obtained from eqs. (4.7) and (5.1), which, taking into account the decorrelation condition (5.14), give immediately:

$$d\langle M(t) \rangle / dt = \Gamma[J + \langle M(t) \rangle] [J - \langle M(t) \rangle + 1]. \quad (5.16)$$

The solution of this equation starting from $M_0 = J - s_0$ at $t = 0$ is:

$$\langle M(t) \rangle = -\frac{N}{2} \tanh \frac{N\Gamma}{2} [t - t_D(s_0)] \quad (5.17)$$

with $t_D(s_0)$ being defined by eq. (5.11).

The solution (5.17) is known as the hyperbolic secant solution to the superradiance problem. Its time variation is represented on fig. 10a. Let us emphasize that it is valid *only* because the system is assumed to have started from a $s_0 = J - M_0 \gg 1$ value, so that the decorrelation hypothesis (5.14) is satisfied at all

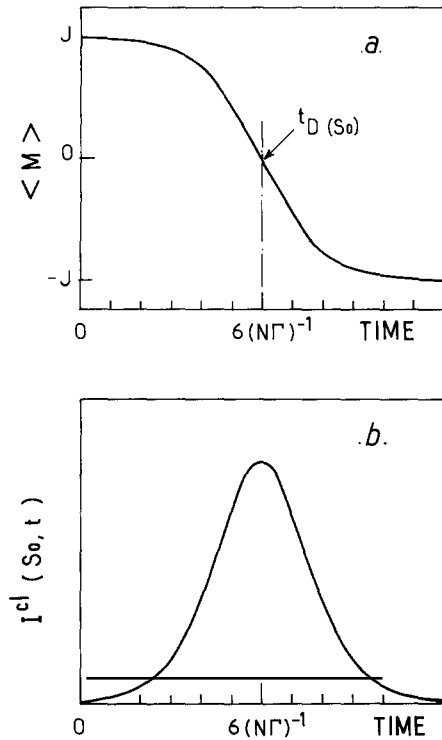


Fig. 10. (a) Time evolution of the center $\langle M(t) \rangle$ of the quasi-classical probability packet starting at time $t = 0$ from $\langle M(0) \rangle = J - s_0$ ($s_0 \ll J$ with $\log N/s_0 = 6$). (b) Time evolution of the corresponding radiated energy $I^{\text{cl}}(s_0, t) = -\hbar\omega_0 d\langle M(t) \rangle/dt$.

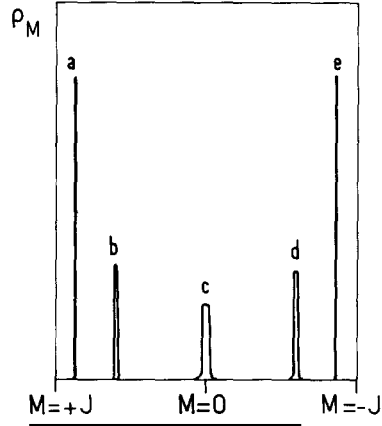


Fig. 11. The $\rho_M^{\text{cl}}(s_0, t)$ distribution corresponding to a system of $N = 2 \times 10^5$ atoms starting at time $t = 0$ from a $|J, M_0 = J - s_0\rangle$ state ($s_0 = 10^3$). Curves a, b, c, d and e correspond to times (in unit of $(N\Gamma)^{-1}$): $t = 9.56, 10.88, 12.20, 13.53$ and 14.86 . Note the big difference with the probability distributions obtained when the system starts from an initially totally inverted system (fig. 9).

times. The radiated energy along the quasi-classical trajectory starting from M_0 at time $t = 0$ is easily deduced from eq. (5.17):

$$I^{\text{cl}}(s_0, t) = -\hbar\omega_0 \frac{d\langle M(t) \rangle}{dt} = \frac{N^2 \hbar\omega_0 \Gamma}{2} \frac{1}{\cosh^2 \frac{1}{2} N\Gamma [t - t_D(s_0)]}. \quad (5.18)$$

Its time variation (see fig. 10b) is represented by a bell-shaped symmetrical function, centered around time $t = t_D(s_0)$, with a full width at half maximum:

$$T_W = 3.5(N\Gamma)^{-1}. \quad (5.19)$$

Knowing the $\langle M(t) \rangle$ evolution law, we know of course also the time evolution of the probability distribution $\rho_M^{\text{cl}}(s_0, t)$ given by eq. (5.15): this distribution remains at all times a quasi-delta-function fluctuation-less quantity whose position on the M -axis obeys the dynamical law of eq. (5.17). The $\rho_M^{\text{cl}}(s_0, t)$ distribution is represented at various times on fig. 11 for $s_0 = 1000$ and for $N = 200\,000$.

Note by comparison of figs. 9 and 11, the completely different behaviour of the superradiant system depending on its initial state at time $t = 0$. This comparison clearly shows that the large

fluctuations exhibited by the superradiant system *when it starts from* a totally inverted $|JJ\rangle$ state are generated at the early stage of the process, before a number of photons of the order of $s_0 \sim N/100$ to $N/1000$ has been emitted. If the system starts from an already correlated atomic state, even if it corresponds to a very small number of emitted photons, the initial quantum fluctuations are no longer effective and the evolution becomes entirely fluctuations-less (i.e. “classical”). This remark will allow us now to describe the evolution of the superradiant system by dividing it into an early quantum stage, where the vacuum fluctuations are essential, and a subsequent classical stage where these fluctuations have become negligible.

5.3. The initial quantum stage of superradiance

In the initial phase of the emission, when $s = J - M \ll N$, the exact equation (4.7) can be approximated by the linearized one:

$$\frac{d\rho_M}{dt} = -\Gamma N (s + 1) \rho_M + \Gamma N s \rho_{M-1}; \quad (s = J - M). \quad (5.20)$$

This equation admits the solution:

$$\rho_M^Q(t) = e^{-\Gamma N t} [1 - e^{-\Gamma N t}]^s. \quad (5.21)$$

The superscript Q in ρ_M^Q is here to recall that we now describe the solution valid at the early quantum stage of the process, corresponding to a system starting from a fully inverted state. As soon as t obeys the condition:

$$t > 1/N\Gamma \quad (5.22)$$

$e^{-\Gamma N t}$ becomes a small quantity and eq. (5.21) can be approximated by:

$$\rho_M^Q(t) = e^{-\Gamma N t} \exp[-s e^{-\Gamma N t}]. \quad (5.23)$$

This expression shows that ρ_M^Q is, at time t , an exponentially decaying distribution of $s = J - M$. At this time, the expectation value for s is:

$$\langle s \rangle = J - \langle M \rangle = \sum_s s \rho_M^Q(t) = e^{N\Gamma t} - 1 \quad (5.24)$$

and the s variance is:

$$\langle s^2 \rangle - \langle s \rangle^2 = e^{N\Gamma t} (e^{N\Gamma t} - 1). \quad (5.25)$$

Eq. (5.24) shows that the system starts to cascade down the ladder of fig. 4 with an exponentially increasing speed. Eq. (5.25) means that the uncertainty in the number of photons emitted at a given time is also increasing exponentially, the relative photon number variance becoming rapidly of the order of unity. These results are of course not surprising in view of the analysis developed in former subsections. This “early stage” solution is valid so long as $\langle s \rangle$ remains much smaller than N , i.e. for

times t such that:

$$t < \frac{1}{N} \log N. \quad (5.26)$$

Note that conditions (5.22) and (5.26) are compatible only if the absolute number of atoms is large, i.e. if:

$$\log N > 1 \quad (5.27)$$

is fulfilled, which is a necessary condition for the foregoing analysis to be valid.

5.4. The superradiance density matrix as a linear superposition of quasi-classical probabilities

Let us choose arbitrarily a time t_0 obeying conditions (5.22) and (5.26). Condition (5.26) means that, up to time t_0 , the linear quantum solution $\rho_M^Q(t)$ is valid. Condition (5.22) entails that at time t_0 , $\langle s \rangle$ is already large in absolute value, which implies that most of the $|JM\rangle$ states onto which the density matrix $\rho_M^Q(t_0)$ is expanded, correspond to $s = J - M$ values much larger than one. As a result, the subsequent evolution of these states for $t > t_0$ will, according to subsection 5.2, follow a classical fluctuation-less trajectory. The probability $\rho_M(t)$ can thus, for $t \geq t_0$, be written as:

$$\rho_M(t) = \sum_{s_0} \rho_{J-s_0}^Q(t_0) \cdot \rho_M^{\text{cl}}(s_0, t - t_0) \quad (5.28)$$

where $\rho_{J-s_0}^Q(t_0)$ and $\rho_M^{\text{cl}}(s_0, t - t_0)$ are given respectively by eqs. (5.23) and (5.15). Expression (5.28) branches continuously into $\rho_M^Q(t_0)$ for $t = t_0$ and is clearly a solution of the superradiant rate equation for $t > t_0$ since it is a superposition of classical trajectories obeying this equation. We have thus found a simple analytical expression for the density matrix of the atomic system valid *beyond* the early linear stage of the emission. This solution is correct only if the procedure of connecting the quantum and classical stages is possible, i.e. if a time t_0 simultaneously obeying conditions (5.22) and (5.26) does exist, which requires the presence of a large absolute number of atoms (condition (5.27)). Eq. (5.28) means that the probability of finding $s = J - M$ photons at time t is a sum of products of probabilities. The probability of finding s_0 photons at an early time t_0 has to be multiplied by the probability that this initial condition will yield $s = J - M$ photons at a later time, the system evolving from t_0 to t along a classical trajectory. One then has to sum over all possible intermediate s_0 values. Equation (5.28) can be replaced, since N is large, by a continuous integral. Replacing ρ^Q and ρ^{cl} by their expressions (5.23) and (5.15) and taking into account eq. (5.17), one finds:

$$\rho_M(t) = \int_0^{+\infty} e^{-\Gamma N t_0} \exp[-s_0 e^{-\Gamma N t_0}] \delta\left[M + \frac{N}{2} \text{th} \frac{N\Gamma}{2} [t - t_0 - t_D(s_0)]\right] ds_0. \quad (5.29)$$

Obviously, this expression should not depend upon the arbitrary time t_0 chosen to connect the “quantum” and “classical” stages. This can be checked by deriving the expression of ρ_M with respect to t_0 and verifying that $d\rho_M/dt_0 = 0$. One can thus formally set t_0 to zero in eq. (5.29) and write more

simply:

$$\rho_M(t) = \int_0^{+\infty} \exp(-s_0) \cdot \delta\left[M + \frac{N}{2} \operatorname{th} \frac{N\Gamma}{2} (t - t_D(s_0))\right] ds_0 \quad (5.30)$$

which shows that the density matrix of the superradiant system is a superposition of classical trajectories with a distribution of initial s_0 values obeying an exponential probability law. It is often convenient to use this expression for ρ_M . If one needs an explicit formula, it is also easy to perform the s_0 integration in (5.30). It implies finding the root \bar{s}_0 of the equation:

$$f(\bar{s}_0) = M + \frac{N}{2} \operatorname{th} \frac{N\Gamma}{2} [t - t_D(\bar{s}_0)] = 0 \quad (5.31)$$

which yields:

$$\bar{s}_0 = N \frac{N - 2M}{N + 2M} e^{-\Gamma N t} \quad (5.32)$$

and replacing the Dirac distribution in eq. (5.30) by $[f'(\bar{s}_0)]^{-1} \delta[s_0 - \bar{s}_0]$. One finally gets [13]:

$$\rho_M(t) = [f'(\bar{s}_0)]^{-1} e^{-\bar{s}_0} = \frac{4N^2}{(N + 2M)^2} e^{-\Gamma N t} \exp\left\{-\frac{N(N - 2M)}{N + 2M} e^{-\Gamma N t}\right\}. \quad (5.33)$$

We have thus obtained a compact analytical expression for $\rho_M(t)$, asymptotically valid for $\log N > 1$, which describes all the quantum fluctuations of the superradiant evolution: when plotted as a function of M for various times t , $\rho_M(t)$ given by eq. (5.33) does coincide remarkably well with the computer solution (fig. 9) as soon as N is larger than a few tens of atoms.

5.5. Physical discussion: The quantum fluctuations of the small sample superradiant system

Once $\rho_M(t)$ is known, the expectation value of the atomic energy, or of the radiated intensity, are readily deduced. For example, one has:

$$\langle I(t) \rangle = \int_0^{+\infty} \exp(-s_0) I^{\text{cl}}(s_0, t) ds_0 \quad (5.34)$$

where $I^{\text{cl}}(s_0, t)$ is the hyperbolic secant solution with delay $t_D(s_0)$ associated with the classical trajectory starting from state $|J; M = J - s_0\rangle$ at time $t = 0$. $\langle I(t) \rangle$ thus appears as a linear superposition of identical bell-shaped pulses with variable delays $t_D(s_0)$. $\langle I(t) \rangle$ has in consequence a somewhat larger width and a smaller peak value ($\langle I_{\max} \rangle < N^2 \hbar \omega_0 \Gamma / 4$) than each fluctuation-less classical solution (see fig. 12).

The above summation procedure has a deep physical meaning, closely related to the quantum mechanical theory of measurement. The expectation value $\langle I(t) \rangle$ is the ensemble average of a large number of “single shot” signals, all measured on identical systems. (In the same way, the well-known

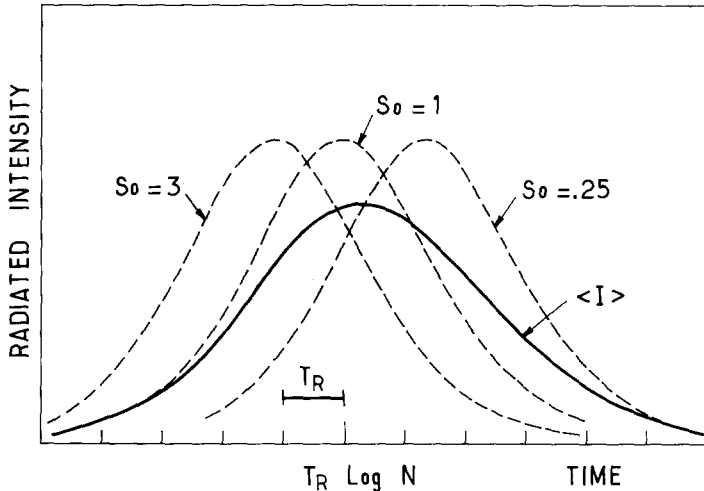


Fig. 12. Time-variation of the average radiated intensity $\langle I(t) \rangle$ of a small sample symmetrical superradiant system (full line). In dashed lines; quasi-classical solutions $I^{cl}(s_0, t)$ corresponding to $s_0 = 0.25, 1$ and 3 .

one atom decay exponential curve is obtained as an average over a large number of single photon detection events.) The time dependence of each “single shot” signal is not $\langle I(t) \rangle$ but precisely $I^{cl}(s_0, t)$. The measurement procedure itself involves indeed a reduction of the probability distribution which, at some early time t_0 , is transformed into a narrow probability packet. The center of this packet can be extrapolated back at time $t = 0$ to the “initial” position s_0 . The evolution of this packet at times $t > t_0$ occurs along the trajectory corresponding to $I^{cl}(s_0, t)$. The single-shot signals are thus – for this small symmetrical sample case – pure hyperbolic secant signals. Equation (5.34) merely states that the expectation value $\langle I(t) \rangle$ results from the average of these signals. It is then very easy to obtain a quantitative expression for the shot to shot delay fluctuations which depend only upon the $\exp(-s_0)$ distribution. The probability $P(t_D) dt_D$ that the delay in a single shot measure is comprised between t_D and $t_D + dt_D$ merely is:

$$P(t_D) dt_D = e^{-s_0} ds_0 \quad (5.35)$$

where s_0 is connected to t_D by relation (5.11). After a straightforward calculation, one finds:

$$P(t_D) = N^2 \Gamma e^{-NT_D} \exp[-N e^{-NT_D}] \quad (5.36)$$

The $P(t_D)$ distribution is represented on fig. 13. It presents a maximum for $\bar{t}_D = [N\Gamma]^{-1} \log N$, which is in fact very close to the average delay $\langle t_D \rangle$ (the $P(t_D)$ distribution is practically symmetrical):

$$\langle t_D \rangle = \frac{1}{N\Gamma} \log N \quad (5.37)$$

The relative variance (average delay dispersion) is:

$$\frac{\Delta t_D}{\langle t_D \rangle} = \frac{\sqrt{\langle t_D^2 \rangle - \langle t_D \rangle^2}}{\langle t_D \rangle} = \frac{1.3}{\log N} \quad (5.38)$$

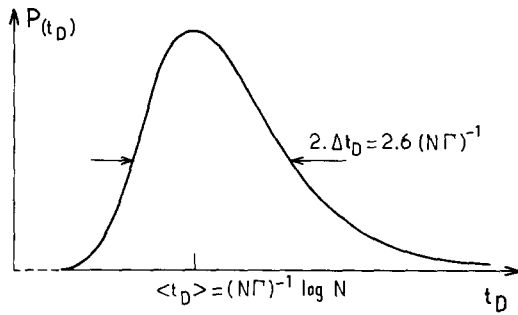


Fig. 13. Probability distribution law $P(t_D)$ for the delay of the superradiant pulse (small sample symmetrical superradiant system).

These exact results are in very good agreement with the values predicted above by qualitative arguments (section 5.1).

6. Large sample superradiance

The ideal superradiance case analysed in the previous section is very difficult to realize in a practical experiment since it involves preparing a large number of excited atoms in a regular pattern within a sample smaller than λ . The regular atomic configuration, which is an essential ingredient to avoid dephasing Van der Waals interactions, is especially hard to achieve. A way of relaxing this requirement for “configuration regularity” could be to place the small sample medium in a resonant cavity [71]. The resonant enhancement due to the cavity finesse permits to achieve superradiance at much lower atomic density than in free space, making the Van der Waals dephasing negligible.* Although the equations describing atomic emission in a cavity are formally identical to the one corresponding to small sample superradiance [9, 71], the physical situation corresponding to the emission in the presence of the cavity walls is different from the case of superradiant emission in free space and we will not discuss it in detail here. We will rather discuss in this section the case of superradiant emission by samples having a volume with linear dimensions much larger than λ . This is the situation realized in most superradiance experiments so far. We will show that the dynamics of the system evolution is in this case qualitatively similar to the one discussed in the previous sections, with some quantitative differences though due to effects connected with the propagation of the electromagnetic field along the emitting sample.

6.1. General considerations concerning propagation and diffraction effects in a large superradiant sample: The pencil-shaped sample case

The general equations (3.18) and (3.27), (3.29), (3.30) represent a formulation of the superradiance problem valid for any shape or size of the atomic sample. They appear however in general extremely

* It might at first sight seem strange that the presence of a resonant cavity can change the relative importance of the real and imaginary parts of the same interatomic coupling. In fact, the introduction of a resonant cavity amounts to concentrate the mode frequency distribution into a spectrum made of narrow peaks, including the resonant frequency k_0 . The contribution to the cooperative decay rate (which involves a product of this spectrum by $\delta(k - k_0)$) is enhanced, whereas the contribution to the Van der Waals dephasing (which is proportional to the integral of the product of the spectrum by the wide $1/(k - k_0)$ distribution) is not modified (intermode separation c/L small compared to c/λ). Physically, it is obvious that the presence of “images” induced in the cavity walls at distance much larger than λ cannot significantly affect the $1/r^3$ Van der Waals interaction.

intricate since they involve a summation over all atoms and – explicitly or implicitly – over all electromagnetic field modes. We have seen in section 4 that the summation over all the modes, even those non-resonant with the atomic transition, are essential to describe such effects as the dipole–dipole $1/r^3$ electrostatic coupling which breaks the symmetry of the system evolution. For a large sample, most pairs of atoms with $i \neq j$ lie at a mutual distance $r_{ij} \gg \lambda$ and the summation over \mathbf{k} vectors, with $|\mathbf{k}|$ much different from $|\mathbf{k}_0|$, leads then to negligible effects (no appreciable Van der Waals dephasing). Even restricted to modes with $|\mathbf{k}|$ close to $|\mathbf{k}_0|$, the summation over field modes remains however very difficult to perform since it involves a priori all directions of \mathbf{k} vectors. The summations over atom pairs and over \mathbf{k} are furthermore not really independent from each other since one knows from diffraction laws that the modes of the field to which an ensemble of radiators is effectively coupled depends upon the shape and size of the radiator pattern. Moreover, the various modes are coupled to the atoms in a non-linear way, which leads to intricate mode coupling effects. In other words, the problem of superradiance in free space is in general a problem of three-dimensional non-linear diffraction theory, further complicated by the quantum nature of the radiated field at the early stage of the emission process.

An important step in the simplification of this problem is to choose for the sample the shape of a long cylinder of length L and transverse dimension $2w$ obeying the relation:

$$L \gg w \gg \lambda . \quad (6.1)$$

This is the so-called pencil-shaped sample case, which has been realized in most experiments so far: it is indeed the “natural shape” for a superradiant medium prepared by a pulsed pumping laser beam acting in a three-level atomic structure (see fig. 2). If the laser beam has a waist $w \gg \lambda$ and intersects an atomic beam of diameter $L \gg w$, or crosses a resonant cell of length L , a cylindrical sample satisfying condition (6.1) is automatically prepared (see fig. 14a). An alternative method for preparing such a cylindrical sample is to excite a collimated atomic beam with an expanded laser beam perpendicular to the atomic beam (see fig. 14b). (These two configurations will be respectively referred to as “longitudinal” and “transverse” superradiance pumping.) It is clear that the field radiated by such a sample will essentially expand along modes with wave-vectors \mathbf{k} pointing within two small cones whose axes are defined by the cylinder longest dimension (which we call the Oz axis). This approximation amounts to neglecting spontaneous emission in off-axis direction as compared to the “cooperative emission” along the Oz axis. This is legitimate only if the number of atoms is large enough (see section 6.5). If this condition is fulfilled, it is natural to expect a physical situation where the radiated field will essentially vary along Oz, with negligible variation along the transverse Ox and Oy directions, which amounts to considering superradiance as being essentially a one-dimensional problem. When looked at more carefully, the situation is somewhat more complicated and the description of superradiance appears to depend upon the Fresnel number:

$$F = \pi w^2 / L \lambda \quad (6.2)$$

of the emitting cylinder, and to change in character whether F is larger or smaller than unity. If $F > 1$, the diffraction of each mode propagating close to the cylinder axis occurs in a small diffraction angle $\theta_D = \lambda/w$, but on the other hand the emission supports off-axial modes within the geometrical angle $\theta_G = w/L > \theta_D$ (see fig. 15a). As a result, if the superradiant process were linear (without mode coupling

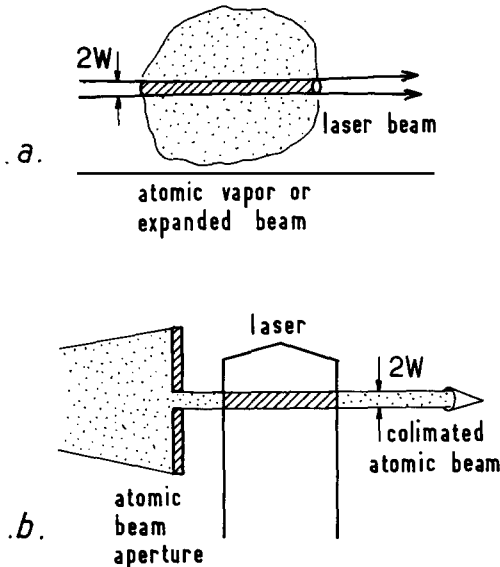


Fig. 14. Two pumping configurations defining a pencil-shaped superradiant sample (shaded area on figures): (a) longitudinal pumping, (b) transverse pumping.

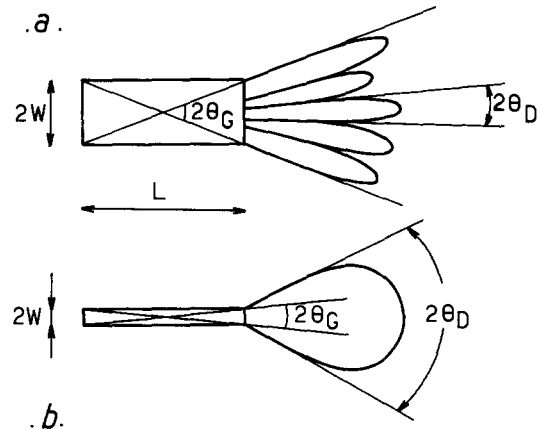


Fig. 15. Schematic representation of the transverse variation of the superradiant field emitted by a pencil-shaped sample, depending upon the Fresnel number: (a) Large Fresnel number ($F \gg 1$): several diffraction limited modes can be sustained within the geometrical angle $\theta_G = w/L$ of the medium. The transverse field variations mainly account for the existence of numerous off-axis modes. (b) Small Fresnel number ($F \ll 1$): a single mode can be sustained by the emission, but it strongly diverges in transverse directions due to diffraction: the transverse field variations mainly describe diffraction effects.

effects), one would expect an emission occurring in $F > 1$ independent “coherence areas”. The transverse variations of the field cannot be neglected if one wants to describe accurately this multiple coherence area structure. If on the other hand $F < 1$, the emission essentially occurs in a single coherence area, but the single mode presents a strong diffraction pattern (see fig. 15b) leading again to an important radial dependance of the emitted field. In other words, for $F < 1$ as well as for $F > 1$, superradiance always remains, strictly speaking, a three-dimensional problem with field varying along the cylinder axis *and* transverse directions as well. The best “compromise” case for which one can expect to have a radiation process not too different from a “one-dimensional” problem is the one corresponding to:

$$F = \pi w^2 / L \lambda \approx 1. \quad (6.3)$$

This choice – resulting from a trade-off between too much off-axis emission and too much diffraction – does not define of course a strictly one-dimensional problem. It is however safe to assume that it should allow us to describe qualitatively the effects of propagation along the superradiant sample within a one-dimensional approximation, the complications due to the transverse variation of the field being not essential ones.

Even if one assumes uni-dimensionality, a last complication arises from the fact that the emission can equally occur in two opposite directions along the cylinder axis. A further simplification amounts to considering the emission along one (arbitrary) direction alone. This again is of course not strictly speaking justified since both emission directions are equivalent. This simplification is shown however

not very much to modify the results obtained when taking into account propagation in both directions as will be discussed at the end of this section. Since it considerably simplifies the analysis, we will make this simplification throughout most of this study.

To summarize this discussion, the simplest assumption that can be made to describe the superradiant emission of a long pencil-shaped sample oriented along the Oz axis, is to consider that the emitted field propagates along a single direction (the positive Oz direction), with negligible transverse field variations. As a consequence, the atomic medium is supposed to be invariant in each plane perpendicular to the cylinder axis. These hypotheses, which are strictly speaking inconsistent with diffraction laws, should allow us however to qualitatively describe the propagation of the emitted field along the cylinder axis. Propagation along Oz makes the radiation field at any given time different at various points along this axis. As a result, the evolution of the atom at various points is no longer identical, in contrast with the small-regular shaped superradiance sample case where all atoms undergo the same evolution. Thus propagation effects, even restricted to one dimension, are expected to break in an essential way the symmetry of the simple superradiant problem described in section 5. This symmetry breaking effect is the fundamental new feature appearing in large sample superradiance. It is thus convenient, in a first stage, to discuss this one-dimensional model of superradiance, even if it is not completely realistic. We will see indeed that it lends itself to a simple discussion with analytical solutions, which is not the case of the three-dimensional superradiance problem which can be studied only by lengthy numerical computation. This is the reason why we will first analyse the one-dimensional model of superradiance, leaving the description of three-dimensional superradiance to subsection 6.4.

6.2. Superradiance equations in the one-dimensional propagation approximation

The evolution of the $F \sim 1$ pencil-shaped sample superradiance can be described either in the Schrödinger or in the Heisenberg point of view. Since the system does not evolve anymore in a small symmetrical subspace of the Hilbert space, the Schrödinger description is, according to the discussion of section 3, less convenient than the Heisenberg one. We thus carry most of the analysis in this section in the more economical Heisenberg point of view. However, in order to stress the basic equivalence of the two descriptions and to make the connection with the analysis of previous sections, we choose to start this study by presenting in this subsection the superradiance equation in both points of view.

6.2.1. Schrödinger point of view

The starting point for the derivation of the one-dimensional model superradiance master equation is the general equation (3.18). Following the arguments of section 6.1, we restrict the summation over Ω to a small solid angle $\Omega_0 \sim \lambda^2/w^2$. This amounts to replacing the Ω integral in (3.18) by Ω_0 . Next, we replace the three-dimensional complex exponential $\exp\{ik(\mathbf{r}_i - \mathbf{r}_j)\}$ by a one-dimensional $\exp\{ik(z_i - z_j)\}$ phase factor ($k = \omega/c$ being the length of the \mathbf{k} vector). This replacement, which is not rigorous, is the essential step of the one-dimensional approximation discussed above. Writing the $\exp(-iH_j\tau/\hbar) D_j \exp(iH_j\tau/\hbar)$ term in eq. (3.18) as $\exp(ick_0\tau) D_j^- + \exp(-ick_0\tau) D_j^+$ ($k_0 = \omega_0/c$), we obtain the following one-dimensional model master equation:

$$\begin{aligned} \frac{d\rho}{dt} = & \frac{1}{i\hbar} \left[\sum_j H_j \rho \right] - \frac{cd^2\Omega_0}{16\varepsilon_0\pi^3\hbar} \sum_{i,j} \int_0^{+\infty} \int_0^{+\infty} d\tau dk k^3 \exp\{i[k(z_i - z_j) - ck\tau]\} \\ & \times \{D_i(\exp(ick_0\tau) D_j^- + \exp(-ick_0\tau) D_j^+) \rho - (\exp(ick_0\tau) D_j^- + \exp(-ick_0\tau) D_j^+) \rho D_i\} \\ & + \text{hermitian conjugate of the integral.} \end{aligned} \quad (6.4)$$

The τ -integral in eq. (6.4) appears as the Fourier transform of the step function $\theta(\tau)$ for the values $k_0 - k$ and $k_0 + k$, according to eq. (4.2).

Among the off-resonant contribution ($k \neq k_0$, Cauchy principal part in eq. (4.2)), it is convenient to distinguish quasi-resonant terms such that:

$$|k - k_0| \ll k_0 , \quad (6.5)$$

from the far-off resonant ones:

$$|k - k_0| \geq k_0 . \quad (6.6)$$

The latter ones essentially describe the dispersive force between very close atoms ($r_{ij} \sim \lambda$). Neglecting them is justified since most pairs of atoms obey the condition $|z_i - z_j| \gg \lambda$ and since we are interested here in collective effects between atoms lying at mutual distances of the order of $L \gg \lambda$. We can thus neglect the k variation in the integral (6.4) and replace k^3 by k_0^3 . Eq. (6.4) becomes:

$$\begin{aligned} \frac{d\rho}{dt} = & \frac{1}{i\hbar} \left[\sum_j H_j, \rho \right] - \frac{3\Gamma\Omega_0}{16\pi^2} \sum_{ij} \exp\{ik_0(z_i - z_j)\} \int_0^{+\infty} \left(\pi\delta(k_0 - k) + i \text{PP} \frac{1}{k_0 - k} \right) \\ & \times \exp\{i(k - k_0)(z_i - z_j)\} dk \{D_i^+ D_j^- \rho - D_j^- \rho D_i^+\} + \text{hermitian conjugate of the integral} \end{aligned} \quad (6.7)$$

(in order to get this equation, we have also performed the secular approximation consisting in neglecting contributions of the form $D_i^- D_j^- \rho$ and $D_j^- \rho D_i^-$).* We now finally remark:

(i) That the $i = j$ term in eq. (6.7) describes the “incoherent part” of the emission, corresponding to the contribution of independent atom emission. The real part of the $i = j$ term is associated to the radiative decay of independently emitting atoms. The imaginary part of the $i = j$ term is the contribution to the Lamb-shift of the axial $k \simeq k_0$ modes which can be reintroduced in the H_j 's as a renormalization of ω_0 .

(ii) That, since only $k \sim k_0$ values contribute to a typical $i \neq j$ integral, we can as well extend the lower bound of the integral to $-\infty$. The k integral then yields a $\theta(z_i - z_j)$ step function. This step function being equal to zero if $z_i < z_j$, it is convenient to express it by ordering the atoms according to increasing z 's and to restrict the sum over pairs of atoms such that $i > j$. Taking these remarks into account and introducing new “phase matched” dipole operators as:

$$D_{k_0 i}^\pm = \exp(\pm ik_0 z_i) D_i^\pm \quad (6.8)$$

* Let us remark that this “rotating wave approximation” is valid only because we neglect here the contribution of the off-resonant processes with $k - k_0 > L/c$. The non-secular term *should* be kept to describe correctly the local dipole-dipole coupling as discussed in refs. [19, 21, 22] and in section 4 of this review.

one finally obtains a one-dimensional superradiance master equation which takes into account the coherent ($i \neq j$) as well as the incoherent ($i = j$) contributions to the emission:

$$\frac{d\rho}{dt} = \frac{1}{i\hbar} \left[\sum_j H_j, \rho \right] - \Gamma\mu \sum'_{i \geq j} \{ D_{k_0i}^+ D_{k_0j}^- \rho + \rho D_{k_0j}^+ D_{k_0i}^- - D_{k_0i}^- \rho D_{k_0j}^+ - D_{k_0j}^- \rho D_{k_0i}^+ \} \quad (6.9)$$

where

$$\mu = \frac{3\Omega_0}{8\pi} \quad (6.10)$$

and $\sum'_{i \geq j}$ means that the summation is restricted to $i \geq j$ terms, with the “incoherent” $i = j$ terms being divided by two.

Equation (6.9) has been first derived in ref. [39]. Its physical interpretation is quite clear. The occurrence of the geometrical factor μ , proportional to the diffraction solid angle of the pencil-shaped volume, amounts to reducing the spontaneous emission rate Γ to a value $\Gamma\mu \ll \Gamma$. Only the photons spontaneously emitted in the diffraction angle of the sample are indeed “useful” to start the superradiant emission process in the “end-fire” mode of the emitting sample. The $i > j$ restriction in the summation over the atom couples clearly describes the effects of propagation. For example, the $D_{k_0i}^+ D_{k_0j}^-$ operators in the right-hand side of eq. (6.9) correspond to emission of a photon by atom j followed by its reabsorption by atom i . The $i > j$ condition merely expresses the fact that this photon is propagating from left to right in the sample. It is worth noticing, after ref. [39], that these propagation effects directly come from the imaginary dispersive term in eq. (6.7), which are necessary in order to introduce the $\theta(z_i - z_j)$ step function. In this imaginary dispersive term, we have seen that it is the contribution of the quasi-resonant processes, with k obeying condition (6.6), which are essential. Dismissing these terms as irrelevant “collective Lamb-shifts”, as it has sometimes been done, amounts to lose completely all the propagation effects in the superradiant sample (see subsection 6.2.4 below).

6.2.2. Heisenberg point of view

In order to describe the pencil-shaped sample superradiance in the Heisenberg picture, we start now from eqs. (3.27), (3.29), (3.30) and assume that the radiated field operator \mathbf{E}^{rad} and the atomic polarization field $\mathbf{P}(r, t)$ can be expressed as products of a fast varying exponential (with time and space frequencies ω_0 and k_0) by “slow varying” envelope operators $\mathcal{E}(z, t)$ and $\mathcal{P}(z, t)$, according to the relations:

$$\mathbf{E}^{\pm\text{rad}} = \mathcal{E}^\pm(z, t) \exp\{\mp i(\omega_0 t - k_0 z)\} \boldsymbol{\epsilon}_a \quad (6.11)$$

$$\mathbf{P}^\pm(r, t) = \mathcal{P}^\pm(z, t) \exp\{\pm i(\omega_0 t - k_0 z)\} \boldsymbol{\epsilon}_a. \quad (6.12)$$

\mathcal{E} and \mathcal{P} are supposed to vary in time over periods much longer than ω_0^{-1} and in space over periods much larger than $k_0^{-1} = \lambda_0/2\pi$. Eqs. (6.11) and (6.12), in which we disregard transverse field variations, express in a very simple way the main assumption of the one-dimensional model of superradiance discussed in subsection 6.1.

Replacing in eqs. (3.27), (3.29) and (3.30) \mathbf{E}^{rad} and \mathbf{P} by their expressions (6.11), (6.12) and neglecting $\partial\mathcal{E}/\partial t$ and $\partial\mathcal{P}/\partial t$ when compared to $\omega_0\mathcal{E}$, or $\omega_0\mathcal{P}$ and $\partial\mathcal{E}/\partial z$ when compared to $k_0\mathcal{E}$, one gets (after

dropping fast oscillating terms) the following Bloch–Maxwell equations for the atom and field envelope operators [30, 40]:

$$\left\{ \begin{array}{l} \frac{\partial \mathcal{N}}{\partial t} = \frac{i}{\hbar} [\mathcal{P}^+ \mathcal{E}^+ - \mathcal{E}^- \mathcal{P}^-] \\ \frac{\partial \mathcal{P}^+}{\partial t} = \frac{2id^2}{\hbar} \mathcal{E}^- \mathcal{N} \end{array} \right. \quad (6.13)$$

$$\left\{ \begin{array}{l} \frac{\partial \mathcal{P}^+}{\partial t} = \frac{2id^2}{\hbar} \mathcal{E}^- \mathcal{N} \end{array} \right. \quad (6.14)$$

$$\left(\frac{1}{c} \frac{\partial}{\partial t} + \frac{\partial}{\partial z} \right) \mathcal{E}^+ = \frac{i\omega_0}{2\varepsilon_0 c} \mathcal{P}^- . \quad (6.15)$$

(Note the normal ordering of the operators in eqs. (6.13) and (6.14).)

Eqs. (6.13) to (6.15) describe superradiance for the one-dimensional model in the Heisenberg point of view. These equations are derived more easily than the corresponding equations in the Schrödinger picture, which illustrates the greater simplicity of the Heisenberg picture for the description of superradiance in the large sample case.

The first two equations (6.13) and (6.14) describe the atoms evolution in the presence of the field envelope $\mathcal{E}(z)$. The last one (eq. (6.15)) describes the propagation of the e.m. field along the Oz axis in the presence of the atomic polarization acting as a source term. It is worth noticing that these equations take a simpler form if one replaces the variables z and t by z and the retarded time $\tau = t - z/c$. Expressing the fields as functions of these new variables, one gets the following equations:

$$\left\{ \begin{array}{l} \frac{\partial \mathcal{N}}{\partial \tau} = \frac{i}{\hbar} [\mathcal{P}^+ \mathcal{E}^+ - \mathcal{E}^- \mathcal{P}^-] ; \quad \frac{\partial \mathcal{P}^+}{\partial \tau} = \frac{2id^2}{\hbar} \mathcal{E}^- \mathcal{N} \end{array} \right. \quad (6.16)$$

$$\left\{ \begin{array}{l} \frac{\partial}{\partial z} \mathcal{E}^+ = \frac{i\omega_0}{2\varepsilon_0 c} \mathcal{P}^- . \end{array} \right. \quad (6.17)$$

The Maxwell equation (6.17) is then readily integrated along the medium to yield inside the sample ($0 < z < L$):

$$\mathcal{E}^+(z, \tau) = \frac{i\omega_0}{2\varepsilon_0 c} \int_0^z \mathcal{P}^-(z', \tau) dz' . \quad (6.18)$$

Again, we note that the system evolution at point z depends only on what happens for $z' < z$, which clearly describes the effect of field propagation in the positive Oz direction.

Let us stress that the slow varying envelope approximation is justified only insofar as the time and space characteristic variation lengths of the envelope \mathcal{E} and \mathcal{P} are very small within ω_0^{-1} and k_0^{-1} . Since the envelope varies over characteristic time $1/N\Gamma\mu$ (see below) and characteristic length L , the one-dimensional equations described here are valid only if the conditions:

$$1/N\Gamma\mu < 1/\omega_0 \quad (6.19)$$

and

$$L > \lambda \quad (6.20)$$

are satisfied. If, moreover, one has:

$$L/c < 1/N\Gamma\mu \quad (6.21)$$

which is known as the Arecchi–Courtens condition [5], one can disregard in eq. (6.16) the difference between t and $\tau - z/c$ and merely replace τ by t in these equations.

6.2.3. Equivalence between the Schrödinger and Heisenberg points of view

Although they may look rather different, eqs. (6.9) and (6.16), (6.17), which respectively describe one-dimensional superradiance in the Schrödinger and Heisenberg pictures, are strictly equivalent when the Arecchi–Courtens condition (6.21) is fulfilled.

In order to show this result, one has merely to express $\mathcal{N}(z, \tau)$ and $\mathcal{P}^\pm(z, \tau)$ in terms of the $D_{k_0 i}^+$ and D_i^3 operators as:

$$\mathcal{N} = \frac{1}{\pi w^2} \sum_i D_i^3 \delta_e(z - z_i) \quad (6.22)$$

$$\mathcal{P}^\pm(z, \tau) = \frac{d}{\pi w^2} \sum_i D_{k_0 i}^\pm e^{\mp i\omega_0 \tau} \delta_e(z - z_i). \quad (6.23)$$

Eliminating from the Bloch equations the electric field operator through equation (6.18) and replacing \mathcal{N} and \mathcal{P} by their expansions (6.22) and (6.23), one readily obtains the following evolution equations for the D_{k_0} operators:

$$\left\{ \begin{array}{l} \frac{d}{d\tau} D_{k_0 i}^+ = i\omega_0 D_{k_0 i}^+ + 2\Gamma\mu \sum_{i \geq j}' D_{k_0 j}^+ D_i^3 \\ \frac{d}{d\tau} D_i^3 = -\Gamma\mu \sum_{i \geq j}' (D_{k_0 j}^+ D_{k_0 i}^- + D_{k_0 j}^- D_{k_0 i}^+) \end{array} \right. \quad (6.24)$$

$$\left\{ \begin{array}{l} \frac{d}{d\tau} D_{k_0 i}^+ = i\omega_0 D_{k_0 i}^+ + 2\Gamma\mu \sum_{i \geq j}' D_{k_0 j}^+ D_i^3 \\ \frac{d}{d\tau} D_i^3 = -\Gamma\mu \sum_{i \geq j}' (D_{k_0 j}^+ D_{k_0 i}^- + D_{k_0 j}^- D_{k_0 i}^+) \end{array} \right. \quad (6.25)$$

where μ is defined as

$$\mu = \frac{3}{8\pi^2} \frac{\lambda^2}{w^2} \quad (6.26)$$

which is consistent with eq. (6.10) provided $\Omega_0 = \lambda^2/\pi w^2$.

If, on the other hand, one adopts the Schrödinger picture, one derives quite similar equations for the expectation values of the D_i 's operators. Starting from:

$$\frac{d}{dt} \langle D_i \rangle = \frac{d}{dt} \text{Tr}(D_i \rho) = \text{Tr}\left(D_i \frac{d\rho}{dt}\right)$$

and expressing $d\rho/dt$ by eq. (6.9), one gets after a straightforward commutation algebra:

$$\left\{ \begin{array}{l} \frac{d}{dt} \langle D_{k_0 i}^+ \rangle = i\omega_0 \langle D_{k_0 i}^+ \rangle + 2\Gamma\mu \sum_{i \geq j}' \langle D_{k_0 j}^+ D_i^3 \rangle \\ \frac{d}{dt} \langle D_i^3 \rangle = -\Gamma\mu \sum_{i \geq j}' \langle D_{k_0 j}^+ D_{k_0 i}^- + D_{k_0 j}^- D_{k_0 i}^+ \rangle \end{array} \right. \quad (6.27)$$

$$\left\{ \begin{array}{l} \frac{d}{dt} \langle D_{k_0 i}^+ \rangle = i\omega_0 \langle D_{k_0 i}^+ \rangle + 2\Gamma\mu \sum_{i \geq j}' \langle D_{k_0 j}^+ D_i^3 \rangle \\ \frac{d}{dt} \langle D_i^3 \rangle = -\Gamma\mu \sum_{i \geq j}' \langle D_{k_0 j}^+ D_{k_0 i}^- + D_{k_0 j}^- D_{k_0 i}^+ \rangle \end{array} \right. \quad (6.28)$$

which could have been directly deduced from eqs. (6.24) and (6.25), provided one could replace τ by t : in other words, the Schrödinger and the Heisenberg pictures are completely equivalent for the description of the evolution of the atomic polarization (and electric field), if one can neglect the difference between t and $t - z/c$. This is not surprising, since the Schrödinger equations have been obtained under the assumption that the propagation time L/c along the sample is completely negligible when compared to the system evolution time (Born–Markov condition). If this assumption is valid, τ and t are practically identical and the two points of view equivalent. If it is no longer valid, eq. (6.9) does not hold anymore and we do not know how to describe the atomic system by a density matrix defined at a single time (see section 7).

6.2.4. Remark: Averaging the electric field in the superradiance sample: the “mean-field” model [9, 11]

Equations (6.9) and (6.16), (6.17) can further be simplified if one gives up the description of propagation effects and relaxes the $i \geq j$ or $z > z'$ condition. One then gets evolution equations in which all atoms play an identical role, i.e. one recovers the symmetry and simplicity of the small sample superradiance problem. In the Schrödinger picture, this is achieved by merely replacing the $\sum_{i \geq j}$ sum in eq. (6.9) by $\frac{1}{2}\Sigma_{i,j}$. This equation then reads:

$$\frac{d\rho}{dt} = \frac{1}{i\hbar} \left[\sum_j H_j, \rho \right] - \frac{\Gamma\mu}{2} \left[D_{k_0}^+ D_{k_0}^-, \rho \right]_+ + \Gamma\mu D_{k_0}^- \rho D_{k_0}^+ \quad (6.29)$$

the $D_{k_0}^+$, $D_{k_0}^-$ being the collective phase-matched operators defined as:

$$D_{k_0}^\pm = \sum_i D_{k_0i}^\pm. \quad (6.30)$$

In the Heisenberg picture, the same result is achieved by computing an “average field” inside the sample as:

$$\bar{\mathcal{E}}^+(\tau) = \frac{i\omega_0}{4\epsilon_0 c} \int_{-L/2}^{L/2} \mathcal{P}^-(z', \tau) dz' \quad (6.31)$$

and by replacing in the Bloch–Maxwell equations the \mathcal{E} , \mathcal{N} and \mathcal{P} operators by their averages $\bar{\mathcal{N}}$, $\bar{\mathcal{P}}$ and $\bar{\mathcal{E}}$. One then gets:

$$\left\{ \begin{array}{l} \frac{\partial \bar{\mathcal{N}}}{\partial \tau} = \frac{i}{\hbar} [\bar{\mathcal{P}}^+ \bar{\mathcal{E}}^+ - \bar{\mathcal{E}}^- \bar{\mathcal{P}}^-]; \\ \frac{\partial \bar{\mathcal{P}}^+}{\partial \tau} = \frac{2id^2}{\hbar} \bar{\mathcal{E}}^- \bar{\mathcal{N}} \end{array} \right. \quad (6.32)$$

$$\bar{\mathcal{E}}^+ = \frac{i\omega_0}{4\epsilon_0 c} L \bar{\mathcal{P}}^-. \quad (6.33)$$

After eliminating the electric field in eq. (6.32) and expressing $\bar{\mathcal{N}}$ and $\bar{\mathcal{P}}$ in terms of the $D_{k_0}^\pm$ operators as:

$$\left\{ \begin{array}{l} \bar{\mathcal{N}} = \frac{1}{\pi L w^2} \sum_i D_i^3 = \frac{1}{\pi L w^2} D^3 \end{array} \right. \quad (6.34)$$

$$\bar{\mathcal{P}}^\pm = \frac{d}{\pi L w^2} e^{\mp i\omega_0 \tau} D_{k_0}^\pm, \quad (6.35)$$

one equivalently gets:

$$\frac{dD_{k_0}^+}{d\tau} = i\omega_0 D_{k_0}^+ + \Gamma\mu D_{k_0}^+ D^3; \quad dD_3/d\tau = -\Gamma\mu D_{k_0}^+ D_{k_0}^- . \quad (6.36)$$

Clearly, equations (6.29) and (6.36) are equivalent if condition (6.21) is fulfilled. They represent what is called, for obvious reasons, the “mean-field” model of large sample superradiance. It is important to stress that this model, which overlooks propagation and the field non-uniformity which it induces in the sample, is not justified by any physical approximation and that its only merit is the simplicity and symmetry of the equations. Since the $D_{k_0}^\pm$ and D_3 operators obey the general angular momentum commutation laws, the density matrix obeying equation (6.29) evolves exactly in the same way as the one of the small sample symmetrical superradiant system, with Γ being replaced by $\Gamma\mu$. The system cascades down the ladder of “symmetrical” $|JM\rangle_{k_0}$ states which are now obtained by repeated action of $D_{k_0}^-$ on the fully excited state:

$$|JM\rangle_{k_0} \propto (D_{k_0}^-)^{J-M} |e, e, \dots e\rangle . \quad (6.37)$$

Hence, the large sample superradiance problem reduces, in the mean-field model, to the simple symmetrical problem analysed in section 5. This explains the success of this model [4, 9, 11, 14] which, in spite of the fact that it neglects important propagation effects, nevertheless qualitatively retains some of the essential features of large sample superradiance.

6.3. Simple analysis of large sample superradiance evolution in the one-dimensional propagation model

We proceed now to solve the superradiance equations derived in subsection 6.2. Similarly to the small sample superradiance discussed in section 5, the evolution of large sample superradiance can be divided into an early linear stage, during which the essential quantum fluctuations do occur and a subsequent “classical phase” during which the system obeys the classical fluctuation-free evolution equation. Since in the large sample case, the system evolution is no longer symmetrical with respect to atom exchange, the Schrödinger description becomes quite intricate and we prefer to adopt the economical Heisenberg point of view which directly deals with the observables of interest ($\mathcal{E}, \mathcal{P}, \mathcal{N}$). Before considering the already rather complex one-dimensional model of superradiance, we will, as an introduction to the Heisenberg point of view, describe the system evolution in the mean-field model of large sample superradiance (subsection 6.3.1). This simple model will of course enable us in this point of view to “revisit” results already derived in section 5 in the Schrödinger picture. At the same time, it will suggest to us a very simple recipe to solve the more complicated one-dimensional propagation equation (subsection 6.3.2). Although the general analysis developed in this section is essentially the same as the one of ref. [30], the development presented here follows a more tutorial pace, with an attempt to make a clear connexion with the small sample superradiance regime and a presentation relying as much as possible on simple analytical expressions.

6.3.1. Evolution of “mean-field” superradiance in the Heisenberg picture:

The Bloch angle representation

The method for solving the mean field Heisenberg equation (6.36) is based on the same physical arguments as the ones used in section 5. The system evolution is analysed into an initial quantum stage and a subsequent classical phase connected at an arbitrary time t_0 . The number of photons emitted at

time t_0 should be small enough so that $\langle D_3(t_0) \rangle$ remains still very close to $N/2$:

$$\langle D_3(t_0) \rangle \sim N/2 \quad (6.38)$$

which implies that the evolution equation (6.36) can be considered as linear for $t < t_0$. This condition is similar to the one expressed by equation (5.26) of section 5. At the same time, t_0 should be large enough so that the $D_{k_0}^+$, $D_{k_0}^-$ and D_3 operators could be considered as “quasi-commuting” classical quantities for $t > t_0$. Since the expectation value of the commutator $[D_{k_0}^+, D_{k_0}^-]$ is practically equal to N around $t = 0$:

$$\langle [D_{k_0}^+, D_{k_0}^-] \rangle = 2\langle D_3 \rangle \simeq N \quad \text{for } t \sim 0 \quad (6.39)$$

and since the expectation value $\langle D_{k_0}^+ D_{k_0}^- \rangle$ can be readily shown to be in the linear regime given by:

$$\langle D_{k_0}^+ D_{k_0}^- \rangle_{t \sim 0} \simeq N e^{NT\mu t}, \quad (6.40)$$

it appears clearly that as soon as $t_0 > 1/NT\mu$, the $D_{k_0}^+$ and $D_{k_0}^-$ operators have a product with an expectation value much larger than their commutator. This justifies a classical treatment of the system evolution from the time t_0 on. This condition is nothing but condition (5.22) of section 5 with $NT\mu$ replacing NT .

Once the time t_0 has been chosen, two questions remain to be answered:

(i) What is the statistics of the results of a “virtual measurement” made at time $t = t_0$ on $D_{k_0}^+$? We will call $\alpha e^{i\phi}$ (α and ϕ real) the result of such a measurement. $P(\alpha^2) d(\alpha^2)$ and $Q(\phi) d\phi$ will be the probabilities that this measurement yields respectively an α^2 value comprised between α^2 and $\alpha^2 + d(\alpha^2)$ and a ϕ value comprised between ϕ and $\phi + d\phi$.

(ii) What is, for a given initial value $\alpha e^{i\phi}$, the subsequent classical trajectory followed by the superradiant system? We will call $D_{cl}^+(\alpha, \phi, t)$ the atomic polarization along this (fluctuation free) trajectory.

Since all the foregoing analysis does not obviously depend upon t_0 , one can as well extrapolate back the classical trajectories to $t_0 = 0$ and determine the statistics of initial conditions for these trajectories at time $t = 0$. Once the answer to these two questions is known, one is able to predict the expectation value of any product of $D_{k_0}^+$ and $D_{k_0}^-$ operators at any times t, t' . For example, the $p+q$ order correlation function of the atomic polarization at times t and t' writes:

$$\langle D_{k_0}^{+(p)}(t) D_{k_0}^{-(q)}(t') \rangle = \int P(\alpha^2) Q(\phi) d(\alpha^2) d\phi [D_{cl}^+(\alpha, \phi, t)]^p [D_{cl}^-(\alpha, \phi, t')]^q. \quad (6.41)$$

As a special case, for $t = t' = 0$, one gets:

$$\langle D_{k_0}^{+(p)}(0) D_{k_0}^{-(q)}(0) \rangle = \int P(\alpha^2) \alpha^{p+q} d(\alpha^2) \int Q(\phi) e^{i(p-q)\phi} d\phi. \quad (6.42)$$

This equation provides us with the answer to question (i). The left-hand side of this equation can indeed be directly calculated at time $t = 0$ since it then coincides with its counterpart in the Schrödinger picture:

$$\langle D_{k_0}^{+(p)}(0) D_{k_0}^{-(q)}(0) \rangle \equiv \langle eee \dots e | D_{k_0}^{+(p)} D_{k_0}^{-(q)} | eee \dots e \rangle. \quad (6.43)$$

After a simple computation based on operator commutation algebra, one finds the following result, valid as soon as $N \gg p, q$:

$$\langle D_{k_0}^{+(p)}(0) D_{k_0}^{-(q)}(0) \rangle = \langle \text{eee} \dots \text{e} | \left(\sum_i D_{k_0 i}^+ \right)^p \left(\sum_j D_{k_0 j}^- \right)^q | \text{ee} \dots \text{ee} \rangle = \delta_{pq} p! N^p. \quad (6.44)$$

Comparing this result with equation (6.42), one then gets the following identities:

$$\left\{ \int Q(\phi) e^{i(p-q)\phi} d\phi = \delta_{pq} \right. \quad (6.45)$$

$$\left. \int P(\alpha^2) d(\alpha^2) \alpha^{2p} = p! N^p \right. \quad (6.46)$$

which allow us to determine unambiguously $Q(\phi)$ and $P(\alpha^2)$. Equation (6.45) implies that $Q(\phi)$ is a constant distribution:

$$Q(\phi) = 1/2\pi \quad (6.47)$$

meaning that the phase ϕ is randomly distributed between 0 and 2π . Equation (6.46) implies that $P(\alpha^2)$ is the probability distribution whose p th moment is $p! N^p$, which allows us to identify $P(\alpha^2)$ with the Gaussian distribution having an average value $\langle \alpha^2 \rangle = N$:

$$P(\alpha^2) = \frac{1}{N} e^{-\alpha^2/N}. \quad (6.48)$$

Equations (6.47) and (6.48) summarize the answer to question (i): the choice of initial atomic polarization obeys Gaussian statistics, with a random phase.

Once the choice of α and ϕ has been made, the answer to question (ii) is readily obtained by solving the Bloch equations (6.36) which are now assumed to describe the evolution of commuting classical quantities $D_{k_0}^{+\text{cl}}$, $D_{k_0}^{-\text{cl}}$, D_3^{cl} :

$$\frac{d}{dt} D_{k_0}^{+\text{cl}} = i\omega_0 D_{k_0}^{+\text{cl}} + \Gamma\mu D_{k_0}^{+\text{cl}} D_3^{\text{cl}}; \quad \frac{d}{dt} D_3^{\text{cl}} = -\Gamma\mu D_{k_0}^{+\text{cl}} D_{k_0}^{-\text{cl}} \quad (\text{we identify here } \tau \text{ and } t). \quad (6.49)$$

These equations conserve the “norm” $D_{k_0}^{+\text{cl}} D_{k_0}^{-\text{cl}} + (D_3^{\text{cl}})^2$. They thus describe the evolution of a “constant length vector” in an abstract space. This vector is called the “Bloch vector”. The initial position $D_3^{\text{cl}}(0) = N/2$, $D^{+\text{cl}}(0) = 0$ is referred to as the “up” position in this space and the angle between the Bloch vector and this vertical position is called the Bloch angle θ (see fig. 16). This geometrical analogy leads us to change to new variables θ and ϕ by writing:

$$\left\{ \begin{array}{l} e^{-i\omega_0 t} \cdot D_{k_0}^{+\text{cl}}(t) = \frac{N}{2} \sin \theta(t) e^{i\phi} \\ D_3^{\text{cl}}(t) = \frac{N}{2} \cos \theta(t) \end{array} \right. \quad (6.50)$$

$$\left\{ \begin{array}{l} D_{k_0}^{+\text{cl}}(t) = \frac{N}{2} \sin \theta(t) e^{i\phi} \\ D_3^{\text{cl}}(t) = \frac{N}{2} \cos \theta(t) \end{array} \right. \quad (6.51)$$

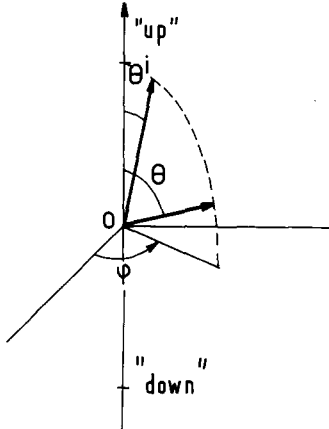


Fig. 16. The Bloch angle representations of mean-field superradiance: the atomic system is formally analogous to a pendulum starting with a small tipping angle θ^i at time $t = 0$ and going down to the $\theta = \pi$ position according to a damped-pendulum equation. The azimuthal angle ϕ of the pendulum varies randomly from one realization of the experiment to the next, but remains constant within a single pulse evolution.

and the Bloch equations (6.49) become:

$$\frac{d\theta}{dt} = \frac{1}{2T_R} \sin \theta \quad (6.52)$$

$$d\phi/dt = 0 \quad (6.53)$$

where we have defined the “characteristic superradiance time”:

$$T_R = (N\Gamma\mu)^{-1}. \quad (6.54)$$

These equations describe the irreversible evolution of the atomic system from the “up” to the “down” ($\theta = \pi$) position (see fig. 16). They are formally analogous to the equations of motion of a damped pendulum immersed in a viscous liquid. It is clear that this equation with the initial condition $\theta(0) = 0$ would not start. This is not surprising, since the beginning of the superradiance evolution precisely depends upon quantum fluctuations which are neglected in the classical Bloch equations. The analysis developed above leads us to choose as initial condition for θ and ϕ a random ϕ value and a θ^i value connected to α by the relation:

$$\theta^i = \frac{2}{N} \alpha \quad (6.55)$$

and thus obeying the Gaussian statistics:

$$P(\theta_i^2) d(\theta_i^2) = \frac{N}{4} e^{-N\theta_i^2/4} d(\theta_i^2) \quad (6.56)$$

with a mean square root value for the initial angle (so-called tipping angle):

$$\bar{\theta}_i = 2/\sqrt{N}. \quad (6.57)$$

The pendulum equation (6.52) with $\theta(0) = \theta^i$ is readily integrated and gives:

$$\operatorname{tg} \frac{\theta}{2} = \operatorname{tg} \frac{\theta^i}{2} e^{-NT\mu t/2}. \quad (6.58)$$

The corresponding radiated intensity is:

$$\begin{aligned} I_{cl}(t) &= -\hbar\omega_0 \frac{dD_3^{cl}}{dt} = \frac{\hbar\omega_0}{2} \frac{N}{T_R} \sin^2 \theta \\ &= \frac{\hbar\omega_0 N}{2T_R} / \cosh^2 \left[\frac{1}{2T_R} (t - t_D(\theta^i)) \right] \end{aligned} \quad (6.59)$$

with

$$t_D(\theta^i) = -2T_R \operatorname{Log}(\theta^i/2). \quad (6.60)$$

One thus finds the same classical trajectories as in the Schrödinger description of the small sample superradiance case (provided NT is replaced by $NT\mu = 1/T_R$), with the initial condition being now described by the “initial tipping angle θ^i ” instead of the parameter s_0 . Clearly, these two descriptions are fully equivalent. A value θ^i corresponds indeed to an initial value $D_3^{cl}(0) \approx \frac{1}{2}N(1 - \frac{1}{2}\theta_i^2)$, i.e. to a number $\frac{1}{4}N\theta_i^2$ of “measured” photons at time $t = 0$. We thus have the correspondence:

$$s_0 = \frac{1}{4}N\theta_i^2. \quad (6.61)$$

This result shows that $t_D(\theta^i)$ given by eq. (6.60) and $t_D(s_0)$ given by eq. (5.11) are identical. Furthermore, one has:

$$P(\theta_i^2) d\theta_i^2 = e^{-s_0} ds_0 \quad (6.62)$$

which also shows that the statistics of the initial condition are identical in the two points of view. We thus conclude that the mean-field model of large sample superradiance yields the same results as the one analysed in section 5: the single shot realization of a superradiance experiment in the mean-field model corresponds to a “damped pendulum classical trajectory” with an initial tipping angle θ^i . The statistics of θ^i values is Gaussian, with a mean square root value $2/\sqrt{N}$. The average pulse delay is:

$$\langle t_D \rangle = T_R \operatorname{Log} N \quad (6.63)$$

and the relative delay variance is:

$$\frac{[\langle t_D^2 \rangle - \langle t_D \rangle^2]^{1/2}}{\langle t_D \rangle} = \frac{1.3}{\operatorname{Log} N}. \quad (6.64)$$

Although we have just shown the complete equivalence of the Schrödinger and Heisenberg pictures

so far the evolution of the superradiant system *energy* is concerned, it is worth noticing that the Heisenberg point of view is in fact much better adapted to provide information concerning the phase and the time correlation functions of the atomic polarization (and hence of the radiated field). An expression such as (6.41) directly yields all correlation functions in terms of a sum over classical trajectories. One immediately sees that the phase of the atomic polarization is random from shot to shot ($\langle D_{k_0}^+(t) \rangle = 0$). At the same time, one notices (eqs. (6.41), (6.50) and (6.58)) that the autocorrelation function $\langle D_{k_0}^+(t) D_{k_0}^-(t') \rangle$ of the atomic polarization is differing from zero for $|t - t'|$ smaller than the typical classical trajectory duration, i.e. a few T_R . In other words, the Heisenberg picture shows that the superradiance field has, in the mean-field model, a coherence time of the order of a few T_R and a coherence length of a few cT_R . These results would be much less obvious to derive in the Schrödinger point of view.

6.3.2. Evolution of “one-dimensional” superradiance in the Heisenberg picture: The Sine-Gordon equation with random initial tipping angle condition

We now have to study the modifications brought to the previous analysis by the propagation of the electromagnetic field along the medium. The method for solving the quantum mechanical evolution equations (6.13) to (6.15) follows the same steps as in the mean-field case. We replace the quantum equations by the corresponding set of semi-classical equations coupling classical quantities $\mathcal{E}_{cl}(z, \tau)$, $N_{cl}(z, \tau)$, $\mathcal{P}_{cl}(z, \tau)$. In order to get the system started, we assume that a “measurement” made at an early arbitrary time yielded a random c-number function $\mathcal{P}(z, 0)$ for the atomic polarization per unit volume at each sample point (the e.m. field being equal to zero at that time). We then solve the semi-classical equation for these random initial conditions and construct as many “classical trajectories” as there are initial random choices possible. Each trajectory represents the result of a particular realization of the experiment. The expectation value of any observable of physical interest is then obtained by performing the weighted average of these classical trajectories.

Propagation effects play a role at the two stages of this procedure:

- (i) The random choice of initial condition is no longer homogeneous throughout the sample, but has to be made independently in each slice of the medium.
- (ii) Even if initial conditions were homogeneous, the symmetry of the medium would be broken by propagation effects during the subsequent “classical stage” of the emission. The atomic polarization and inversion density as well as the electromagnetic field quickly take different values in the various slices of the medium. Let us study in more detail these two effects.

(i) Statistics of initial conditions in the one-dimensional propagation model [30]

Let us divide the medium into n identical slices of mean position $z_p = pL/n$ ($p = 1, 2, \dots, n$). The length of each slice is large compared to λ , but small compared to L ($\lambda < L/n < L$). The atomic polarization $\mathcal{P}^+(z, \tau)$ and population inversion $\mathcal{N}(z, \tau)$ are “smoothed” by assuming them to be constant in each slice:

$$\left\{ \begin{array}{l} \mathcal{P}^+(z_p, \tau) = \frac{n}{\pi L w^2} d\epsilon_a e^{-i\omega_0 \tau} D_{k_0 p}^+ \\ \mathcal{N}(z_p, \tau) = \frac{n}{\pi L w^2} D_p^3 \end{array} \right. \quad (6.65)$$

$$\left\{ \begin{array}{l} \mathcal{P}^+(z_p, \tau) = \frac{n}{\pi L w^2} d\epsilon_a e^{-i\omega_0 \tau} D_{k_0 p}^+ \\ \mathcal{N}(z_p, \tau) = \frac{n}{\pi L w^2} D_p^3 \end{array} \right. \quad (6.66)$$

with

$$D_{k_0 p}^+ = \sum_{i \in p^{\text{th}} \text{ slice}} D_{k_0 i}^+ ; \quad D_p^3 = \sum_{i \in p^{\text{th}} \text{ slice}} D_i^3 . \quad (6.67)$$

We assume that each slice contains a large absolute number N_p of atoms, so that statistics can be performed in each slice:

$$N_p = N/n \gg 1 . \quad (6.68)$$

By analogy with what has been done in the mean-field case, we assume that the initial condition in each slice:

$$D_{k_0 p}^{+\text{cl}}(\tau = 0) = \alpha_p e^{i\phi_p} \quad (6.69)$$

has a random phase with a probability law:

$$Q(\phi_p) = 1/2\pi \quad (6.70)$$

and an amplitude obeying Gaussian statistics:

$$P(\alpha_p^2) = \frac{1}{N_p} \exp(-\alpha_p^2/N_p) . \quad (6.71)$$

A given choice (α_p, ϕ_p) leads to the following value for the initial atomic polarization:

$$\mathcal{P}_{\text{cl}}^+(z_p, \tau = 0) = \frac{n}{\pi L_w^2} d\varepsilon_a \alpha_p e^{i\phi_p} . \quad (6.72)$$

The statistics for different slices are independent (uncorrelated random choices). These results can be demonstrated exactly in the same way as in subsection 6.3.1.

Equation (6.72) describes the quantum initiation for a medium prepared in the upper atomic level at time $\tau = t - z/c = 0$, i.e. prepared by an excitation “sweeping” along the medium at speed of light. This condition is realized in “a three-level atom” scheme where the initial excitation is provided by a short pulse of light propagating along the sample axis (longitudinal pumping; see fig. 14a). If one prepares on the other hand the medium instantaneously at the same time $t = 0$ for all z values (transverse pumping; see fig. 14b), the initial condition should read instead:

$$\mathcal{P}_{\text{cl}}^+(z_p, t = 0) = \frac{n}{\pi L_w^2} d\varepsilon_a \alpha_p e^{i\phi_p} . \quad (6.73)$$

These two kinds of initial conditions do not practically differ from each other if the medium is short enough to satisfy relation (6.21). In that case, τ and t can be used indifferently and there is no physical distinction to be made between longitudinal or transversal superradiance pumping. We assume in this section this condition to be fulfilled and use eq. (6.72) as the initial condition for the superradiant system.

The procedure outlined above for the description of the initial quantum fluctuations seems to depend upon the arbitrary number n of slices. Obviously, such a model is satisfactory only if the statistics of classical trajectories obtained in this way tends to a limit when n is increased. It has been shown by numerical calculations in ref. [30] that this is indeed the case and that increasing beyond a few units the number of uncorrelated initial slices does not appreciably modify the statistics of the subsequent classical trajectories (this result being true only if condition (6.21) is fulfilled). This interesting feature, which considerably simplifies the analysis to come, can be explained intuitively. On fig. 17a, we have sketched an initial condition corresponding to a relatively large number of uncorrelated slices. The local tipping angle $\theta_p^i = (2/N_p)\alpha_p$ has a typical value $\bar{\theta}_p^i = 2/\sqrt{N_p}$ proportional to \sqrt{n} and varies randomly from slice to slice. On fig. 17b, the number of slices is smaller and so is the tipping angle in each slice. At last, on fig. 17c, we consider the case of a single slice extending throughout the medium, with a very small tipping angle θ^i , typically of the order of $2/\sqrt{N}$. It is now easy to understand that the subsequent evolution of pulses obtained with these three types of initial conditions should look very similar. The atomic polarization throughout the medium, which is initially uncorrelated for different slices, will eventually lock to a common phase to yield a macroscopic N^2 intensity pulse radiation. The locking is due to the coupling of all the atomic dipoles to their common radiation field. The “efficiency” of this locking which will eventually govern the time scale of the emission process – and the statistics of pulse to pulse fluctuation – depends upon the magnitude of this common “driving” field. At the beginning of the emission, when the radiation is still emitted by uncorrelated sources in various slices, the magnitude of the “driving” field at each point in the sample results from a quadratic summation of the fields radiated by each slice. Since, in each slice the atomic polarization has an average amplitude $\bar{\alpha}_p = \frac{1}{2}N_p\bar{\theta}_p^i = \sqrt{N_p}$, one expects a global radiated intensity at each point proportional to $\sum_p N_p = N$, i.e. n -independent! In other words, n random oscillators each with an amplitude of the order of $1/\sqrt{n}$ radiate just as much as a single one with an amplitude 1. The common field to which the atomic polarization eventually locks does not change too much when the number of initial incoherent slices is increased. Another way to express this result is to remark that a large n value means a lot of incoherent sources with large relative polarizations partially cancelling each other, whereas a small n value means a smaller initial polarization per atom cooperating more efficiently throughout the medium. It is important to notice that this analysis is valid only because condition (6.21) is fulfilled. If it were not the case, it is obvious that atomic polarization belonging to slices far away from each other could never lock to a common phase and an initial condition homogeneous throughout a large section of the medium would not be realistic. We discuss qualitatively this situation in section 7 and we restrict ourselves here

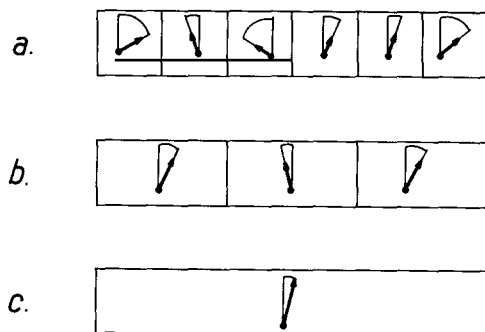


Fig. 17. Sketch of initial conditions in the one-dimensional propagation model: (a) Large number of slices with small-Bloch-vector-large tripping angle condition in each slice. (b) The number of slices is reduced by a factor two: there is a larger Bloch vector in each slice, with a smaller tipping angle. (c) Single slice: the uniform initial Bloch vector is still larger but the tipping angle is now very small.

to the Arecchi–Courtens regime of condition (6.21). To summarize, we will assume in the following that the initial condition is chosen homogeneous *throughout the whole medium*. This amounts to considering that *the early stage* of the emission process obeys to the *mean-field description* of subsection 6.2: the quantum fluctuations initiating the superradiant emission are described by a single random tipping angle variable throughout the medium with a mean square root value $2/\sqrt{N}$ and a statistics obeying eq. (6.56). This assumption considerably simplifies the description of the subsequent classical trajectories without altering in a qualitative way the results of a more refined description of the initial conditions based on a division into a large number of slices [30].

(ii) *Classical trajectories in the one-dimensional model corresponding to homogeneous initial conditions*

The classical equations describing the one-dimensional propagation model of superradiance are readily deduced from the quantum mechanical equations ((6.13) to (6.15)):

$$\frac{\partial N_{\text{cl}}}{\partial \tau} = \frac{i}{\hbar} [\mathcal{P}_{\text{cl}}^* \mathcal{E}_{\text{cl}}^* - \mathcal{P}_{\text{cl}} \mathcal{E}_{\text{cl}}] ; \quad \frac{\partial \mathcal{P}_{\text{cl}}^*}{\partial \tau} = \frac{2id^2}{\hbar} \mathcal{E}_{\text{cl}} N_{\text{cl}} ; \quad \frac{\partial \mathcal{E}_{\text{cl}}^*}{\partial z} = \frac{i\omega_0}{2\varepsilon_0 c} \mathcal{P}_{\text{cl}} . \quad (6.74)$$

They are conveniently solved by introducing a time and space varying tipping angle $\theta(z, \tau)$ generalizing the procedure of subsection 6.3.1:

$$\mathcal{N}_{\text{cl}}(z, \tau) = \frac{N}{2\pi L w^2} \cos \theta(z, \tau) ; \quad \mathcal{P}_{\text{cl}}^*(z, \tau) = id \frac{N}{2\pi L w^2} \sin \theta(z, \tau) e^{i\phi} . \quad (6.75)$$

The Bloch equations then reduce to:

$$\frac{2d}{\hbar} \mathcal{E}_{\text{cl}} = e^{i\phi} \frac{\partial \theta}{\partial \tau} \quad (6.76)$$

and the Maxwell equation to:

$$\frac{\partial^2 \theta}{\partial z \partial \tau} = \frac{1}{L \cdot T_R} \sin \theta \quad (6.77)$$

with T_R being defined by eq. (6.54).

We can also write (6.77) in a dimensionless form as:

$$\frac{\partial^2 \theta}{\partial(z/L) \partial(\tau/T_R)} = \sin \theta . \quad (6.78)$$

This equation, known as the Sine–Gordon one, has been used in many studies dealing with optical pulse propagation in non-linear media. It has been introduced in the context of superradiance studies in ref. [17]. It clearly shows that the “natural length” of the problem is L and the “natural time” T_R . It describes the flipping of the local tipping angle $\theta(z, \tau)$ from a value close to zero at time $t=0$ to the value $\theta=\pi$ at $\tau=\infty$. The initial conditions to choose for solving this equation are:

$$\theta(z, \tau=0) = \theta^i \quad (6.79)$$

$$\frac{\partial \theta}{\partial \tau}(z, \tau = 0) = 0. \quad (6.80)$$

(Equation (6.80) expresses that the electromagnetic field at time $\tau = 0$ is equal to zero.) A mere inspection of eq. (6.78) shows that θ is in fact a function of the single dimensionless quantity:

$$q = 2 \left(\frac{z}{L} \frac{\tau}{T_R} \right)^{1/2}. \quad (6.81)$$

Replacing z and τ by q in eq. (6.78), the Sine–Gordon equation is transformed into:

$$\theta''(q) + \frac{1}{q} \theta'(q) - \sin \theta = 0 \quad (6.82)$$

with the initial conditions $\theta(0) = \theta^i$ and $\theta'(0) = 0$.

Numerical computation of eq. (6.82) is easy to perform. Once $\theta(q)$ is obtained, one computes $\mathcal{E}_{cl}(z, \tau)$ with the help of eq. (6.76) and the emitted intensity at the end of the medium is given by:

$$I^{cl}(\tau) = \mathcal{E}_{cl}^*(L, \tau) \mathcal{E}_{cl}(L, \tau). \quad (6.83)$$

A typical $I^{cl}(\tau)$ trajectory is displayed on fig. 18. The main differences with the mean-field trajectories (compare with fig. 10b) are:

- (a) The occurrence of several emission maxima (the so-called superradiance ringings [80]).
- (b) The fact that not only the delay but also the shape of single shot trajectories depend upon the choice of the initial tipping angle. In particular, the ringing contrast depends upon θ^i , with more important ringings obtained for small θ^i values [64]. The intensity of the first radiation burst also fluctuates from shot to shot. These properties have been extensively studied [30]. Let us simply focus here on some of the basic features of these “one-dimensional propagation” trajectories.

The occurrence of ringings in the radiation output of the superradiance sample can be understood simply from eqs. (6.77) and (6.81). The equilibrium solution of the Sine–Gordon equation is:

$$\theta(z, \tau = +\infty) = \pi, \quad (6.84)$$

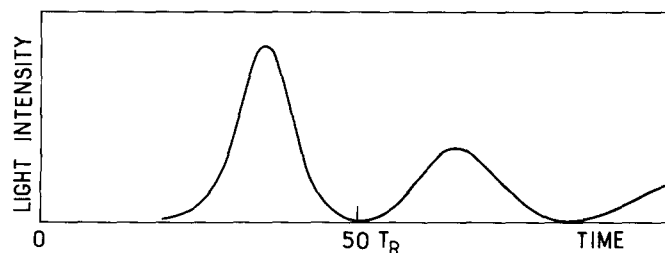


Fig. 18. Example of one-dimensional propagation superradiant pulse. The initial tipping angle is here $\theta^i = 2 \times 10^{-4}$ (uniform throughout the sample). The number of atoms is $N \sim 10^8$. Note the ringing (not present in the mean-field solution).

which means that all atoms eventually end-up in the lower g level. However, due to propagation, the various slices do not evolve at the same speed. Since a given Bloch angle corresponds to a definite q value, which is reached at earlier time for a larger z value according to eq. (6.81), one understands that the atoms reaching first the $\theta = \pi$ position are those located at the end of the medium ($z = L$). These atoms have indeed experienced the largest field, amplified by all the other atoms along the medium. Integration of the Sine–Gordon equation for $z = L$ yields:

$$\frac{\partial \theta}{\partial z}(z = L, \tau) = \frac{1}{LT_R} \int_0^L dz \sin \theta(z, \tau). \quad (6.85)$$

At the time τ_0 corresponding to $\theta = \pi$ for $z = L$, $\theta(z, \tau_0)$ with $z < L$ is still smaller than π and hence $\sin \theta$ in eq. (6.85) is positive. As a result, $\partial \theta(z = L)/\partial \tau$ given by the integral is positive. This means that $\theta(L, \tau)$ keeps increasing for $\tau > \tau_0$, $\theta(z = L)$ going beyond the π value: the atoms at the end of the medium begin at $\tau = \tau_0$ to reabsorb the field still emitted by the $z < L$ atoms. The Bloch vector of the $z = L$ atoms thus “overshoots” and exhibits an oscillating behaviour around $\theta = \pi$, a new feature not present in the mean-field model. Other atoms in the sample undergo a similar evolution at later times. The electric field, proportional to $\partial \theta(z = L, \tau)/\partial \tau$ oscillates as θ does and changes sign from one ringing lobe to the next. (This means that the phase of the field undergoes a π shift from one radiation ringing to the next.)

(iii) *The statistics of superradiant pulse delays* can also be calculated in a simple way and approximate analytical formulae can be obtained for the average delay [17] and delay variance [40]. Following refs. [17, 40], we notice that the maximum of the first emission ringing corresponds, with a good approximation, to the time when $\theta(z = L)$ is equal to one. To determine this time, we solve the Sine–Gordon equation for $0 < \theta < 1$ by assuming that $\sin \theta$ can be replaced by θ (linearization procedure):

$$\theta'' + \frac{1}{q} \theta' - \theta = 0. \quad (6.86)$$

This equation, with the initial conditions (6.79) and (6.80), admits the following solution [80]:

$$\theta(q) = \theta^i J_0(iq). \quad (6.87)$$

(Easily checked by replacing $J_0(iq)$ by its series expansion and identifying in (6.86).)

The corresponding emission delay τ_D is thus given by:

$$J_0[2i(\tau_D/T_R)^{1/2}] \simeq 1/\theta^i. \quad (6.88)$$

Replacing the function J_0 by its asymptotic value:

$$J_0(iq) \simeq \frac{1}{\sqrt{2\pi q}} e^q, \quad (6.89)$$

eq. (6.88) can be rewritten as:

$$\tau_D = \frac{1}{4} T_R [\text{Log}(A/\theta^i)]^2, \quad (6.90)$$

where $A = 2(\pi^2 \tau_D / T_R)^{1/4}$ can be taken as a constant (of the order of 10).

The average delay $\langle \tau_D \rangle$ is obtained with $\theta_i = 2/\sqrt{N}$:

$$\langle \tau_D \rangle = \frac{1}{4} T_R [\text{Log}(A\sqrt{N}/2)]^2. \quad (6.91)$$

The delay fluctuations are obtained from eq. (6.90) and from the statistics of θ^i (eq. (6.56)). The probability $P(\tau_D - \langle \tau_D \rangle)$ for a given difference $\tau_D - \langle \tau_D \rangle$ between the measured and the average delay is:

$$P(\tau_D - \langle \tau_D \rangle) = \exp\left\{-\left(\frac{\tau_D - \langle \tau_D \rangle}{\Delta \tau_D}\right)\right\} \exp\left\{-\exp\left\{-\left(\frac{\tau_D - \langle \tau_D \rangle}{\Delta \tau_D}\right)\right\}\right\} \quad (6.92)$$

with

$$\Delta \tau_D = \frac{1}{2} \sqrt{T_R \langle \tau_D \rangle}. \quad (6.93)$$

Comparing the “one-dimensional propagation” and the mean-field case, we notice that the average delays given respectively by formulae (6.63) and (6.91) are not too much differing from each other, the ratio between them being a logarithmic factor slowly varying with N . For large atom numbers ($N \geq 10^6$), the delay of the one-dimensional propagation model is somewhat larger than the one of the mean-field case. For example, the ratio between the two delays is equal to 1.5 for $N = 10^9$ ($\langle \tau_D \rangle \approx 21 T_R$ in the mean-field model and $\langle \tau_D \rangle = 31 T_R$ in the one-dimensional propagation case).

As for the delay fluctuations, a simple comparison between formulae (5.36) and (6.92) shows that their statistics is given in the one-dimensional model by exactly the same analytical expression as in the mean-field case, provided one replaces in eq. (5.36) $(NT)^{-1}$ by $\Delta \tau_D$. The relative delay fluctuation is thus, in the one-dimensional propagation model:

$$\frac{[\langle \tau_D^2 \rangle - \langle \tau_D \rangle^2]^{1/2}}{\langle \tau_D \rangle} \approx \frac{1.3 \Delta \tau_D}{\langle \tau_D \rangle} \approx \frac{2.6}{\text{Log } N} \quad (6.94)$$

approximately twice larger than in the mean-field case (compare with eq. (5.38)). For example, the relative delay fluctuations are equal to 12% for $N = 10^9$ [66].

The results have been presented here in the form of very simple analytical expressions, which have been made possible because of the choice of a uniform initial tipping angle and because of the assumption that the delay can be accurately estimated with the linear equation (6.86). Most of these expressions [eqs. (6.90), (6.91), (6.94)] have been previously derived in ref. [40], although we believe that eq. (6.92) has been first obtained in ref. [24]. When non-uniform initial conditions are assumed, the calculations become much more intricate. However, an expression for the delay statistics can be obtained within the linear regime, which involves complex error functions [31]. This expression does not notably differ from the much simpler one presented above. A description of delay fluctuation statistics has also been obtained by numerical solution of the non-linear equations (6.74) with non-uniform initial conditions [30]. Fig. 19 presents a histogram of relative $\tau_D/\langle \tau_D \rangle$ delays corresponding to classical

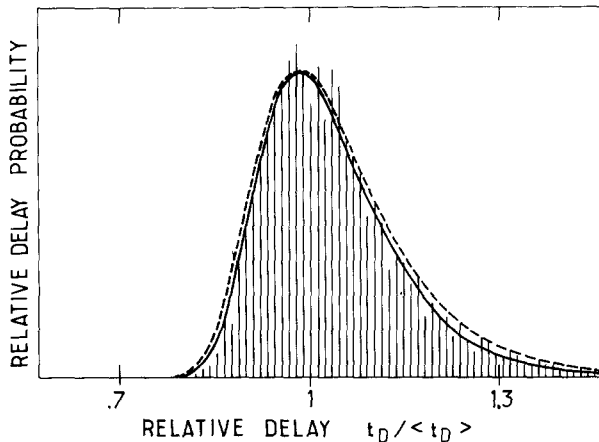


Fig. 19. Histogram of relative delays $t_D / \langle t_D \rangle$ corresponding to one dimensional propagation classical trajectories with non-uniform initial conditions (from ref. [31]). The solid line curve represents formula (6.92) based on a uniform tipping angle model, the dashed line curve the theoretical expression obtained in ref. [31] using complex error functions.

trajectories. The solid line curve displayed on the histogram represents the predictions of eq. (6.92), the dashed line the result obtained in ref. [31], using complex error functions. Note the fair agreement between the result of the calculation taking into account local fluctuations and non-linear propagation with the much simpler theory outlined above, which assumed uniform fluctuations and linear propagation equations until the first emission maximum.

A similar analysis can be performed to describe the fluctuations of the first emission peak maximum intensity, the fluctuations of the first to second ringing maxima ratio and so on. Description of some of these fluctuations within the one-dimensional propagation model can be found in ref. [30], with histograms displaying statistics corresponding to a large number of single shot trajectories.

6.4. Numerical solution of three-dimensional large sample superradiance equations (pencil-shaped case)

The one-dimensional propagation model of superradiance developed in the previous subsection can only be considered as an approximation to the correct description of propagation effects in superradiance. Some of its predictions – in particular the occurrence of strong coherent ringings in a long pulse tail – are not consistently observed in the superradiance experiments, so that several authors have recently tried to investigate more precise models of superradiance taking into account transverse effects in the emitting sample. In this subsection, we present some results of these studies and discuss some problems still open for a complete analysis of three-dimensional superradiance evolution.

The main result of this section is to show that transverse effects can be simply taken into account in a *very small Fresnel number sample* for which the coherent ringings are indeed washed out and a hyperbolic secant pulse emission very reminiscent of the mean-field evolution case is obtained. Unfortunately, no such simple results exist for Fresnel numbers of the order of unity or larger and the solution of the superradiance evolution problem relies in these cases on lengthy numerical computations still in progress [83, 87].

6.4.1. Three-dimensional Bloch–Maxwell equations in the Heisenberg picture

In order to allow for slow variations of the field and atomic polarizations along the x and y directions, we now define slow varying envelopes $\mathcal{E}^\pm(x, y, z, t)$ and $\mathcal{P}^\pm(x, y, z, t)$ by the equations:

$$E^{\pm(\text{rad})} = \mathcal{E}^+(x, y, z, t) e^{\pm i(\omega_0 t - k_0 z)} \boldsymbol{\epsilon}_a \quad (6.95)$$

$$P^\pm = \mathcal{P}^\pm(x, y, z, t) e^{\pm i(\omega_0 t - k_0 z)} \boldsymbol{\epsilon}_a. \quad (6.96)$$

Replacing in eqs. (3.27) and (3.29)–(3.30) $E^{\pm(\text{rad})}$ and \mathbf{P} by these expressions and neglecting, as in section 6.3 $\partial\mathcal{E}/\partial t$ and $\partial\mathcal{P}/\partial t$ compared to $\omega_0\mathcal{E}$ and $\omega_0\mathcal{P}$ and $\partial\mathcal{E}/\partial z$ compared to $k_0\mathcal{E}$, one gets a new three-dimensional Maxwell equation:

$$\frac{\partial\mathcal{E}^+}{\partial z} - \frac{i}{2k_0} \left(\frac{\partial^2}{\partial x^2} + \frac{\partial^2}{\partial y^2} \right) \mathcal{E}^+ = \frac{i\omega_0}{2\epsilon_0 c} \mathcal{P}^- \quad (6.97)$$

whereas the Bloch equations remain identical to the ones derived in the one-dimensional propagation model (eq. (6.16)). The Maxwell equation (6.97) is modified as compared to eq. (6.17) by the addition of the transverse term $-(i/2k_0)(\partial^2/\partial x^2 + \partial^2/\partial y^2)\mathcal{E}^+$ whose physical meaning depends upon the value of the Fresnel number F . For $F \gg 1$, this term mainly describes the possibility of off-axis emission in the geometric angle θ_G of the sample. For $F \ll 1$, it accounts on the other hand for the diffraction of the emitted field in the angle θ_D . Note that the model presented here assumes, as in section 6.3, that the field propagates only along *one direction* (defined by \mathbf{k}_0). The complication introduced by propagation in the opposite direction will be briefly discussed below (subsection 6.4.5).

6.4.2. The initial condition in the three-dimensional model of superradiance

The solution of eqs. (6.16) and (6.97) is obtained by a simple generalization of the method outlined in section 6.3. These quantum mechanical equations involving non-commuting quantities are replaced by similar equations between classical quantities \mathcal{N}_{cl} , \mathcal{E}_{cl} and \mathcal{P}_{cl} . At time $\tau = 0$, it is assumed that the electric field is equal to zero:

$$\mathcal{E}_{\text{cl}}(x, y, z, \tau = 0) = 0 \quad (6.98)$$

whereas the initial atomic inversion density is distributed throughout the medium:

$$\mathcal{N}_{\text{cl}}(x, y, z, \tau = 0) = \mathcal{N}_0(x, y, z). \quad (6.99)$$

In order to represent the effect of the quantum field fluctuations, a random atomic polarization is also distributed throughout the sample. In order to define this polarization, we follow a procedure which generalizes the one of subsection 6.3: the medium is divided into three-dimensional boxes whose longitudinal (l_z) and transverse (l_x , l_y) dimensions are small compared to L and w but large compared to λ . Each box is assumed to contain a large absolute number of atoms (N_p atoms in the p th box). The initial polarization in the p th box is taken as:

$$\mathcal{P}_{\text{cl}}(x_p, y_p, z_p, \tau = 0) = \frac{1}{l_x l_y l_z} d \cdot \boldsymbol{\epsilon}_a \alpha_p e^{i\phi_p} \quad (6.100)$$

with ϕ_p and α_p being random quantities obeying respectively the probability laws (6.70) and (6.71).

For each choice $\{\alpha_p, \phi_p\}$ of the random polarization, a solution of the classical equation is computed, obeying the boundary conditions (6.98), (6.99), (6.100), with the extra condition:

$$\mathcal{E}_{\text{cl}}(x, y, z = 0, \tau) = 0 \quad (6.101)$$

which means that the electromagnetic field is propagating along the positive Oz direction in the medium. This solution corresponds to a possible realization of the superradiant pulse, whose probability is given by the laws (6.70), (6.71).

From this analysis, it results clearly that the three-dimensional character of superradiance does not only appear in the Maxwell equation (6.97), but also intervenes at two different levels in the definition of the initial conditions of the system evolution:

(i) First, we must now take into account the possibility of a transverse variation of the atomic inversion distribution at time $\tau = 0$. Clearly, the initial condition depends upon the shape of the $\mathcal{N}_0(x, y, z)$ distribution and the statistics of the initial polarization (through the N_p coefficients in eq. (6.71)) also depends upon this distribution. For a longitudinally pumped superradiant system using an axial pulsed laser-beam resonant on the f → e transition to prepare the inverted medium (see fig. 14a), the distribution of initially excited atoms is determined by the transverse intensity-distribution of the laser beam. If it is Gaussian, with a waist $w/\sqrt{2}$, and if the pumping process is not saturated, one has:

$$\mathcal{N}_0(x, y, z) = \mathcal{N}_0 e^{-(x^2 + y^2)/w^2}. \quad (6.102)$$

If, on the other hand, the laser beam waist is expanded to a value $w' \gg w$ and the beam sent through a pinhole with a radius w placed in front of the sample, one has:

$$\begin{cases} \mathcal{N}_0(x, y, z) = \mathcal{N}_0 & \text{if } x^2 + y^2 \leq w^2 \\ \mathcal{N}_0(x, y, z) = 0 & \text{if } x^2 + y^2 > w^2. \end{cases} \quad (6.103)$$

Clearly, the superradiant evolution will be different for these two distributions.

(ii) The transverse fluctuations, not existing in the one-dimensional propagation model, may also play a very important role. Depending upon these fluctuations, the emission may start slightly off-axis, in a direction making a random angle with the sample axis. If $F \gg 1$, the off-axis gain of the medium is very close to the axial gain and the emitted pulse is expected to reflect this initial randomness and exhibit strong direction fluctuations. A large ensemble of initial conditions must then be considered to reconstruct the pulse statistics. This statistics and the individual pulse shapes should furthermore depend upon the initial atomic distribution (e.g. eq. (6.102) or (6.103)).

On the contrary, if $F \ll 1$, the off-axis gain is significantly smaller than the on-axis one and the emission, even if it starts on an off-axis direction, will very rapidly become axial. We thus expect the transverse fluctuations not to be significant in that case, with most individual pulse realizations being correctly described by initial polarizations corresponding to a uni-dimensional – or even uniform – distribution (see discussion of subsection 6.3.2).

6.4.3. Mathematical and numerical difficulties related to the solution of the three-dimensional equations of superradiance

The system of equations ((6.16) and (6.97)), although it looks very similar to the one-dimensional propagation ones (eqs. (6.16) and (6.17)), is much more difficult to solve. It is impossible to find an analytical solution, even with a uniform initial condition – not to speak about three-dimensional ones – and the only method left is numerical computation using computers. This type of problem, involving a non-linear set of four-dimensional differential equations (in x, y, z, τ) with random initialization is quite

reminiscent of other situations encountered in physics (turbulence, phase transition problems) and certainly is a challenge for computing science.

One of the main difficulties in looking for a solution comes from the fact that these equations involve a mixture of first and second order partial derivatives. Furthermore, the transverse boundary condition for the field [$\mathcal{E}_{\text{cl}}(x, y = +\infty, z, \tau) = 0$] makes it necessary to extend the transverse dimensions of the integration space far enough from the actual boundary of the active medium. In order to overcome these difficulties by direct integration of eqs. (6.16), (6.97), it is necessary to develop rather complex and lengthy mathematical and numerical procedures [81]. An alternative method [82] consists in transforming the problem into a transverse Fourier space. The basic idea is to introduce the transverse Fourier transformed polarization $\hat{\mathcal{P}}$ by the equations:

$$\hat{\mathcal{P}}_{\text{cl}}(k_x, k_y, z, \tau) = \frac{1}{2\pi} \int_{-\infty}^{+\infty} e^{-ik_x x} dx \int_{-\infty}^{+\infty} e^{-ik_y y} dy \mathcal{P}^+(x, y, z, \tau) \quad (6.104)$$

with a similar definition for the Fourier transformed electric field $\hat{\mathcal{E}}_{\text{cl}}$.

This transformation changes the Maxwell equation (6.97) into:

$$\frac{\partial \hat{\mathcal{E}}_{\text{cl}}^*}{\partial z} + i\kappa \hat{\mathcal{E}}_{\text{cl}}^* = \frac{i\omega_0}{2\epsilon_0 c} \hat{\mathcal{P}}_{\text{cl}} \quad (6.105)$$

with

$$\kappa = (k_x^2 + k_y^2)/2k_0$$

without changing the Bloch equations.

The Fourier transformed function $\hat{\mathcal{E}}_{\text{cl}}$ represents incidentally the far-field component of the emitted field in the direction $\mathbf{k}(k_x, k_y, k_z \sim k_0)$, which is a quantity directly accessible to measurement.

The solution of equation (6.105) with the boundary condition $\hat{\mathcal{E}}_{\text{cl}}(z = 0) = 0$ can be readily expressed by iteration of small integration steps, under a form suitable for numerical computation:

$$\hat{\mathcal{E}}_{\text{cl}}^*(z + \Delta z) = e^{-i\kappa \Delta z} \hat{\mathcal{E}}_{\text{cl}}^*(z) + e^{-i\kappa \Delta z} \int_z^{z + \Delta z} dz' \hat{\mathcal{P}}_{\text{cl}}(z') e^{i\kappa(z' - z)} \quad (6.106)$$

with Δz being a small integration step over z .

In this equation, the right-hand side integral can be easily evaluated from the knowledge of $\hat{\mathcal{P}}_{\text{cl}}(z + \Delta z)$, $\hat{\mathcal{P}}_{\text{cl}}(z)$, $\hat{\mathcal{P}}_{\text{cl}}(z - \Delta z)$ even if $\kappa \Delta z \gg 1$, since one can show that either $\hat{\mathcal{P}}_{\text{cl}}(z')$, or $\hat{\mathcal{P}}_{\text{cl}}(z') e^{i\kappa(z' - z)}$, or both these quantities do not vary too much in a numerical step Δz ($F \ll 1$, $F \gg 1$, $F \sim 1$ respectively). Once $\hat{\mathcal{E}}_{\text{cl}}(z + \Delta z)$ is known from $\hat{\mathcal{E}}_{\text{cl}}(z)$, one can get \mathcal{E}_{cl} and \mathcal{P}_{cl} in the plane $z + \Delta z$ by inverse Fourier transform and integration of the Bloch equations (6.16) and so on.

The main advantage of this method is to deal with the atomic evolution (Bloch equation), and with the field amplification and propagation (Maxwell equation) in different spaces (real and transverse Fourier space respectively), each well adapted to the corresponding problem.

Using either the direct integration method in real space, or the Fourier transform one, several

authors have recently investigated various aspects of the transverse effects in superradiance [34, 83, 87] and tried to analyse in which way they modify the simple results of the one-dimensional propagation model. We summarize now some of the results of these studies.

6.4.4. Analysis of some transverse effects in superradiance

The main difficulty for analysing these effects is due to the fact that the transverse properties of the medium enter into play at different levels in the superradiant process. If there is a transverse variation of the initial atomic inversion (eq. (6.102)), it is expected that various lines of atoms parallel to the sample axis and located at different distances from it will tend to evolve at different speeds, thus resulting in some averaging of the superradiant ringings. The transverse fluctuations of the initial polarization will also, in case of large Fresnel number, introduce large fluctuations of pulse shape, intensity and direction. These effects are complicated by the presence of the transverse term in the Maxwell equation (6.97) which couples to each other the evolution of the various lines of atoms and the different field modes. In order to classify these complex effects, it is convenient to successively consider various situations in which some of them are dominant and the others negligible.

(i) Transverse population averaging effect

Let us first consider a situation in which the transverse dependence of the initial polarization is neglected, as well as the transverse term in the Maxwell equation. This case corresponds to an "on-axis" single shot realization of the superradiant emission in a large Fresnel number sample (so that diffraction and off-axis contribution can be disregarded). The only transverse effect left is then the possibility of a non-uniform atomic distribution. Figure 20 represents the time variation of the total light intensity radiated at the end of the sample, for two different initial population distributions (and the same sample size and atom number: the first maximum of both curves has been normalized to unity).

Figure 20a corresponds to a uniform but transversally limited medium (eq. (6.103)) and fig. 20b to a Gaussian distribution (eq. (6.102)). In both cases, the emission is initiated by an initial uniform

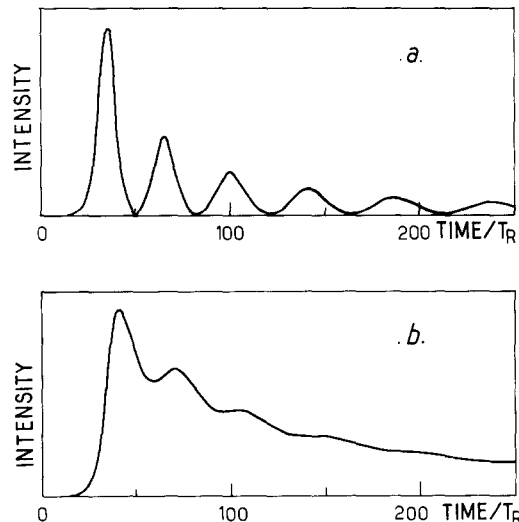


Fig. 20. Transverse population averaging effects: time variation of intensity radiated at the end of the sample ($N = 10^8$); (a) for a transversally uniform pumping (eq. (6.103)); (b) for a transversal Gaussian distribution of the initial inversion (eq. (6.102)).

polarization corresponding to a tipping angle $\theta^i = 2/\sqrt{N}$ with $N = 10^8$. The fig. 20a curve represents the one-dimensional propagation solution of subsection 6.3, exhibiting large coherent ringings. On fig. 20b, the ringings have been to a large extent washed out. This washing out comes obviously from an averaging of the contribution of lines of atoms with partial superradiant times varying proportionally to $N_0(x, y) \sim \exp\{-(x^2 + y^2)/w^2\}$ and thus evolving at different speeds. Hence, the non-uniform transverse distribution of atoms in actual superradiance experiments appears to be one possible reason for the fact that the observed ringings are smaller than the one predicted by the one-dimensional propagation model.

(ii) Diffraction effects in small Fresnel number superradiance

We assume now a non-uniform initial population inversion (eq. (6.102)) and we also include the transverse term in the Maxwell equation, but we still neglect the transverse dependence of the initial atomic polarization. This model is supposed to correctly describe most of the single shot superradiant pulses emitted by a *small Fresnel number* medium (for which the transverse fluctuations of the initial polarizations are expected to have a negligible effect) and some single shot pulses emitted by a sample with a Fresnel number $F \geq 1$ (those which happen to have been started by an axial polarization wave). In order to analyse the effects of diffraction on the pulse characteristics as a function of the Fresnel number, it is convenient to compare the pulse shapes corresponding to the *same* superradiant rate $T_R^{-1} = \Gamma N \mu = (3/8\pi)\Gamma N \lambda^2 / w^2$, but to *different* values of $F = \pi w^2 / L \lambda$. We consider for example an ensemble of samples with the same transverse dimension w and the same number of atoms N , but different lengths L or else an ensemble of samples with a field length L , a fixed atomic density N/Lw^2 and different transverse dimensions w . Figure 21, a, b, c, d, from ref. [34], present numerically computed pulse shapes corresponding to decreasing F values (with fixed T_R). For large Fresnel number (fig. 21, a), one finds of course the same results as in fig. 20, b (diffraction is then negligible since $F \gg 1$). For a Fresnel number of the order of unity (fig. 21, b and c), one notices a slight increase in emission delay and a reduction of the remaining ringings (for $F = 0.4$, the pulse delay is $\sim 55T_R$, as compared to $\sim 35T_R$ in the one-dimensional solution model). These changes become even

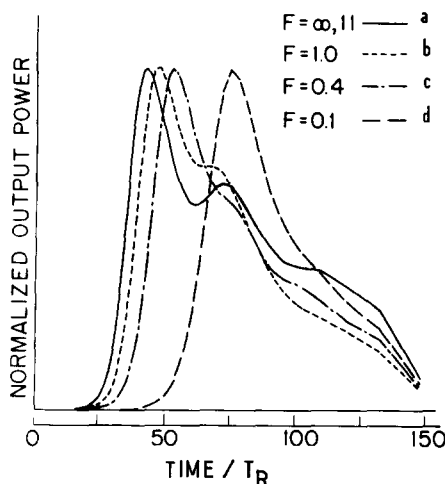


Fig. 21. Time variation of superradiant pulses for various values of the Fresnel number F for $N = 10^8$ atoms (from ref. [34]). Transverse terms in the Maxwell equation are included, with a Gaussian transverse population distribution and a uniform tipping angle initial condition. Traces a, b, c, d correspond to the decreasing F values indicated on the figure.

more important for smaller F values (fig. 21, d) for which one obtains longer delays, narrower pulse widths with a pulse shape becoming more and more symmetrical.

It is indeed possible to understand the results corresponding to small F values by using a simpler model [10, 90], replacing the diffraction term in eq. (6.97) by a “loss term” describing the “escape” of the electromagnetic field occurring over a characteristic “diffraction length” L_{diff} , the Maxwell equation (6.97) being replaced by:

$$\frac{\partial}{\partial z} \mathcal{E}_{\text{cl}} + \frac{\mathcal{E}_{\text{cl}}}{L_{\text{diff}}} = \frac{i\omega_0}{2\epsilon_0 c} \mathcal{D}_{\text{cl}}. \quad (6.107)$$

The diffracted field, for small F values, does indeed transversally extend over a distance much larger than w , which makes it possible to assume that all atoms, independently of their transverse location, see the same field. As a consequence, it seems logical that the one-dimensional propagation model should become valid provided one adds-up a diffraction loss term accounting for the field divergence. To estimate the L_{diff} parameter, we have to compute the length $L_{\text{diff}}/2$ over which an emitted photon leaves the medium. The intensity diffraction angle of emission being $\theta_D = \lambda/(\sqrt{2}\pi w)$, one has obviously:

$$\frac{1}{2}L_{\text{diff}} \cdot \theta_D \sim w$$

or else:

$$(L/L_{\text{diff}}) \times F \simeq 0.35 \quad (6.108)$$

(ref. [87] gives a similar relation between L_{diff} and F).

Eq. (6.108) means that the sample may be divided in $L/L_{\text{diff}} \sim 1/3F$ sections of length L_{diff} , each having a partial Fresnel number $\pi w^2/\lambda L_{\text{diff}} \sim 0.35$. Changing the Fresnel number F with a fixed length L thus amounts to change proportionally the L_{diff} coefficient in eq. (6.107). Fig. 22, a, b, c and d present the numerical solutions for the total light emission at the end of the sample corresponding to this loss-factor model for $L/L_{\text{diff}} = 0, 1, 5$ and 10 . The small L/L_{diff} solution (fig. 22, a; small loss case) not surprisingly yields a solution identical to the one-dimensional model of superradiance (fig. 18 or 20, a). For larger L/L_{diff} values (fig. 22, c and d; larger loss factor), one gets pulse shapes looking more and

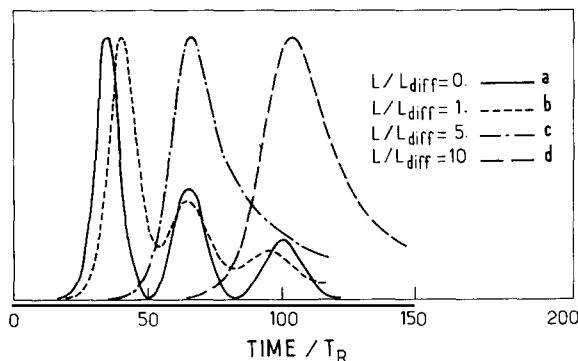


Fig. 22. Numerical solutions of the loss factor models for increasing values of L/L_{diff} . Traces a, b, c, d correspond respectively to $L/L_{\text{diff}} = 0, 1, 5, 10$.

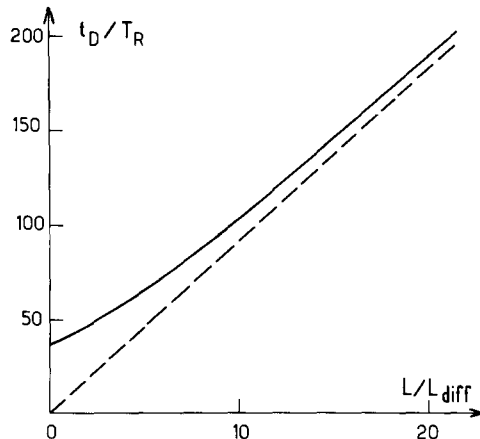


Fig. 23. Pulse delay for a fixed T_R value as a function of L/L_{diff} in the loss factor model (solid line) for $N = 10^8$. The dashed line represents the delay in the mean-field model with an effective superradiant time $T'_R = \frac{1}{2}(L/L_{\text{diff}})T_R$.

more like the solution of the diffraction equation (6.97) (compare with fig. 21, d). The loss term, as does the “true” diffraction term, reduces the coherent ringings and lengthens the pulse delay, making the pulse shape more symmetrical.

Figure 23 represents the variation of the pulse delay as a function of $L/L_{\text{diff}} \sim F^{-1}$ for a fixed T_R value, as it is given by this model. For a very small Fresnel number ($L/L_{\text{diff}} > 10$), the delay appears to increase linearly with L/L_{diff} and becomes close to $\frac{1}{2}(L/L_{\text{diff}})T_R \log N$ (dashed line). The correspondence between L_{diff} and F , established by intuitive arguments above (eq. (6.108)) can now be derived more precisely by comparing for $F \ll 1$ the respective delays of the numerical solutions of eqs. (6.97) and (6.107) (true diffraction and loss factor models respectively). For $F = 0.0125$, one gets for example $\tau_D = 250T_R$ by solving eq. (6.97); this delay corresponds to a diffraction loss factor $L/L_{\text{diff}} = 27$ and to a product $(L/L_{\text{diff}}) \times F = 0.33$, in fair agreement with eq. (6.108).

The asymptotic behaviour of the pulse shape and delay for small F values can be understood very easily. For small F (i.e. small L_{diff} values), the loss factor is so large that the $\mathcal{E}_{\text{cl}}/L_{\text{diff}}$ term dominates the $\partial\mathcal{E}_{\text{cl}}/\partial z$ one in eq. (6.107) which can thus be neglected. As a result, \mathcal{E}_{cl} becomes merely proportional to \mathcal{P}_{cl} (and z independent) and one retrieves the simple result of the mean-field model with L being replaced by $L_{\text{diff}}/2$ and T_R by $\frac{1}{2}(L/L_{\text{diff}})T_R$.

The field expression is now (compare with eq. (6.33)):

$$\mathcal{E}_{\text{cl}} = \frac{i\omega_0}{2\varepsilon_0 c} L_{\text{diff}} \mathcal{P}_{\text{cl}}. \quad (6.109)$$

In other words, a *very small Fresnel number medium tends to asymptotically obey the equation of mean-field superradiance* with an effective superradiant time $T'_R = \frac{1}{2}(L/L_{\text{diff}})T_R$, i.e. with an average superradiance delay varying as $\frac{1}{2}L/L_{\text{diff}} \propto F^{-1}$. These results are qualitatively in agreement with the model of a medium divided into $\sim(3F)^{-1}$ sections with a partial Fresnel number of the order of unity, each of them containing $\sim N/3F$ atoms and emitting practically independently from each other (since the field emitted by one section leaves the medium before entering into the next one).

(iii) *Off-axis emission in large Fresnel number samples*

In order to study the effect of non-axial emission in the case of a large Fresnel number, it is necessary to deal both with the non-axial term in eq. (6.97) and with the initial transverse fluctuations of \mathcal{P}_{cl} . The study of this problem, which offers the maximum computational difficulties is presently under progress. A complete analysis of the phenomenon involves indeed a very large amount of calculations since the number of observable quantities is formidable: one can consider the field received at a given spot and observed by a point-size detector whose location can be varied in front of the medium; one can also consider the total field integrated over all possible directions. For each of these observables, one can define fluctuations in intensity, delay, pulse shape, etc. Correlations between fields emitted in various directions might also be considered and all these quantities should be studied as a function of the Fresnel number F .

Quite generally, and without entering into too much details, it is expected to get for each realization of the experiment a directive emission (within an angle of the order of θ_d), with large shot to shot fluctuations of the emission direction (within a solid angle of the order of θ_G or smaller if non-linear mode coupling effects are significant). At the same time, a partial washing out of the coherent ringings in each realization of the experiment is also expected.

6.4.5. Propagation in the two opposite directions

We briefly consider here another complication of three-dimensional pencil-shaped sample superradiance: the possibility for the emission to take place in two opposite directions along the positive and negative Oz axis. Clearly, the formalism developed above can be generalized to include this possibility, the electric field being now the sum of two counterpropagating (left and right) components:

$$E^{\pm(\text{rad})}(x, y, z, \tau) = \mathcal{E}_{(q=+1)}^{\pm}(x, y, z, \tau) \exp\{\mp i(\omega_0 t - k_0 z)\} \boldsymbol{\epsilon}_a + \mathcal{E}_{(q=-1)}^{\pm}(x, y, z, \tau) \exp\{\mp i(\omega_0 t + k_0 z)\} \boldsymbol{\epsilon}_a \quad (6.110)$$

with a similar definition for P :

$$P^{\pm}(x, y, z, \tau) = \sum_{q \text{ odd}} \mathcal{P}_q^{\pm}(x, y, z, \tau) \exp\{\pm i(\omega_0 t - qk_0 z)\} \boldsymbol{\epsilon}_a. \quad (6.111)$$

Furthermore, the inversion population operator will write now:

$$\mathcal{N}(x, y, z, \tau) = \sum_{q \text{ even}} \mathcal{N}_{(q)}(x, y, z, \tau) e^{iqk_0 z} \quad (6.112)$$

(as \mathcal{N} is a real quantity, one has $\mathcal{N}_{(q)} = \mathcal{N}_{(-q)}^*$). The new modulated contributions, ($\mathcal{N}_{(q)}$ with $q \neq 0$) describe a spatial modulation of the inversion density resulting from the creation of a standing wave in the medium which, through non-linear atom-field coupling, induces a population grating. Replacing E , P and \mathcal{N} by their expressions in the Bloch-Maxwell equations (3.27), (3.29) and (3.30) and making the usual slow varying approximations, one gets non-linear equations generalizing (6.16) and (6.97) and coupling now $\mathcal{E}_{(q=\pm 1)}$ to $\mathcal{P}_{(q \text{ odd})}$ and $\mathcal{N}_{(q \text{ even})}$. These equations should be numerically solved according to the method described above in the running wave case.

These equations have indeed been solved – under a simplified version neglecting the population grating contributions ($\mathcal{N}_{(q \neq 0)} = 0$) in ref. [30] – and calculations including these contributions are

planned. These calculations should yield for each realization of the superradiant experiment, two opposite pulses with random intensities, delays and shapes. A new type of correlation has to be calculated, namely the “forward-backward” one concerning intensities, pulse delays, ringing contrast. In fact, the conclusion which seems to emerge from preliminary calculations is that the two counter-propagating pulses corresponding to a single superradiant event behave to a large extent as two independent superradiant pulses, the correlations between the two pulses being very small. This numerical result can be understood by noticing that both pulses are triggered by independent fluctuations (corresponding to left and right propagating polarization waves respectively) and that the first maximum of the pulse emission in a given direction is essentially radiated by the atoms close to the corresponding sample end (see discussion of section 6.3). These atoms have undergone a negligible interaction with the field amplified in the other direction and emitted by atoms located at the other sample end. In other words, neither the quantum initiation, nor the classical non-linear stage of the superradiant pulse evolution do couple efficiently these two pulses.

6.5. Superradiance equations taking into account competing effects:

Doppler shifts, spontaneous emission in off-axis directions or on other transitions

[11, 17, 31, 32, 41, 84, 86]

To conclude this section, we indicate briefly how one can add to the superradiance equations analysed in the previous sections the terms describing effects neglected in this study: Doppler dephasing due to atomic motion, spontaneous emission along modes \mathbf{k} very different from \mathbf{k}_0 or emission towards levels g' different from g , collisions.

In order to deal with the effects due to atomic motion, one has to divide the atom ensemble into atomic velocity groups corresponding each to a given value v of the velocity along the sample axis. For a thermal distribution, v is distributed over an interval symmetrical around $v = 0$, of the order of $\Delta v = \sqrt{k_B T/M}$ where T is the atom temperature and M the atomic mass. We thus define new atomic operators \mathcal{P}_v^\pm and \mathcal{N}_v depending on x , y , z , τ and v . The Bloch–Maxwell equation obeyed by these operators can be simply generalized from eqs. (6.17) and (6.97). If one neglects the existence of a counterrunning wave, one gets for example [31]:

$$\frac{\partial \mathcal{N}_v}{\partial \tau} = \frac{i}{\hbar} [\mathcal{P}_v^+ \mathcal{E}^+ - \mathcal{E}^- \mathcal{P}_v^-] \quad (6.113)$$

$$\frac{\partial \mathcal{P}_v^+}{\partial \tau} = ikv \mathcal{P}_v^+ + \frac{2id^2}{\hbar} \mathcal{E}^- \mathcal{N}_v \quad (6.114)$$

$$\frac{\partial \mathcal{E}^+}{\partial z} + \frac{i}{2k_0} \left(\frac{\partial^2}{\partial x^2} + \frac{\partial^2}{\partial y^2} \right) \mathcal{E}^+ = \frac{i\omega_0}{2\varepsilon_0 c} \int \mathcal{P}_v^- \mathcal{F}(v) dv \quad (6.115)$$

where $\mathcal{F}(v)$ is the Boltzmann velocity distribution.

The Doppler shift of atoms with velocity v appears in the new $ikv \mathcal{P}_v^+$ term in the Bloch equation (6.114). The various velocity groups are non-linearly coupled to each other via their interaction with the common electromagnetic field.

Relaxation due to spontaneous emission along modes not taken into account in the $\mathbf{k} \sim \mathbf{k}_0$ summation (transverse spontaneous emission on the $e \rightarrow g$ transition) and spontaneous emission towards other g'

levels results in a damping of the e and g levels with a total rate:

$$\Gamma_e = \Gamma + \sum_{g' \neq g} \Gamma_{e \rightarrow g'} \quad (6.116)$$

$$\Gamma_g = \sum_{g' \neq g} \Gamma_{g \rightarrow g'} \quad (6.117)$$

These decays can be introduced in the equation by the addition of the following extra terms:

$$\frac{\partial}{\partial \tau} \mathcal{N}_v = - \left(\frac{\gamma + \Gamma}{2} \right) \mathcal{N}_v - \left(\frac{\gamma' + \Gamma}{2} \right) \left(\frac{\mathcal{N}_e + \mathcal{N}_g}{2} \right)_v \quad (6.118)$$

$$\frac{\partial}{\partial \tau} \mathcal{P}_v^\pm = - \frac{\gamma^*}{2} \mathcal{P}_v^\pm \quad (6.119)$$

$$\frac{\partial}{\partial \tau} \left(\frac{\mathcal{N}_e + \mathcal{N}_g}{2} \right)_v = - \left(\frac{\gamma - \Gamma}{2} \right) \left(\frac{\mathcal{N}_e + \mathcal{N}_g}{2} \right)_v - \left(\frac{\gamma' - \Gamma}{2} \right) \mathcal{N}_v \quad (6.120)$$

with

$$\gamma = \gamma^* = \Gamma_e + \Gamma_g \quad (6.121)$$

$$\gamma' = \Gamma_e - \Gamma_g \quad (6.122)$$

(in (6.118) and (6.120), \mathcal{N}_e and \mathcal{N}_g represent the respective population density operators in the upper and lower levels: $\mathcal{N}_e = (\pi w^2)^{-1} \cdot \sum_i D_i^+ D_i^- \cdot \delta_e(z - z_i)$).

Similarly, other relaxation mechanisms such as collisions can be added in order to provide a complete description of the phenomenon. γ , γ' and γ^* have then to be slightly modified (in particular the equality $\gamma = \gamma^*$ does not remain necessary valid). Clearly the new terms described by eqs. (6.117), (6.118), (6.119) and (6.120) will have a negligible effect on the system evolution if the condition:

$$t_D^{-1}, T_R^{-1} \gg \gamma, \gamma', \gamma^*, k_0 \Delta v \quad (6.123)$$

is fulfilled, which means that the superradiant decay occurs faster than these other processes. This is the situation implicitly assumed throughout this review. If it is not the case, these extra terms contribute to alter the shape, delay and statistics of the superradiant emission in a more or less simple way.

If T_R^{-1} or t_D^{-1} becomes smaller than γ , γ' , γ^* or $k_0 \Delta v$, these dephasing effects will obviously tend to destroy the phase matching responsible for superradiance and the system will rather evolve as an ensemble of independent emitters (ordinary fluorescence). Thus, the condition for superradiance *threshold* expresses that $T_R^{-1} = NT\mu$ is large enough (t_D is roughly proportional to T_R). The exact value of the threshold depends on sample shape, respective importance of Doppler and natural widths, and condition (6.123) puts – as expected – a lower limit to the number of atoms in the superradiant sample.

7. Discussion of the “slow variation-approximations”: The various regimes of superradiance

In this section, we intend to discuss the validity of the Born–Markov and slow varying envelopes approximations made to obtain the equations whose solutions have been presented in sections 5 and 6. It is not necessary to have read this section to understand the material of sections 8 and 9.

The characteristic superradiance time has been shown in sections 5 and 6 to be $(N\Gamma)^{-1}$ or $T_R = (N\Gamma\mu)^{-1}$ in the small sample and large pencil-shaped sample cases respectively. It can in principle be made as small as desired by merely increasing N enough. Obviously, at some point, the slow variation assumptions made to derive the evolution equation of the superradiant system in the Schrödinger or in the Heisenberg picture become no longer valid and the theory developed in previous sections breaks down. It is interesting to understand what happens in that case, both theoretically and practically: is it possible to describe the phenomenon of superradiance beyond the N values for which the slow variation approximations are satisfied? Is it possible to experimentally realize and observe physical situations corresponding to these new N domains? We will analyse here this problem and show that, in large sample superradiance, one can actually distinguish various regimes of emission associated to successive domains of N values. The transitions between these various regimes correspond to critical numbers of atoms which are functions of the optical wavelength and of the size of the emitting sample. One of these critical numbers, which has already been encountered in the previous section, corresponds to the Arecchi–Courtens limit (eq. (6.21)). A careful analysis of the slow variation approximation shows that the Arecchi–Courtens limit is only one of many such transitions occurring when N is increased from very small to very large values. We will show that the physical quantities which can be actually calculated and measured in an experiment depend upon the N -domain one considers, which will give a strong physical basis to the division of superradiance into these various regimes. For small enough N values, we will see that one could in principle determine and measure all the correlation functions of the electromagnetic field (or of the atomic polarization) in photon-counting type experiments: this is what we will call the “microscopic” domain of superradiance which could be considered as a mere extension to the many-atom case of single-atom spontaneous emission. For large N values, the successive photons are emitted so close to each other that it is no longer possible, even in principle, to count them separately. One then finds “macroscopic regimes” of superradiance in which only large scale observables such as the total field amplitudes or the macroscopic local atomic polarization and their lowest order correlation functions can be calculated and measured. This is the regime of all superradiance experiments performed so far. At last, for very large N values, the atoms can no longer be considered as individual radiators coupled through their common radiation field and short range interactions (including electron exchange) not included in the Hamiltonian of eq. (3.6) have to be taken into account, leading to a complete collapse of the superradiance description presented in this report. The distinction between these different regimes of superradiance will be shown to depend upon the point of view one chooses in order to describe the system evolution: since the observables introduced in the Schrödinger and in the Heisenberg pictures differ by the time at which they are defined (t or τ), the transition between the various regimes is different in the two points of view. This will lead us to consider successively the Schrödinger and the Heisenberg pictures.

7.1. Validity of the Schrödinger picture: The break-down of the Born–Markov approximation

The rate equations (3.18) and (6.9) have been obtained under the assumption that the correlation time τ_c of the emission process is “short enough” compared to the characteristic evolution time of the superradiant system (τ_c is of the order of λ/c or L/c for small sample and large pencil-shaped samples respectively). This approximation, known as the Born–Markov one, is simply expressed by writing in the right-hand side of eq. (3.14) the global density matrix $\tilde{\phi}(t - \tau)$ as:

$$\tilde{\phi}(t - \tau) = \tilde{\phi}(t) - \tau\tilde{\phi}'(t) + \dots \quad (7.1)$$

with

$$\tilde{\phi}(t) = \tilde{\rho}(t) \otimes |0\rangle_R \langle 0| + \Delta\tilde{\phi}(t). \quad (7.2)$$

The Markov approximation consists in neglecting in eq. (7.1) the $-\tau\tilde{\phi}'(t)$ term describing the system evolution during the correlation time of the emission process. The Born approximation consists in neglecting the higher order $\Delta\tilde{\phi}(t)$ term which describes the correlation build-up between the atomic system and the field. Both approximations should be made at once, since the neglected $-\tau\tilde{\phi}'(t)$ and $\Delta\tilde{\phi}(t)$ terms are quite generally of the same order of magnitude [75]. The condition for the Markov approximation validity in the mean-field case can be found by the very simple following argument. According to eq. (5.33), the matrix element $\rho_M(t)$ has the following logarithmic derivative at time $t = 0$:

$$\frac{d}{dt} \text{Log } \rho_M \Big|_{t=0} = \frac{1}{\rho_M} \frac{d\rho_M}{dt} \Big|_{t=0} \sim \frac{1}{T_R} \frac{N(N-2M)}{N+2M}. \quad (7.3)$$

(Here $T_R = (NT\mu)^{-1}$ with $\mu = 1$ in the small sample case and $\mu = 3\lambda^2/8\pi^2w^2$ in the pencil-shaped case.) For matrix elements with $M \ll N$, this corresponds to a logarithmic increase rate of the order of N/T_R . Accordingly, the Markov approximation correctly describes the ρ_M matrix element evolution for $M \ll N$ if the sufficient condition:

$$N/T_R \ll 1/\tau_c \quad (7.4)$$

is fulfilled. In terms of atom numbers, this condition reads:

$$N < (c/\Gamma\lambda)^{1/2} \quad (7.5)$$

for the small sample superradiance case, and:

$$N < (c/\Gamma\mu L)^{1/2} = (8\pi c/3\Gamma\lambda)^{1/2} \quad (7.6)$$

for the case of a large pencil-shaped sample with a Fresnel number 1 ($\mu L = (3\lambda^2/8\pi w^2)L = (3/8\pi)\lambda$). (We assume here a mean-field model description, so that the density matrix evolution of the system is ruled by eq. (6.29) very similarly to eq. (4.7).

As for the Born approximation, an estimate of the $\Delta\tilde{\phi}(t)$ term shows that its matrix elements are of the order of $N\tau_c/T_R$ times smaller than those of $\tilde{\rho}(t)$, which justifies that one can indeed neglect $\Delta\tilde{\phi}(t)$ as soon as the Markov condition (7.4) is fulfilled. This condition can be understood physically in a very simple way: in the mean field model, the superradiant emission can be seen as a cascade emission down the ladder of states of fig. 4. Each step down is a process with a “memory time” of the order of τ_c . The convolution of the N steps corresponds to a global memory time $N\tau_c$. The Markov approximation is thus certainly valid if $N\tau_c$ is shorter than the overall evolution time of the order of T_R : one finds thus again condition (7.4).

The break-down of the Markov condition for the calculation of the ρ_M coefficients can also be checked by numerical computation. One replaces eq. (4.7) by an integrodifferential equation with a kernel $\kappa(\tau)$ of width τ_c , mimicking the finite memory time of the system:

$$\begin{aligned} \frac{d}{dt} \rho_M = & -\frac{1}{T_R} (J+M)(J-M+1) \int_0^t \rho_M(t-\tau) k(\tau) d\tau \\ & + \frac{1}{T_R} (J+M+1)(J-M) \int_0^t \rho_{M+1}(t-\tau) \kappa(\tau) d\tau \end{aligned} \quad (7.7)$$

and one numerically solves this equation for a given finite number of atoms [89]. When condition (7.4) is not fulfilled, the obtained solution departs from the solution (5.33) and starts to develop strong oscillations reflecting the effect of the finite memory time. These non-physical oscillations (which can even yield negative values for ρ_M) are corrected by the higher order terms in the Born expansion ($\Delta\tilde{\phi}(t)$), which also become important when eq. (7.4) is not satisfied.

For most superradiant systems, condition (7.5) or (7.6) imposes an upper limit to the number of atoms of the order of 10^3 to 10^4 . This condition is not very restrictive for *small sample superradiance*, since so many atoms distributed along a ring with a perimeter l smaller than λ would correspond to an interatomic distance l/N of the order of or smaller than a characteristic atom size: condition (7.5) is thus certainly fulfilled if one considers independent well separated radiators interacting through their common radiation field (the case of closely spaced atoms with interpenetrating orbitals which would not satisfy condition (7.5) is clearly beyond the description of this paper, since the Hamiltonian H does not include interatomic close coupling terms. The dominant process would not be in that case the radiative one and one could not term it “superradiance”).

The situation is however very different for large sample superradiance for which, in all experiments so far, the atom number exceeds the limit (7.6) which we will call “the restrictive Born–Markov condition”. The question is then to understand what happens beyond this restrictive limit. In fact, one is interested not in the matrix elements themselves, but rather in an expectation value of some physical observables (atomic energy, light intensity, etc.) which is expressed as a linear superposition of a large number of ρ_M with different M values. In such superpositions, the fast logarithmic rate components of the ρ_M cancel out. For example, the light intensity $\langle I \rangle = \sum_M M d\rho_M/dt$ appears as a weighted average of hyperbolic secant curves (see eq. (5.34)), whose logarithmic increase rate is only $1/T_R$ (and not N/T_R). In other words, the non-physical oscillations which develop in ρ_M in the non-Markovian eq. (7.7) are washed out in the superposition of ρ_M ’s occurring in the expression of the measured quantities [24, 89]. In the same way, it can be shown that the higher order term in the Born expansion of the evolution equation for these quantities cancels out. For these observables, which we will call “slow observables” as opposed to the “fast varying” matrix elements of ρ , the true Born–Markov condition appears to be $T_R > L/c$ or:

$$N < c/L\Gamma\mu \approx 8\pi c/3\lambda\Gamma \quad (7.8)$$

which is the already encountered Arecchi–Courtens condition (eq. (6.21)). When N satisfies condition (7.8), but not condition (7.6), one can still use the rate equation (6.29) provided one is aware that the $\rho_M(t)$ determined by these equations are intermediate steps in the calculation of slow varying linear superpositions. (Note that we are in this section reasoning on the mean-field equations and not on the one-dimensional propagation one. The evolution times of both models being of the same order, our conclusions obviously apply to both cases.)

Since we are not able, beyond the limit of equation (7.6), to accurately calculate individual matrix elements of the atomic system, it is important to discuss the “physical reality” of these quantities. If instead of measuring a “slow varying” observable such as the total light emitted, one wants to “measure” ρ_M , one would have to count the number of photons emitted by the system up to a time t and to determine, by a large set of identical experiments, the probability for this number to be equal to $J - M$. Such a hypothetical experiment would require a detection procedure whose “response time” δt is fast enough to resolve N photons in a time T_R :

$$\delta t < T_R/N. \quad (7.9)$$

At the same time, there will always be an intrinsic uncertainty of the order of L/c on the definition of the emission time t , since a photon detected at time t_0 at the end of the cell might have been emitted any time between t_0 and $t_0 - L/c$ by the collective atomic system:

$$\delta t > L/c. \quad (7.10)$$

For conditions (7.9) and (7.10) to be compatible, the restrictive Born–Markov condition (7.6) has to be satisfied. In other words, beyond condition (7.6) not only we do not know how to calculate exactly the evolution of the $\rho_M(t)$ defined at a unique time t for the whole sample, but we are unable to measure them by photon counting. This is a quite interesting and fortunate result, which amounts to say that we are able in fact to calculate all the quantities of physical interest up to the Arecchi–Courtens limit (6.21).

7.2. Validity of the Heisenberg picture: The break-down of the slow varying envelope approximation

Let us now resume the discussion in the Heisenberg picture. The quantities \mathcal{E} , \mathcal{P} , \mathcal{N} are typically slow varying observables (with a time constant $\sim T_R$) whose evolution equations are valid under the “slow varying envelope” condition (6.19). This condition is the counterpart of the “weak” Born–Markov (or Arecchi–Courtens) condition (7.8) with L being replaced by λ . As λ is much smaller than L , the validity condition (6.19) is less restrictive than in the Schrödinger picture. This is not surprising, since we are dealing here with *local* operators defined in terms of retarded time τ instead of *collective* observables defined at a single time t . The correlation time (which is the intrinsic duration of each photon process) is thus λ/c instead of L/c . If the more restrictive Arecchi–Courtens condition (6.21) is also fulfilled, not only are the Bloch–Maxwell equations valid, but one can also replace in them τ by t and the Schrödinger and Heisenberg pictures become completely equivalent (see section 6).

What are, in the Heisenberg picture, the counterparts of the ρ_M quantities? Photon counting signals correspond in this picture to high-order correlation expectation values such as:

$$\langle \mathcal{E}^+(\tau_1) \mathcal{E}^+(\tau_2) \cdots \mathcal{E}^+(\tau_n) \mathcal{E}(\tau_n) \cdots \mathcal{E}(\tau_2) \mathcal{E}(\tau_1) \rangle$$

which represents for example the probability of detecting a series of photons at times $\tau_1, \tau_2, \dots, \tau_N$. Such a quantity, which appears as a high power of \mathcal{E} or \mathcal{P} operators, has at most a time rate of evolution of the order of N/T_R (for an N photon correlation signal) and will be measurable only if the condition:

$$N/T_R > \lambda/c \quad (7.11)$$

is fulfilled. Here again, we find a condition similar to the corresponding Schrödinger case (eq. (7.6)) with L being replaced by λ . Since the shortest possible detection time is, for any kind of detector, at least of the order of λ/c , it is again clear in this picture that if condition (7.11) is not fulfilled, the corresponding quantities loose their physical meaning.

7.3. The various regimes of large sample superradiance

The above discussion leads us quite naturally to distinguish various domains of superradiance when N is increased for a cylindrical atomic sample of fixed shape and size. We have to consider separately the cases of an instantaneous system excitation at time $t = 0$ and the case of a swept excitation along the medium at $\tau = t - z/c = 0$ (see fig. 14).

7.3.1. Instantaneous transverse excitation of the whole sample

The following situations are successively encountered when N is increased:

$$(i) \text{ if } N < (c/L\Gamma\mu)^{1/2}. \quad (\text{condition 7.6})$$

The restrictive Born–Markov condition is fulfilled in the Schrödinger picture. One can calculate by rate equations and (at least in principle) measure any matrix element of the collective system. Photon correlation experiments involving the detection of all the photons and the determination of their emission times are possible and calculable. This case corresponds to what we call “microscopic superradiance”, starting in principle from a system of two atoms, up to a few hundred.

Note that in this case, there is no physical difference to be made between t and τ and hence no distinction between instantaneous and swept excitation.

$$(ii) \text{ if } [c/L\Gamma\mu]^{1/2} < N < [c/\lambda\Gamma\mu]^{1/2}. \quad (7.12)$$

The high-order correlation functions cannot any longer be measured in terms of the actual emission time t , but can still be determined in terms of the retarded time τ (i.e., one cannot for these quantities deduce the time t at which the processes have actually occurred in the medium from the time the photons have been received by the detector). This means that the equivalence between t and τ breaks down for the high-order correlation photon experiments, which should be calculated in the Heisenberg and not in the Schrödinger picture. The equivalence remains however for the “slow observable” like $\mathcal{E}, \mathcal{P}, \mathcal{N}$ which evolve with the time constant T_R .

$$(iii) \text{ if } (c/\lambda\Gamma\mu)^{1/2} < N < c/L\Gamma\mu. \quad (7.13)$$

One can only measure the “slow observables” such as $\mathcal{E}, \mathcal{P}, \mathcal{N}$ and no longer try to determine all the photon arrival times on a detector. For these “slow observables”, t and τ are still equivalent and there is no difference between longitudinal and transverse excitation. The Schrödinger and Heisenberg pictures can be used.

$$(iv) \text{ if } c/L\Gamma\mu < N < (c/\lambda\Gamma\mu)(L/\lambda). \quad (7.14)$$

The Arecchi–Courtens condition is now also violated. This situation has not been explicitly considered

in section 6. Let us discuss briefly what happens in this case. The identity between t and τ breaks down, even for “slow observables”. One can still study the evolution of these observables in terms of the retarded time τ in the Heisenberg picture (the Schrödinger picture is no longer valid even for the slow observables). As the superradiance time T_R is now shorter than the light propagation time through the medium, the notion of collective emission of the whole system becomes meaningless (if the medium is instantaneously excited). Each part of the system now emits before having interacted with the rest of the sample: the superradiance is “broken”. The random initial conditions have of course to be chosen independently in the various slices of the sample. The maximum length l of each slice should contain at most N' atoms such that the corresponding partial superradiance time $T'_R = T_R N/N'$ satisfies in the slice the Arecchi–Courtens limit:

$$T'_R = T_R N/N' = T_R L/l > l/c \quad (7.15)$$

(it has been noted in section 6 that a division into smaller slices will not appreciably change the description of the phenomenon). The minimum number of slices is thus $(L/cT_R)^{1/2} = (N\Gamma\mu L/c)^{1/2}$. The characteristic evolution time of each piece of the medium is then:

$$T'_R = (T_R L/c)^{1/2} \quad (7.16)$$

and the signal is made of a random succession of pulses each of which has a characteristic duration $T'_R > T_R$. The statistics of these pulses could be easily determined by the numerical calculation of a large number of classical trajectories.

$$(v) \text{ if at last } N > (c/\lambda\Gamma\mu)(L/\lambda). \quad (7.17)$$

The “slow envelope” approximation breaks down even for the “broken superradiance” phenomenon, since one has now:

$$T'_R = (T_R L/c)^{1/2} = (L/N\Gamma\mu c)^{1/2} < \lambda/c. \quad (7.18)$$

One cannot use any longer the Heisenberg equations. This regime is not physical: in order to observe it, one would have to realize the inversion of the medium in a time shorter than the optical period. More basically, condition (7.18) can be written as:

$$N/Lw^2 \geq 1/\alpha a_0^2 \lambda \quad (7.19)$$

where a_0 is the typical atomic size (Bohr radius) and α the fine structure constant ($\alpha = q^2/4\pi\epsilon_0\hbar c$). To get this condition, we have replaced Γ and μ in eq. (7.18) by their expressions (4.5) and (6.10) and the dipole matrix element d in Γ by its order of magnitude qa_0 . Remarking now that $\alpha\lambda$ is also of the order of a_0 , we find that the atom density N/Lw^2 has to be larger than one atom per a_0^3 , which means that the atoms are closely packed with interatomic distance of the order of their sizes. It is clear that the formalism developed in this article, which considers each atom as an isolated system interacting with the field emitted by the others, is no longer valid in this case. One should then take into account short range interaction, wave function overlapping and so on.

7.3.2. Swept excitation

If instead of having an instantaneous excitation at time $t = 0$, one performs a longitudinal excitation, swept through the medium at time $\tau = 0$, the description of the phenomenon for the slow varying observables is not modified below the Arecchi–Courtens limit (eq. (6.21)). Above it, the physics of the superradiance phenomenon is strongly modified. Contrary to what happens in the instantaneous excitation case, the Heisenberg equations of motion and their initial conditions remain the same below and above this limit. The medium can still behave collectively as a whole for N larger than $c/L\Gamma\mu$ since the excitation “follows” the superradiant signal along the sample: the system starts on the random polarization in the first slices excited by the pulse inverting the system. The shape and the statistics of the emitted pulse is then identical to the one calculated in subsection 6.3. The phenomenon occurs as if the medium was “compressed” along the propagation direction [90]. The emission time is then T_R , shorter than T'_R . The theoretical compression limit of the pulse is $T_R = \lambda/c$. Above this value, the Heisenberg description (slow envelope) breaks down.

8. Superradiance in multilevel systems, light beating and polarization effects

In most realistic cases, the superradiant medium is an ensemble of multilevel atoms more complex than the two-level atom system considered in the previous sections. As a result, the emission might exhibit new interesting features, lacking in the two-level case: emission of successive pulses of different wavelengths on cascading transitions, competition between different polarizations, light beating between nearly degenerate transitions. The two-level atom formalism can be easily generalized to describe all these effects. In this section, we discuss some of the phenomena expected in multilevel system superradiance, we present the equations which allow us to describe them and – as an illustration – we analyse in detail some simple effects.

8.1. Description of multilevel systems with various types of initial preparation

Figure 24 shows various possible cases of multilevel superradiance. The emission can occur successively on two cascading transitions at two different frequencies ω_1 and ω_2 (fig. 24a), or two transitions with different frequencies sharing a common upper level can be in competition for the depletion of this

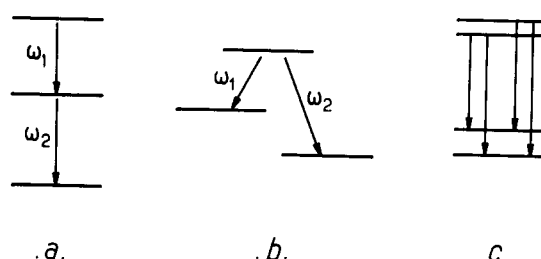


Fig. 24. Various level schemes in which multilevel superradiance can occur: (a) cascading transitions, (b) competing transitions, (c) degenerate or quasi-degenerate level superradiance.

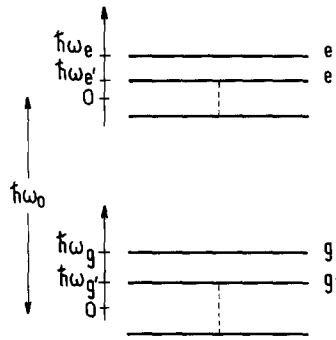


Fig. 25. Superradiance between two nearly degenerate levels. Level scheme with indication of the various frequencies: ω_0 is the average optical frequency; ω_e , $\omega_{e'}$, ω_g , $\omega_{g'}$ are the frequency splittings in the upper and lower levels.

level (fig. 24b). Another interesting and very usual situation corresponds to the case of an optical transition with degenerate or nearly degenerate upper and lower levels (fig. 24c) (contrary to the previous cases, the various transition frequencies are now considered to be very close to each other). Of course, any combination of these situations can also be considered, leading to more complex cases. Although the cascades or branching transitions can also give rise to interesting effects [25], we will restrict here our study to the very important case of fig. 24c and analyse various effects related to the degeneracy or near-degeneracy of a single optical transition.

The level scheme under consideration is specified on fig. 25. We call e, e', \dots and g, g', \dots the upper and lower sublevels of the transition, the average frequency of which is ω_0 . We call $\hbar\omega_e, \hbar\omega_{e'}, \dots$ and $\hbar\omega_g, \hbar\omega_{g'}, \dots$ the energies of the upper and lower levels respectively, each of these energies being measured with respect to the average energy of the corresponding level. The transition frequency between level e and g is thus:

$$\omega_{eg} = \omega_0 + (\omega_e - \omega_g) \quad (8.1)$$

and one assumes the inequalities:

$$\omega_e, \omega_{e'}, \omega_g, \omega_{g'}, \dots \ll \omega_0 \quad (8.2)$$

which means that the upper and lower levels are nearly degenerate. We call $d_{eg}\epsilon_{eg}$ the electric dipole between levels e and g , ϵ_{eg} being a (complex) unit vector defining the polarization of this transition (we assume $d_{ee'} = d_{gg'} = 0$).

At time $t = 0$, each atom of the system is prepared in some initial state corresponding to a total inversion of the transition (no atoms in levels g, g', g'', \dots). In order to specify this preparation, it is convenient to introduce the one-atom local density matrix of the atomic system, that we will call $\rho_i(z)$. Calling:

$$\rho_i = \text{Tr}_{j \neq i} \rho \quad (8.3)$$

the partial density matrix of atom i , we define $\rho_i(z_p)$ in the p th slice of the medium as the average of the

density matrices of all the atoms belonging to this slice:

$$\rho_1(z_p) = \frac{1}{N_p} \sum_{i \in \text{slice } p} \rho_i \quad (8.4)$$

(where N_p is, as in section 6, the number of atoms in the p th slice). $\rho_1(z)$, which is a one-particle quantity, should not be confused with the total density matrix ρ of the atomic system defined in section 3.

At time $\tau = 0$, the system is supposed to be homogeneously excited:

$$\rho_1(z, 0) = \text{constant} \quad (8.5)$$

and the excitation is completely specified by the value of the matrix elements $\rho_{1ee'}(\tau = 0)$ (all the $\rho_{1eg}(0)$ and $\rho_{1gg}(0)$ are zero). As an illustration, we consider below several simple typical situations involving three or four level systems (see fig. 26). On fig. 26a, we have represented the situation of a “λ-shaped” transition with a near-degeneracy in the lower level only. The initial condition is then identical to the two-level atom case: all atoms are prepared in the same way in the unique e level. Figures 26b and 26c represent a “V-shaped” transition with an upper degenerate or nearly degenerate level. The initial condition might then be either a pure population excitation ($\rho_{1ee'} = 0$, fig. 26b) or a “coherent excitation” of a linear superposition of states e and e' ($\rho_{1ee'} \neq 0$, fig. 26c). In the former case, a fraction ρ_{1ee} of the atom has been prepared in sublevel e and a fraction $\rho_{1e'e'}$ in sublevel e'. These atoms can – at least in principle – be distinguished by their initial preparation. The system is then made of two classes of identical atoms superradiating together and distinguishable by the preparation process. The trace of the square of the initial density matrix is then strictly smaller than one (ρ_1 describes a “statistical mixing” of states).

In the latter case (fig. 26c), the excitation can be either “fully coherent” ($\rho_{1ee'} = \sqrt{\rho_{1ee}\rho_{1e'e'}}$; density matrix corresponding to a “pure case” with $\text{Tr } \rho_1^2 = 1$) or “partially coherent” (statistical mixture; $\rho_{1ee'} < \sqrt{\rho_{1ee}\rho_{1e'e'}}$ and $\text{Tr } \rho_1^2 < 1$). The initial state then describes an intrinsic quantum mechanical superposition within each atom, and the system cannot be analysed in terms of a statistical superposition of classes of atoms belonging to energy eigen-states. The cases a, b and c just described are simplifications of situations which occur quite generally when dealing with the superradiance of a transition between levels with non-zero angular momentum J, J' . The “coherent” or “incoherent” character of the initial excitation is then dependent upon the pumping process which initially prepares the upper J level. In the most common case of an optical excitation, the polarization of the pumping light pulse determines the initial state density matrix [91]. By conveniently choosing this polarization, one can perform either a “population excitation” ($\rho_{1ee'} = 0$) or a coherent excitation ($\rho_{1ee'} \neq 0$). At last,

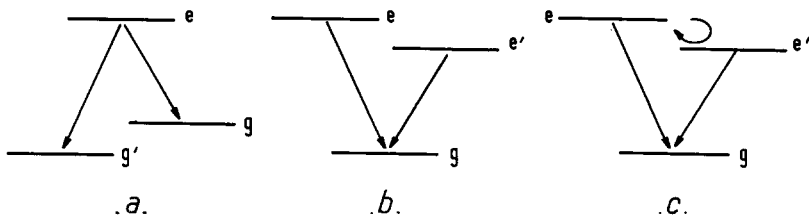


Fig. 26. Three-level superradiance schemes: (a) λ-shaped transition (one excited and two lower states); (b) V-shaped transition with pure population excitation (two excited states with $\rho_{1ee'} = 0$ and one lower state); (c) V-shaped transition with an initial coherence symbolized by the circular arrow (two excited states with $\rho_{1ee'} \neq 0$).

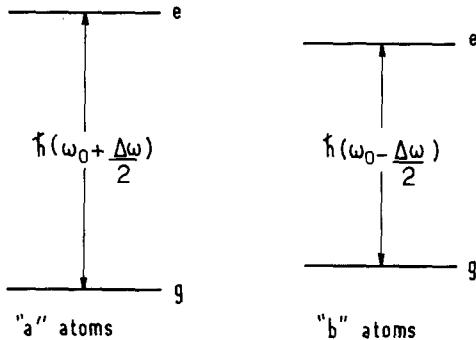


Fig. 27. Level scheme corresponding to the superradiance of a mixture of two ensembles of atoms a and b with slightly different frequencies.

fig. 27 represents a four-level system with only two allowed transitions $e \rightarrow g$ and $e' \rightarrow g'$, without initial coherence between levels e and e' . The two classes of atoms then evolve on independent transitions and this case describes the superradiance of two physically different types of atoms (such as two isotopic varieties) mixed together in the sample. For each of these cases, one can also choose the polarization ϵ_{eg} of the various competing transitions. They can be either identical ($\epsilon_{eg} \parallel \epsilon_{e'g'}$) or orthogonal ($\epsilon_{eg} \perp \epsilon_{e'g'}$). The possibilities are obviously quite numerous, which explains the wealth of physical effects which might be expected from such multilevel superradiant systems.

8.2. New physical effects in multilevel superradiance

The superradiant field radiated by the multilevel system results now from the competition and the interference of several degenerate or nearly degenerate transitions. If the degeneracy of the levels is removed, one expects to observe beatings between the various transitions giving rise to modulations of the superradiant signal. The beatings, which come from interatomic interferences are basically different from the intra-atomic quantum interference effects (quantum beats) observed on ordinary (single-atom) fluorescence light [92]. The phase of the beats and their modulation depth will obviously depend upon the nature of the initial excitation (percentage of atoms in each sublevel at $t = 0$, coherent or incoherent preparation). These beats will also undergo pulse to pulse phase and modulation depth fluctuations, reflecting the initial quantum fluctuation of the system. If the levels are degenerate, the beats will disappear, but polarization effects, not existing on two-level systems will occur. The competition between different transitions with different polarizations will result in the emission of a light field whose polarization will strongly depend upon the initial preparation of the system. This polarization might also fluctuate from one realization of the experiment to the next, due to the intrinsic randomness of the initial atomic polarization starting the system evolution.

At last, it often occurs that a complete destructive interference between the emission of various classes of atoms terminates the superradiant emission before all the atoms have decayed to the lower state. This latter effect – called limited superradiance or subradiance [49] – will be described in the next section. To summarize, there is indeed a whole stock of new effects, exhibiting a large variety of statistical fluctuations, which might be studied in the superradiance of a degenerate or nearly degenerate atomic transition. We present in the next subsection the general theoretical framework for the description of these effects.

8.3. Superradiance equations generalized to multilevel systems

We restrict here the description to the cases of the one-dimensional (or mean-field) models introduced in section 6 and make use of the Heisenberg picture. It is convenient to generalize the D_i^\pm operator of the two-level case and to define $D_i^{XX'}$ as the operator which changes in atom i the sublevel X into X' (X, X' might be any e, e', g, g'):

$$D_i^{XX'}|X\rangle_i = |X'\rangle_i. \quad (8.6)$$

In terms of these operators, the Hamiltonian of the atom + field system is now:

$$H = H_{\text{at}} + H_{\text{rad}} + V \quad (8.7)$$

with:

$$H_{\text{at}} = \sum_{i,e} \hbar(\omega_0 + \omega_e) D_i^{ee} + \sum_{i,g} \hbar\omega_g D_i^{gg} \quad (8.8)$$

$$H_{\text{rad}} = \sum_{k,\alpha} \hbar\omega_k a_{k,\epsilon_\alpha}^+ a_{k,\epsilon_\alpha} \quad (8.9)$$

$$V = \sum_{\substack{k,\alpha \\ e,g \\ i}} \sqrt{\frac{\hbar ck}{2\epsilon_0\vartheta}} [a_{k,\epsilon_\alpha} D_i^{ge} d_{ge}(\boldsymbol{\epsilon}_\alpha \cdot \boldsymbol{\epsilon}_{ge}) + a_{k,\epsilon_\alpha}^+ D_i^{eg} d_{eg}(\boldsymbol{\epsilon}_\alpha \cdot \boldsymbol{\epsilon}_{ge}^*)]. \quad (8.10)$$

It is important, in the multilevel case, to retain the vector character of the electromagnetic field:

$$\mathbf{E}^\pm = \sum_{\alpha=1,2} E_\alpha^\pm \boldsymbol{\epsilon}_\alpha \quad (8.11)$$

and to keep in (8.10) and (8.11) the summation over two orthogonal polarizations ($\alpha = 1, 2$) perpendicular to the main propagation direction k_0 .

The atomic system is now described by generalized atomic polarization operators:

$$\sigma_{XX'}(z, t) = \frac{1}{\pi w^2} \sum_i D_i^{XX'} \delta_e(z - z_i). \quad (8.12)$$

The $\sigma_{XX'}(z, t)$ describe populations and low frequency coherences if XX' both belong to the e or g manifold, and optical coherences if X and X' belong respectively to the upper and lower level. In this latter case, one introduces the slow-varying envelope operator $\tilde{\sigma}_{eg}(z, t)$ defined as:

$$\sigma_{eg}(z, t) = \tilde{\sigma}_{eg}(z, t) \exp\{-i(\omega_0 t - k_0 z)\} \quad (8.13)$$

which generalizes eq. (6.12), and in a similar way the envelope \mathcal{E}_α of the α component of the electric field operator.

From the expressions (8.8), (8.9) and (8.10) of the Hamiltonian and from the obvious commutation rules of the $D_i^{XX'}$ and a_{k,ϵ_α} operators, one readily obtains the following Heisenberg equations which

generalize eqs. (6.13), (6.14) and (6.15) and which are valid under the same general assumptions:

$$\frac{\partial}{\partial z} \mathcal{E}_\alpha^+ = + \frac{i k_0}{2 \varepsilon_{e,g}} \sum d_{eg}^\star \{ \boldsymbol{\epsilon}_{eg} \cdot \boldsymbol{\epsilon}_\alpha \} \tilde{\sigma}_{eg} \quad (8.14)$$

$$\frac{\partial}{\partial \tau} \sigma_{ee'} = -i(\omega_e - \omega_{e'}) \sigma_{ee'} - \frac{i}{\hbar} \sum_{\alpha,e} [\mathcal{E}_\alpha^- \tilde{\sigma}_{eg} d_{ge'}^\star \{ \boldsymbol{\epsilon}_{ge'} \cdot \boldsymbol{\epsilon}_\alpha \} - d_{eg}^\star \{ \boldsymbol{\epsilon}_{eg} \cdot \boldsymbol{\epsilon}_\alpha \} \sigma_{e'g}^+ \mathcal{E}_\alpha^+] \quad (8.15)$$

$$\frac{\partial}{\partial \tau} \sigma_{gg'} = -i(\omega_g - \omega_{g'}) \sigma_{gg'} - \frac{i}{\hbar} \sum_{\alpha,e} [\sigma_{eg}^+ \mathcal{E}_\alpha^+ d_{eg}^\star \{ \boldsymbol{\epsilon}_{eg'} \cdot \boldsymbol{\epsilon}_\alpha \} - d_{ge}^\star \{ \boldsymbol{\epsilon}_{ge} \cdot \boldsymbol{\epsilon}_\alpha \} \mathcal{E}_\alpha^- \tilde{\sigma}_{eg'}] \quad (8.16)$$

$$\frac{\partial}{\partial \tau} \tilde{\sigma}_{eg} = -i(\omega_e - \omega_g) \tilde{\sigma}_{eg} - \frac{i}{\hbar} \left\{ \sum_{\alpha,e'} \sigma_{ee'} \mathcal{E}_\alpha^+ d_{e'g}^\star \{ \boldsymbol{\epsilon}_{e'g} \cdot \boldsymbol{\epsilon}_\alpha \} - \sum_{\alpha,g'} d_{eg'} \{ \boldsymbol{\epsilon}_{eg'} \cdot \boldsymbol{\epsilon}_\alpha \} \sigma_{g'g} \mathcal{E}_\alpha^+ \right\}. \quad (8.17)$$

In these equations, in which normal ordering is used, the populations and low-frequency coherences are coupled to the optical polarizations (eqs. (8.15) and (8.16)) and reciprocally (eq. (8.17)). This coupling occurs through the envelope of the radiated field, itself related to the optical polarization through the Maxwell equation (8.14). It is easy to check that these equations reduce to eqs. (6.13), (6.14) and (6.15) if e and g are not degenerate.

Let us finally remark that the expectation values of the $\sigma_{XX'}$ operators are very simply related to the one-atom local density matrix elements. One has indeed:

$$\langle \sigma_{XX'} \rangle = \frac{1}{\pi w^2} \sum_i \text{Tr}\{\rho_i D_i^{XX'}\} \delta_\epsilon(z - z_i) \quad (8.18)$$

which, averaged in the p th slice, gives:

$$\langle \sigma_{XX'}(z_p) \rangle = \frac{N}{\pi w^2 L} \langle X | \rho_1(z_p) | X' \rangle. \quad (8.19)$$

The general method to solve eqs. (8.14) to (8.17) is exactly the same as in the two-level case. Disregarding the non-commuting character of the σ and \mathcal{E}_α operators, one numerically solves these equations as if all quantities were classical, after assuming *random initial conditions* in each slice of the medium for the *optical polarizations* of the various initial transitions. [The initial populations and low frequency coherences are obtained from the initial values of the $\rho_{1ee'}$ matrix elements, using eq. (8.19).] Each set of random initial optical coherence corresponds to a classical trajectory which represents a possible realization of the experiment. The fluctuation of these classical trajectories depends upon the statistics of the initial optical coherences. The expectation values of physical quantities are obtained by averaging all the classical trajectories with their statistical probabilities. We extend in the next subsection the results of subsection 6.3 and give the general statistical laws obeyed by the initial optical coherences in the multilevel case.

8.4. Statistics of initial condition for the classical trajectories

Each classical trajectory is defined by a set of initial amplitudes α_p^{eg} and phases ϕ_p^{eg} chosen in each slice of the medium for each atomic optical coherence. One will note the corresponding classical trajectory as $\sigma_{cl}^{XX'}(z, \tau; \{\alpha_p^{eg}, \phi_p^{eg}\})$ with the condition (generalizing eq. (6.72)):

$$\sigma_{\text{cl}}^{\text{eg}}(z, \tau = 0; \{\alpha_p^{\text{eg}}, \phi_p^{\text{eg}}\}) = \frac{n}{\pi w^2 L} \alpha_p^{\text{eg}} \exp(i\phi_p^{\text{eg}}). \quad (8.20)$$

The statistics of these trajectories is determined when one knows the probability law for each random choice of initial condition. We will call $\bar{P}\{\alpha_p^{\text{eg}}, \phi_p^{\text{eg}} \dots\}$ this law which generalizes in an obvious way the definition of section 6.3.2.

As in the two-level atom superradiance case, the correlation functions of the optical dipole at time $\tau = 0$ can be expressed as:

$$\langle (\sigma_{\text{ge}}(z, \tau = 0))^l (\sigma_{g'e'}^+(z', \tau = 0))^m \rangle = \left(\frac{n}{\pi w^2 L} \right)^{l+m} \sum_{\substack{\alpha_p^{\text{ge}}, \phi_p^{\text{ge}} \\ \alpha_p^{g'e'}, \phi_p^{g'e'}}} \bar{P}\{\alpha_p^{\text{ge}}, \phi_p^{\text{ge}} \dots\} (\alpha_p^{\text{ge}})^l (\alpha_p^{g'e'})^m \exp(il\phi_p^{\text{ge}} - im\phi_p^{g'e'}). \quad (8.21)$$

The left-hand side of eq. (8.21) can be computed for any exponents l and m from the knowledge of the atomic system density matrix at time $t = 0$ and this equation can thus be used to determine all the moments of the generalized probability law $\bar{P}\{\alpha_p^{\text{eg}}, \phi_p^{\text{eg}} \dots\}$ in the same way as in section 6.3. In order to perform this computation, each $\sigma_{\text{xx'}}$ has to be expressed as a sum of $D_i^{\text{XX'}}$ operators (eq. (8.12)). For $l=m=1$, the calculation introduces a priori the correlation terms $\langle D_i^{\text{ge}} D_i^{\text{eg}} \rangle$, $\langle D_i^{\text{ge}} D_i^{g'e} \rangle$, $\langle D_i^{\text{eg}} D_i^{g'e} \rangle$ and $\langle D_i^{\text{eg}} D_i^{g'e'} \rangle$. The first term is the same as the one obtained in a two-level atom case and is different from zero. The second one is non-zero only if there is an initial coherence in the upper level of the atomic transition at $\tau = 0$ and is proportional to $\rho_{1ee}(0)$. The last two terms are obviously zero since all atoms are initially in upper states. The existence of the cross-correlation term $\langle D_i^{\text{ge}} D_i^{g'e'} \rangle$ is a source of complication for the solution of eq. (8.21) since it means that the initial choices for ϕ_p^{eg} and $\phi_p^{g'e}$ are not independent: the phase difference $\phi_p^{\text{ge}} - \phi_p^{g'e}$ is obviously, for each random choice, equal to the phase of $\rho_{1ee}(0)$. In order to avoid this complication, it is possible to make a state basis change in the upper level which diagonalizes the matrix $\rho_{1ee}(0)$. This basis change allows us to define new excited state vectors i, i', \dots such that ρ_1 is diagonal in the new basis:

$$\rho_1 = \frac{1}{N} \begin{bmatrix} N_i & & & \\ & N_{i'} & & \\ & & \ddots & \\ & & & \ddots \end{bmatrix} \quad (8.22)$$

where $N_i, N_{i'}, \dots$ represent the total number of atoms in each of the new basis substates. Since the statistics of the initial condition is determined at time $\tau = 0$, before any evolution has occurred, eq. (8.21) does not depend upon the basis choice and one can as well determine the statistics for the new optical coherences $\sigma_{\text{cl}}^{\text{ig}}$. One defines new amplitudes and phases $\alpha_p'^{\text{ig}}$ and $\phi_p'^{\text{ig}}$ whose statistics is much simpler than the one of α_p^{eg} and ϕ_p^{eg} : since the cross-correlation terms all vanish in the new basis, the choices of initial condition are statistically independent for any two different optical coherences in each slice of the medium (and of course for the same coherence in two different slices). The probability law thus factorizes in the new basis:

$$\bar{P}\{\alpha_p'^{\text{ig}}, \phi_p'^{\text{ig}}\} = \prod_{p,i,g} P[(\alpha_p'^{\text{ig}})^2] \cdot Q(\phi_p'^{\text{ig}}) \quad (8.23)$$

with:

$$P[(\alpha_p'^{ig})^2] = \frac{1}{N_{p,i}} \exp(-(\alpha_p'^{ig})^2/N_{p,i}), \quad (8.24)$$

$$Q[(\phi_p'^{ig})] = \frac{1}{2\pi}. \quad (8.25)$$

In eq. (8.24) $N_{p,i}$ is the number of atoms in the p th slice in the new basis substate i ($N_{p,i} = N_i/n$).

The statistics for the α_p^{eg} and ϕ_p^{eg} is then deduced from eqs. (8.23) to (8.25) by application of the inverse basis transformation. We will now illustrate on some simple examples the general theory that we have just developed.

8.5. First example: Beats radiated by a mixture of two isotopes

The first case we will discuss corresponds to the superradiance of a mixture of two ensembles a and b of two-level atoms (such as two isotopes) having slightly different optical frequencies. The corresponding level scheme is shown on fig. 27. We suppose that both systems have the same transition polarization ϵ_1 . Without loss of generality, we choose ω_0 so that the respective transition frequencies of systems a and b are:

$$\omega_a = \omega_0 + \Delta\omega_a = \omega_0 + \frac{\Delta\omega}{2}, \quad \omega_b = \omega_0 + \Delta\omega_b = \omega_0 - \frac{\Delta\omega}{2}. \quad (8.26)$$

Making the following notation changes:

$$\omega_0 + \omega_e - \omega_g = \omega_0 + \Delta\omega_a \quad (8.27)$$

$$\omega_0 + \omega_{e'} - \omega_{g'} = \omega_0 + \Delta\omega_b \quad (8.28)$$

$$d_{eg} = d_a; \quad d_{e'g'} = d_b \quad (8.29)$$

$$d_{eg}\tilde{\sigma}_{eg} = \mathcal{P}_a^-; \quad d_{e'g'}\tilde{\sigma}_{e'g'} = \mathcal{P}_b^- \quad (8.30)$$

$$\sigma_{ee} - \sigma_{gg} = 2\mathcal{N}_a; \quad \sigma_{e'e'} - \sigma_{g'g'} = 2\mathcal{N}_b \quad (8.31)$$

and remarking that the low frequency coherences $\sigma_{ee'}$ and $\sigma_{gg'}$ are obviously lacking in this case, one easily transforms the general equation [(8.14), (8.15), (6.16), (8.17)] into the following set of equations:

$$\frac{d}{dz} \mathcal{E}^+ = \frac{i k_0}{2\epsilon_0} \sum_x \mathcal{P}_x^- \quad (8.32)$$

$$\frac{\partial}{\partial \tau} \mathcal{P}_x^- = -i \Delta\omega_x \mathcal{P}_x^- - 2i \frac{|d_x|^2}{\hbar} \mathcal{N}_x \mathcal{E}^+ \quad (8.33)$$

$$\frac{\partial}{\partial \tau} \mathcal{N}_x = \frac{i}{\hbar} [\mathcal{P}_x^+ \mathcal{E}^+ - \mathcal{E}^- \mathcal{P}_x^-] \quad (8.34)$$

where X is used for a and b and \mathcal{E} is the field component along the common polarization ϵ_1 of the two transitions.

Equations (8.32), (8.33) and (8.34) describe the evolution of two complex “oscillators” \mathcal{P}_a and \mathcal{P}_b coupled to the same radiation field. The free-evolution frequencies of these oscillators being different

(respectively $\Delta\omega_a$ and $\Delta\omega_b$), one expects that the electric field will exhibit these two frequency components and that the light intensity, proportional to $\mathcal{E}^+ \mathcal{E}^-$, will be modulated around frequency $\Delta\omega = \Delta\omega_a - \Delta\omega_b$.

The exact shape of a given classical trajectory (single realization of the experiment) depends upon the initial random condition given by:

$$\mathcal{P}_X(z, \tau = 0) = \frac{n}{\pi L w^2} d_X \alpha_X e^{i\phi_X} \quad (8.35)$$

with independent probability distributions for α_X ($X = a, b$) and ϕ_X .

The statistics of the beat pattern can be numerically obtained by solving the classical counterpart of eqs. (8.32), (8.33) and (8.34) assuming all possible initial conditions (8.35). One could in this way study the pulse to pulse fluctuations of the beat phase and modulation depth and construct the corresponding histograms. The expectation value of the light intensity would then be obtained by averaging over all the classical trajectories. The modulation depth of the average obviously depends on the randomness of the beat phase in the various classical trajectories. If this phase reflects exactly the statistics of the initial condition, it will be completely random and the expectation value will not be modulated at all. If, on the contrary, the two coupled transitions experienced some kind of phase locking during the emission process, this will produce a partial modulation of the averaged signal. At the same time, such a coupling should also cause some kind of frequency shift of the beat note. All these effects are expected to build up during the linear phase of the emission, when the number of atoms in the lower state is still small. Although it is easy to calculate exactly these effects by solving numerically the non-linear equations (8.32), (8.33) and (8.34), we think that a simple analytical analysis of this linear regime will provide a deeper physical insight into the phenomenon. We will thus solve eq. (8.33) with the assumption that:

$$\mathcal{N}_X(z, \tau) \sim \mathcal{N}_X(z, 0) \quad (X = a, b). \quad (8.36)$$

And we will also, for the sake of simplicity, consider that the two systems are equally excited at $\tau = 0$:

$$\mathcal{N}_a(z, 0) = \mathcal{N}_b(z, 0) \quad (8.37)$$

and that they have the same oscillator strength:

$$d_a = d_b \quad (8.38)$$

so that one can define a single superradiance time:

$$[T_R]^{-1} = [T_{Ra}]^{-1} = [T_{Rb}]^{-1} = \frac{|d_a|^2 k_0 L \mathcal{N}_a(0)}{\epsilon_0 \hbar}. \quad (8.39)$$

Furthermore, the calculation will be performed in the mean-field approximation. With all these hypotheses, eq. (8.33) can be written as:

$$\frac{d}{dt} \begin{bmatrix} \mathcal{P}_{a\text{cl}} \\ \mathcal{P}_{b\text{cl}} \end{bmatrix} = \frac{1}{2} \begin{bmatrix} \frac{1}{T_R} - i\Delta\omega & \frac{1}{T_R} \\ \frac{1}{T_R} & \frac{1}{T_R} + i\Delta\omega \end{bmatrix} \begin{bmatrix} \mathcal{P}_{a\text{cl}} \\ \mathcal{P}_{b\text{cl}} \end{bmatrix}. \quad (8.40)$$

The eigenvalues of the matrix in the right-hand side of eq. (8.40) are:

$$\omega_{\pm} = \frac{1}{2T_R} [1 \pm \sqrt{1 - \eta^2}] \quad (8.41)$$

and the corresponding eigenvectors:

$$\begin{bmatrix} V_{\pm a} \\ V_{\pm b} \end{bmatrix} = \begin{bmatrix} 1 - i\eta \pm \sqrt{1 - \eta^2} \\ 1 + i\eta \pm \sqrt{1 - \eta^2} \end{bmatrix} \quad (8.42)$$

with:

$$\eta = \Delta\omega T_R \quad (8.43)$$

being a dimensionless measure of the reciprocal of the coupling strength between the two oscillators (strong couplings correspond to short T_R and hence small η).

The solution of the linearized equation (8.40) is then obviously:

$$\begin{bmatrix} \mathcal{P}_{a cl}(t) \\ \mathcal{P}_{b cl}(t) \end{bmatrix} = \mathcal{P}_+(0) e^{\omega_a t} \begin{bmatrix} V_{+a} \\ V_{+b} \end{bmatrix} + \mathcal{P}_-(0) e^{\omega_b t} \begin{bmatrix} V_{-a} \\ V_{-b} \end{bmatrix} \quad (8.44)$$

with the initial conditions:

$$\begin{bmatrix} \mathcal{P}_+(0) \\ \mathcal{P}_-(0) \end{bmatrix} = \frac{1}{4\eta\sqrt{\eta^2-1}} \begin{bmatrix} -V_{-b} \mathcal{P}_{a cl}(0) + V_{-a} \mathcal{P}_{b cl}(0) \\ V_{+b} \mathcal{P}_{a cl}(0) - V_{+a} \mathcal{P}_{b cl}(0) \end{bmatrix} . \quad (8.45)$$

The beats will exist only if ω_{\pm} has an imaginary part, that is if the coupling is weak enough so that:

$$\eta = \Delta\omega T_R > 1 . \quad (8.46)$$

One then has:

$$\omega_{\pm} = 1/2T_R \pm i\Delta\omega'/2 \quad (8.47)$$

with:

$$\Delta\omega' = \Delta\omega\sqrt{1 - 1/\eta^2} < \Delta\omega \quad (8.48)$$

and the light intensity on a given classical trajectory:

$$I_{cl} \sim |\mathcal{P}_{a cl}(z, t) + \mathcal{P}_{b cl}(z, t)|^2 \quad (8.49)$$

can be expressed with the help of eq. (8.45) as a function of $\mathcal{P}_+(0)$ and $\mathcal{P}_-(0)$:

$$I_{cl} \sim \eta^2 e^{i/T_R} \{ |\mathcal{P}_+(0)|^2 + |\mathcal{P}_-(0)|^2 + (\mathcal{P}_+(0) \mathcal{P}_-^*(0) e^{i(\Delta\omega' t + \phi)} + c.c.) \} \quad (8.50)$$

with:

$$e^{i\phi} = \frac{2 - \eta^2 + 2i\sqrt{\eta^2 - 1}}{\eta^2}. \quad (8.51)$$

The classical signal starts to increase exponentially with the time constant T_R and exhibits a modulation at the shift frequency $\Delta\omega'$, whose depth is proportional to $\mathcal{P}_+(0)\mathcal{P}_-^\star(0)$. Whereas $\mathcal{P}_{a\text{cl}}(0)$ and $\mathcal{P}_{b\text{cl}}(0)$ are completely uncorrelated, this is not the case of the linear superpositions $\mathcal{P}_+(0)$ and $\mathcal{P}_-(0)$ given by eq. (8.45). One easily gets:

$$\langle|\mathcal{P}_+(0)|^2\rangle = \langle|\mathcal{P}_-(0)|^2\rangle = \frac{1}{4(\eta^2 - 1)} \langle|\mathcal{P}_a|^2\rangle = \frac{1}{4(\eta^2 - 1)} \langle|\mathcal{P}_b|^2\rangle \quad (8.52)$$

and

$$\langle\mathcal{P}_+(0)\mathcal{P}_-^\star(0)\rangle = \frac{-1}{4(\eta^2 - 1)} \langle|\mathcal{P}_a|^2\rangle \left(\frac{1 + e^{-i\phi}}{2}\right) \quad (8.53)$$

which finally gives:

$$\langle I \rangle = \frac{\eta^2}{4(\eta^2 - 1)} \langle|\mathcal{P}_a(0)|^2 + |\mathcal{P}_b(0)|^2\rangle e^{i\psi/T_R} \left(1 + \frac{1}{\eta} \cos(\Delta\omega't + \psi')\right), \quad (8.54)$$

ψ' being a phase related to η .

In the linear regime, the expectation value is thus found to be modulated at $\Delta\omega'$, with a modulation depth $1/\eta$. Figure 28 represents the ratio $\Delta\omega'/\Delta\omega$ of the shifted to the unperturbed atomic frequency and the relative modulation depth as a function of η . The weaker the coupling between the two species, the less is the expectation value modulated and the less the beat frequency shifted with respect to the atomic frequency. For very large η values, the two systems indeed behave as independent oscillators with random phases, so that the average signal is only very weakly modulated. It is also worth noticing that the relative frequency shift decreases much faster than the modulation depth when η increases. For

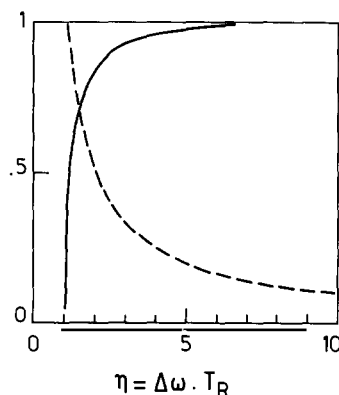


Fig. 28. Superradiance beats between two ensembles of atoms a and b: variation of the relative beat frequency $\Delta\omega'/\Delta\omega$ (solid line) and of the expectation value modulation depth (dashed line) as a function of $\eta = \Delta\omega T_R$.

$\eta \sim 10$, the former is already negligible whereas the expectation value remains appreciably modulated. This property is interesting for spectroscopic applications (possibility of measuring nearly unperturbed atomic frequencies on averaged signals). Finally, for $\eta < 1$, the two oscillators are so strongly coupled that they do not precess any longer and the superradiance takes place without oscillation. The above results remain qualitatively valid throughout the system evolution, even during its non-linear phase. The calculation can be extended without difficulty to non-equivalent transition ($d_a \neq d_b, N_a \neq N_b$) and generalized to include propagation effects.

If, instead of being emitted by two sets of physically distinct atoms, the superradiance beats are radiated by an ensemble of three-level systems (fig. 26, b or c), new effects related to the existence of low frequency coherences in the upper level at time $t = 0$ do occur [93, 63]. In particular, the pulse to pulse phase correlation of the beat pattern depends upon the value of $\rho_{1ee}(0)$. If this initial coherence is large, the modulations of single pulse signals are all in phase with each other and the *expectation value* of the light intensity is strongly modulated for a reason quite different from the one discussed above in the case of independent atom beats. Whereas in this latter case this “average” modulation is due to a coupling between initially uncorrelated oscillations, in the case of a coherent preparation of levels e and e', the phase correlation between the two frequency components is achieved by the excitation process itself at time $t = 0$. We will not discuss further these different light beating effects and rather conclude this section by the description of some simple polarization effects occurring when the transitions are exactly degenerate (zero-frequency beat limit).

8.6. Second example: Polarization fluctuations in superradiance

We consider here again the superradiant emission of a mixture of two ensembles a and b of two-level atoms. The situation differs however in two respects from the one discussed in the previous subsection. The two systems have now exactly the same optical frequency ω_0 and their transition polarizations ϵ_a and ϵ_b are *orthogonal* to each other. To be specific, the situation we have in mind corresponds to the superradiance of a $J = \frac{1}{2} \rightarrow J' = \frac{1}{2}$ transition. The initial and final states then decompose respectively into two degenerate $|e\rangle = |m_J = +\frac{1}{2}\rangle$, $|e'\rangle = |m_J = -\frac{1}{2}\rangle$ and $|g\rangle = |m_{J'} = +\frac{1}{2}\rangle$, $|g'\rangle = |m_{J'} = -\frac{1}{2}\rangle$ substates (quantization direction parallel to the emission axis Oz). If the preparation of the upper level is incoherent ($\rho_{1ee} = 0$) with equal excitations in both substates ($\rho_{1ee} = \rho_{1e'e'}$), the emission is the superposition of two independent and strictly equivalent superradiant processes (transition $|e\rangle \rightarrow |g\rangle$ with a right-handed circular polarization $\epsilon_a = \epsilon_+$ and transition $|e'\rangle \rightarrow |g'\rangle$ with a left-handed circular polarization $\epsilon_b = \epsilon_-$; see fig. 29a).

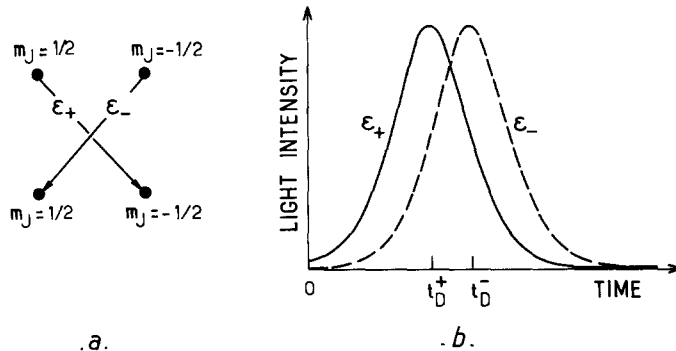


Fig. 29. Polarization fluctuations in the superradiance of a $J = \frac{1}{2} \rightarrow J' = \frac{1}{2}$ transition: (a) level diagram showing the two magnetic sublevels in the upper and lower states. The two arrows correspond to the independent ϵ_+ and ϵ_- emission; (b) time variation of the ϵ_+ and ϵ_- polarization components for one possible realization. In the event shown here, the emission starts with a ϵ_+ polarization and ends with the other ϵ_- polarization.

Let us first discuss this emission in the *mean-field model*. The two ϵ_+ and ϵ_- components are then emitted as two hyperbolic secant pulses with equal amplitudes. The initial quantum fluctuations being uncorrelated for the two field components, there is for each realization of the experiment a random phase and delay difference between these two components. According to eq. (6.47), the phase difference $\phi_+ - \phi_-$ is completely random. The average value of the pulse delay difference $t_B^+ - t_B^-$ is of the order of $1.3T_R$ (eq. (6.64)), i.e. only about one third of the width of each pulse. As a result, the total radiated field is the sum of two slightly-shifted ϵ_+ and ϵ_- polarized bell-shaped pulses with random phases (see fig. 29b). The resulting field has a time-varying polarization. It starts with the circular polarization of the component which happens to have been triggered by the larger fluctuation and ends with the other circular polarization. For most of the field emission however, the two components have comparable amplitudes and the field polarization is elliptical. At emission maximum, the ϵ_+ and ϵ_- amplitudes are equal and the polarization is linear, with a direction defined by $\phi_+ - \phi_-$. These polarization features randomly change from one realization of the experiment to the next, with a statistics entirely determined by eqs. (6.45) and (6.46).

In the one-dimensional propagation model of superradiance, the above description is slightly modified by the fact that not only the delay, but also the peak intensity and shape of the two-level system single pulses fluctuate (see subsection 6.3.2). The two ϵ_+ and ϵ_- components are now slightly unequal at emission maximum and the resulting polarization is then elliptical, with a big axis randomly rotating from pulse to pulse [54].

It is remarkable that the initial quantum fluctuations of superradiance induce in this case extremely large macroscopic fluctuations in the polarization of the emitted field. The analysis of these fluctuations is a very simple and convenient way to study the quantum noise responsible for the superradiance initiation: in the situation we have just described, one prepares indeed at the same time two independent systems with identical initial conditions and the randomness observed in the resulting pulse polarization reflects the intrinsic fluctuations existing between two equivalent realizations of a two-level superradiant emission.

Other interesting polarization effects in superradiance can be found in multilevel systems prepared with non-vanishing initial coherences $\rho_{1ee'}$ (quenching or initiation of one polarization component by the emission of another). These effects can be simply analysed with the formalism introduced in subsections 8.3 and 8.4 and their description can be found in refs. [25, 53].

9. Limited superradiance

In two-level atom superradiance (mean-field or one-dimensional propagation models), all the atoms end-up in the lower state of the superradiant transition: the system emits a π pulse and all the available atomic energy is changed into radiation. This basic feature is quite clear to understand, at least in the mean-field case. So long as some atoms remain in the upper level, there is necessarily a non-zero optical dipole in the medium (conservation of the Bloch vector length). This dipole radiates and the atomic system still loses energy. The only stable state is thus the one in which all atoms are de-excited. When propagation is taken into account (one-dimensional model), the situation is a little bit more complicated since the evolution rate of the dipoles depends upon their location along the medium, but the conclusion remains the same: the atomic system stops radiating when all its energy has been emitted.

In multilevel-atom superradiance, the situation is quite different. Numerical integration of eqs. (8.14, 15, 16, 17) shows that in most cases the equilibrium position of the atomic system corresponds to a state where a lot of atoms remain in the upper level of the atomic transition.

Often, the limited superradiance effect is merely due to the fact that a transition with a larger gain quenches the emission on another transition sharing a common lower level and prevents the upper level of this latter transition to decay.

More interestingly, even when the gain of two competing transitions are close or equal, a partial quenching of the emission on these transitions is *still observed*. This quenching might be due to random differences in the quantum initiation of both transitions. In this case, the respective percentages of quenching on the competing transitions fluctuate from pulse to pulse, reflecting the random character of the emission initiation. In other cases, the effect of limited superradiance is related to some kind of destructive interference between the emissions of physically distinguishable optical dipoles. These dipoles might correspond to different transitions having the same polarization (subsections 9.1 and 9.2) or to different classes of atoms radiating on the same transitions (subsection 9.3). In all cases, these dipoles evolve at different rates in the common radiation field because they are differently coupled to it. After some time, the phase distribution of these dipoles becomes such that the field they radiate completely vanishes by negative interference. The system thus remains in a very peculiar equilibrium situation in which large macroscopic, but non-radiating optical coherences are distributed along the medium (this situation is also called subradiance by some authors [49]).

These various aspects of the limited superradiance phenomenon will be analysed on three simple examples in the next subsections.

9.1. First example: Case of two independent degenerate transitions with the same polarization and different matrix elements

Let us first consider the simple situation illustrated on fig. 30. Two “parallel” transitions a and b, with identical polarization $\epsilon_a = \epsilon_b = \epsilon$, have different matrix elements. We write without loss of generality:

$$d_a = \alpha d ; \quad d_b = \beta d \quad (9.1)$$

with α and β ($\alpha \neq \beta$) being real numbers.

The system is quite similar to the one considered in subsection 8.5, now with $\Delta\omega_a = \Delta\omega_b = 0$ and $d_a \neq d_b$. The evolution equations are simply deduced from eqs. (8.32, 33, 34). To solve these equations, it is convenient to introduce – as in subsection 6.3.1 – a Bloch angle θ_x ($x = a, b$) for each transition: (we replace $\mathcal{N}_x(0)$ by \mathcal{N}_{0x}):

$$\mathcal{N}_x = \mathcal{N}_{0x} \cos \theta_x \quad (9.2)$$

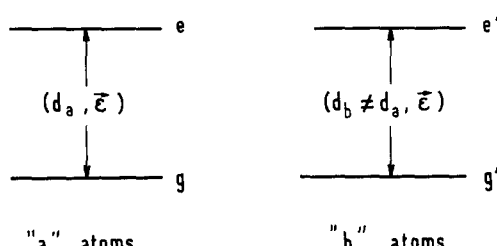


Fig. 30. Level scheme illustrating a first example of limited superradiance: case of two ensembles of atoms “a” and “b” with degenerate frequencies, identical polarization, but different dipole matrix elements.

$$\mathcal{P}_x = i d_x \mathcal{N}_{0x} \sin \theta_x . \quad (9.3)$$

The Bloch equations then become:

$$\dot{\theta}_x = \frac{2}{\hbar} \int_0^\tau d_x \mathcal{E} d\tau . \quad (9.4)$$

It is then convenient to define a “common” tipping angle $\bar{\theta}$

$$\bar{\theta} = \frac{2}{\hbar} \int_0^\tau d \mathcal{E} d\tau \quad (9.5)$$

which is related to the θ_x by:

$$\theta_a = \alpha \bar{\theta}; \quad \theta_b = \beta \bar{\theta}. \quad (9.6)$$

With these notations, it is clear that the tipping angles associated to the two classes of atoms a and b are at all times proportional to each other (in the ratio α/β) and are thus never equal. Hence, the two transitions cannot both undergo a π pulse at the end of the superradiant emission.

The atomic energy per unit volume $W(z, \tau)$ is then readily obtained from eqs. (9.2) and (9.6). It can be expressed as a function of $\bar{\theta}$ alone:

$$W(z, \tau) = \frac{\hbar \omega}{2} [\mathcal{N}_{0a} \cos \alpha \bar{\theta} + \mathcal{N}_{0b} \cos \beta \bar{\theta}] . \quad (9.7)$$

This function has been plotted against $\bar{\theta}$ on fig. 31 in the case $\mathcal{N}_{0a} = \mathcal{N}_{0b}$ and $\alpha/\beta = 2$. The atomic energy density appears as the sum of two cosine functions which, for $\alpha \neq \beta$ never reaches the value $-\frac{1}{2}\hbar\omega_0[\mathcal{N}_{0a} + \mathcal{N}_{0b}]$ corresponding to all atoms in the ground state. The system will thus exhibit the limited superradiance effect.

The $W(\bar{\theta})$ function has in fact a very simple physical meaning. From eqs. (9.3), (9.5), (9.6) and (8.32),

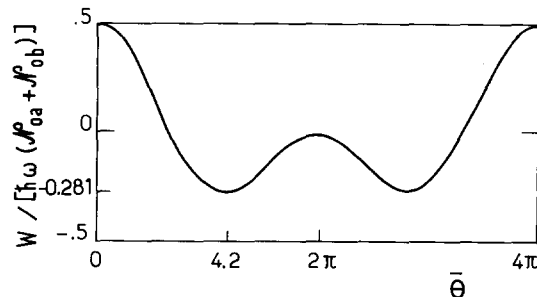


Fig. 31. Limited superradiance in the case of two ensembles of atoms emitting on degenerate transitions with different dipole matrix elements: variation of the atomic energy W versus $\bar{\theta}$ in the case $\mathcal{N}_{0a} = \mathcal{N}_{0b}$ and $\alpha/\beta = 2$. Note that W never reaches the value $(-\hbar\omega_0/2)(\mathcal{N}_{0a} + \mathcal{N}_{0b})$ corresponding to a total deexcitation of the system.

one obtains:

$$\frac{\partial^2 \bar{\theta}}{\partial(z/L)\partial(\tau/T_R)} = \frac{-2}{(\mathcal{N}_{0a} + \mathcal{N}_{0b})\hbar\omega_0} \frac{\partial W(\bar{\theta})}{\partial\bar{\theta}} \quad (9.8)$$

with

$$T_R^{-1} = \frac{k_0 d^2}{\hbar\epsilon_0} (\mathcal{N}_{0a} + \mathcal{N}_{0b}). \quad (9.9)$$

Eq. (9.8) is a simple generalization of the Sine-Gordon equation (6.78) of the two-level atom case. It means that $W(\bar{\theta})$ plays the role of a potential well for the superradiant system, whose evolution can end only when $W(\bar{\theta})$ is minimum, for the $\bar{\theta}_{\min}$ value such that:

$$\partial W(\bar{\theta}_{\min})/\partial\bar{\theta} = 0. \quad (9.10)$$

In the case of fig. 31, this minimum is reached for $\bar{\theta}_{\min} = 4.2$ and corresponds to a value $-0.281\hbar\omega_0[\mathcal{N}_{0a} + \mathcal{N}_{0b}]$ for $W(\bar{\theta})$, that is to a ratio of 21.9% of the atoms remaining in the upper level at all points in the sample.

In order to physically understand this effect of limited superradiance, let us calculate the optical dipoles \mathcal{P}_a and \mathcal{P}_b corresponding to this equilibrium state. From eq. (9.3), one gets:

$$\mathcal{P}_a(\tau = \infty) = -i\alpha d \mathcal{N}_{0a} \sin \alpha \bar{\theta}_{\min} \quad (9.11)$$

$$\mathcal{P}_b(\tau = \infty) = -i\beta d \mathcal{N}_{0b} \sin \beta \bar{\theta}_{\min}. \quad (9.12)$$

One readily checks that eq. (9.10) precisely corresponds to:

$$\mathcal{P}_a(\tau = \infty) + \mathcal{P}_b(\tau = \infty) = 0. \quad (9.13)$$

In other words, the evolution comes to an end when the two classes of dipoles corresponding to the two transitions a and b radiate fields in phase opposition.

9.2. Second example: Degenerate transitions with identical polarizations sharing a common lower level

Let us now turn to the situation corresponding to two degenerate transitions $e \rightarrow g$ and $e' \rightarrow g$ with identical polarization ϵ and same matrix element ($d_{eg} = d_{e'g} = d$), sharing a common lower level g .

Assume the very simple initial condition

$$\rho_{1ee}(0) = 1; \quad \rho_{1e'e'}(0) = 0 \quad (9.14)$$

which expresses that all atoms are prepared in a single sublevel. Let us introduce again a Bloch angle:

$$\frac{1}{2\sqrt{2}} \theta = \frac{id}{\hbar} \int_0^t \mathcal{E} d\tau \quad (9.15)$$

where \mathcal{E} is the field component along the common polarization direction of both transitions. It is easy to show in that case that the atomic populations and optical coherences are related to θ by simple relations:

$$\rho_{1ee} = \frac{1}{4}(1 + \cos \frac{1}{2}\theta)^2 \quad (9.16)$$

$$\rho_{1e'e'} = \frac{1}{4}(1 - \cos \frac{1}{2}\theta)^2 \quad (9.17)$$

$$\rho_{1gg} = \frac{1}{2} \sin^2 \frac{1}{2}\theta \quad (9.18)$$

$$\rho_{1eg} = (1 + \cos \frac{1}{2}\theta)(\sin \frac{1}{2}\theta)/(2\sqrt{2}) \quad (9.19)$$

$$\rho_{1e'g'} = (\cos \frac{1}{2}\theta - 1)(\sin \frac{1}{2}\theta)/(2\sqrt{2}) \quad (9.20)$$

The stable position of minimum energy for the atomic system (maximum ρ_{gg} value) is reached for $\theta = \pi$. Equations (9.19) and (9.20) then show that the two dipoles ρ_{1eg} and $\rho_{1e'g'}$ are again in phase opposition at each point of the sample:

$$\rho_{1eg}(\tau = \infty) = -\rho_{1e'g'}(\tau = \infty). \quad (9.21)$$

The physical explanation of this effect is the following: the field emitted with polarization ϵ on the $e \rightarrow g$ transition can be reabsorbed on the $g \rightarrow e'$ transition and excite the level e' initially empty. The system evolution stops when an equilibrium is reached in which the fields emitted on these two transitions destructively interfere. In that position, 1/2 of the atoms are in the lower level and 1/2 in each of the upper states. Furthermore, there is a non-vanishing coherence between these two upper levels.

The above simple discussion can be easily generalized to the more general situation ($\rho_{1ee'}$, $\rho_{1ee'}$, $\rho_{1ee'} \neq 0$, $d_{eg} \neq d_{e'g}$). Similar results are obtained, with a limited superradiance effect resulting from an exact cancellation of the macroscopic dipoles $\rho_{1eg}(\tau = +\infty)$ and $\rho_{1e'g'}(\tau = +\infty)$ at the end of the emission process.

9.3. Third example: Degenerate transitions with orthogonal polarizations sharing a common lower level

We consider now the case illustrated on fig. 32, which is similar to the previous one, except for the fact that the two polarizations ϵ_{eg} and $\epsilon_{e'g}$ are now orthogonal. The two electric dipole matrix elements are still supposed to be equal to d .

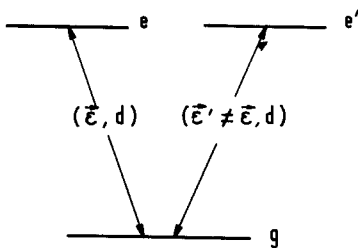


Fig. 32. Level scheme illustrating the case of limited superradiance discussed in section 9.3.

Suppose first that one excites only level e (condition (9.14)). It is clear now that the superradiant emission will be total, without any atom left in the upper levels. The field radiated on the $e \rightarrow g$ transition cannot be reabsorbed on the orthogonally polarized $g \rightarrow e'$ transition and we are in fact in a two-level atom case, the state e' playing no role in the process.

Let us see now what happens if both levels are initially populated. If ρ_{1ee} is larger than $\rho_{1e'e'}$, the emission takes place first on the $e \rightarrow g$ transition and quenches the $e' \rightarrow g$ orthogonal polarization process. Nearly all the atoms initially in the e' level remain in this state and limited superradiance does occur.

Suppose, on the other hand, that the e and e' levels are initially equally populated (for sake of simplicity, we assume incoherent pumping):

$$\rho_{1ee}(0) = \rho_{1e'e'}(0) = \frac{1}{2}, \quad \rho_{1e'e} = 0. \quad (9.22)$$

The numerical calculation shows that the effect of limited superradiance does occur in this case whatever the initial fluctuations are. For the classical trajectories which start on very different fluctuations on both transitions, the limited superradiance effect is easy to understand: one transition starts first and quenches the other. For the classical trajectories which happen to start on nearly equal fluctuations on both transitions, the above explanation does not hold. Another hypothesis to explain limited superradiance in this situation would be to assume, as in the previous subsection that the dipoles on the $e \rightarrow g$ and $e' \rightarrow g$ transitions have reached an equilibrium value in phase opposition. This is however certainly wrong, since both transitions are now polarized at right angle: if the electric dipoles were non-zero on each transition, they could not interfere and would certainly go on radiating and the decay could not stop. The limited superradiance has thus to be explained otherwise:

As it has been noticed in subsection 8.1, this excitation procedure allows us to consider – at least in principle – two classes of physically distinct atoms: those which have been initially prepared in state e , which we will call “a atoms” and those which have been initially prepared in state e' (“b atoms”). These two classes of atoms are sketched on fig. 33(i). Let us try to track these two classes of atoms throughout

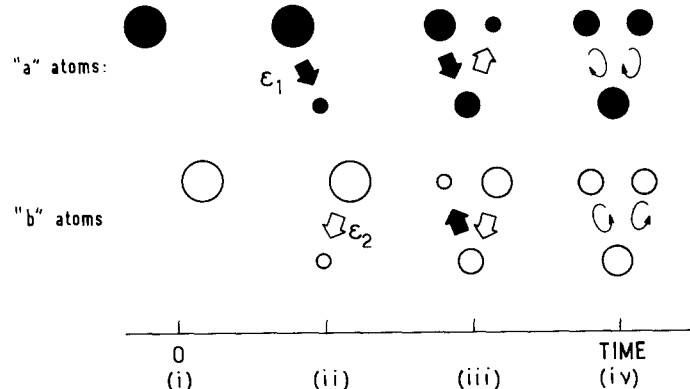


Fig. 33. Illustration of the symmetrical emission process in the case of limited superradiance discussed in section 9.3: the two classes of atoms a and b interact with two field components E_1 and E_2 . Atomic level populations for atoms a and b are represented by black and white dots respectively, the size of the dot being proportional to the population of the corresponding level. Transition induced by fields components E_1 and E_2 are represented by black and white arrows respectively. Time evolves from left to right. (i) sketch of the initial state, (ii) beginning of the emission: atoms a and b emit fields E_1 and E_2 respectively, (iii) the emission proceeds: atoms a start to absorb field E_2 and atoms b absorb field E_1 : all sublevels start to be populated for each ensemble of atoms, (iv) equilibrium state ($t = +\infty$): in each subgroup a or b, half of the atoms remain excited. There is a non-zero optical dipole on each transition (circular arrows). Fields emitted on each transition by atoms a and b interfere destructively.

the system evolution and study what happens to the superradiant emission. The atoms interact now with two electric field components: one is polarized along ϵ_{eg} and will be called \mathcal{E}_1 , the other along $\epsilon_{e'g}$ and will be called \mathcal{E}_2 . At the beginning of the emission (fig. 33(ii)), “atoms a” start to emit field \mathcal{E}_1 and “atoms b” radiate \mathcal{E}_2 . After some time, both classes of atoms have a non-zero probability of being in the lower state g . Then they start to interact with both fields components at the same time (fig. 33(iii)). We have thus to solve a rather complicated problem involving the interaction of two classes of atoms with two electric fields. The actual system evolution in a given realization of the experiment depends on the exact balance of initial quantum fluctuations on both transitions. For sake of simplicity, let us at first consider a *fully symmetrical classical trajectory* starting on *identical* optical coherences on both transitions. In this case, \mathcal{E}_1 and \mathcal{E}_2 will obviously remain equal throughout the evolution and it is convenient to define a common Bloch angle:

$$\frac{1}{2\sqrt{2}} \theta = \frac{id}{\hbar} \int_0^t \mathcal{E}_1 d\tau = \frac{id}{\hbar} \int_0^t \mathcal{E}_2 d\tau. \quad (9.23)$$

Writing separately the Bloch equation for the two classes of atoms, one then finds quite similarly to eqs. (9.16) to (9.20):

$$\rho_{1ee'}^{(a)} = \rho_{1e'e'}^{(b)} = (1 + \cos \frac{1}{2}\theta)^2/8 \quad (9.24)$$

$$\rho_{1e'e'}^{(a)} = \rho_{1ee'}^{(b)} = (1 - \cos \frac{1}{2}\theta)^2/8 \quad (9.25)$$

$$\rho_{1eg}^{(a)} = \rho_{1e'g}^{(b)} = (1 + \cos \frac{1}{2}\theta)(\sin \frac{1}{2}\theta)/4\sqrt{2} \quad (9.26)$$

$$\rho_{1e'g}^{(a)} = \rho_{1eg}^{(b)} = (\cos \frac{1}{2}\theta - 1)(\sin \frac{1}{2}\theta)/4\sqrt{2}. \quad (9.27)$$

The equilibrium position again corresponds to $\theta = \pi$ (maximum ρ_{gg} value). Then, one obviously has the relations:

$$\rho_{1eg}(\tau = \infty) = \rho_{1eg}^{(a)}(\tau = \infty) + \rho_{1eg}^{(b)}(\tau = \infty) = 0 \quad (9.28)$$

and

$$\rho_{1e'g}(\tau = \infty) = \rho_{1e'g}^{(a)}(\tau = \infty) + \rho_{1e'g}^{(b)}(\tau = \infty) = 0 \quad (9.29)$$

which means that the overall optical dipole on each transition is zero, as it could have been guessed from the orthogonality of ϵ_{eg} and $\epsilon_{e'g}$. However, this null result is, on each transition, due to destructive interference between the dipoles belonging to class a and class b. Here again, the limited superradiance effect comes from an interference between physically different dipoles but this time, as opposed to section 9.2, these dipoles correspond to the same transition and to *physically distinguishable* atoms. Figure 33(iv) illustrates this result and symbolizes the final state described by eqs. (9.24) to (9.29) with $\theta = \pi$. Let us recall that the situation studied above represents a very specific realization of the experiment, in which identical fluctuations have started on both transitions. When performing a statistical study involving all possible initiations, it is found that half of the atoms always stay in the upper level at the end of the process, with large fluctuations in the distribution between levels e and e'.

In particular, in the mean-field model, the statistics of ρ_{1ee} (and $\rho_{1e'e'}$) at the end of the evolution is represented by a flat histogram (all values of ρ_{1ee} between 0 and 0.5 are equiprobable). The quantum noise initiating superradiance randomly favors one of the two transitions, resulting in macroscopic population fluctuations in the final state. This effect is similar to the polarization fluctuation phenomenon discussed in subsection 8.6 and could also be used to study the quantum initiation of superradiance.

Remark: The occurrence of limited superradiance in the present case (initial condition given by eq. (9.22)) can be inferred without any calculation from simple arguments concerning the statistical character of the density matrix of the system: the initial state is here a “mixture of states” corresponding to:

$$\text{Tr } \rho_1^2 < 1. \quad (9.30)$$

On any classical trajectory, the interaction with a classical field conserves the value of $\text{Tr } \rho_1^2$ and cannot change the initial mixture of the state into a “pure” g state. As a result, the system must necessarily remain partially in the upper levels. Let us notice however that this “statistical argument” cannot explain the limited superradiance situation described in sections 9.1 and 9.2.

9.4. Conclusion: Relation with the limited superradiance phenomenon in a two-level atom small sample system

The various examples discussed above show that limited superradiance follows in multilevel systems from a decrease of the “symmetry” as compared to the two-level-atom mean-field or one-dimensional situations. In this latter case, all dipoles evolve in a “similar” way, either at exactly the same rate (mean-field situation), or according to the same law in “reduced time” $q = 2(z\tau/LT_R)^{1/2}$ (one-dimensional propagation). As a result, all atoms have the possibility to end up at $t = +\infty$ in the same lower state. In multilevel situations, on the contrary, the evolution of different transitions, or the evolution of the same transitions on different classes of atoms follow quite distinct “paths”. This occurs either because they are several electric dipole matrix elements with different values (subsection 9.1), or because transitions are excited successively (one transition starts first and then induce a dipole on another one; subsection 9.2), or else because different classes of atoms are interacting with various field polarizations (subsection 9.3). The consequence is always the same: the loss of symmetry in the system evolution prevents all atoms from emitting a π pulse and leaves some energy in the system at the end of the emission.

It is worth noticing that the effects discussed in this section bear some similarity with the phenomenon of superradiance quenching encountered in a small sample of two-level atoms (see section 4). In this latter case, we have seen that the limitations to superradiance are due to Van der Waals interaction breaking the high symmetry of the atomic system: in other words, the Van der Waals forces make the atoms “distinguishable” from each other and reduce the high correlation of the pure symmetrical states. In multilevel systems, the “symmetry breaking” has another physical origin, but its effect is the same: the rate of superradiant emission is reduced. The generality of the limited superradiance phenomenon encountered in these various situations can be stressed in treatments describing the various degree of symmetry of the multilevel N -atom state by group theory representations [94].

10. Conclusion

We have presented in this review various aspects of superradiant emission. We have emphasized both the quantal and classical aspects of the phenomenon. We have tried to make the connexion between the very simple small sample superradiance effect predicted by Dicke and the very complicated behaviour of an extended medium in which field propagation and diffraction effects are essential. We have also discussed special effects due to the degeneracy or near degeneracy of the superradiant transition.

The formalism we have described gives a simple recipe for the calculation of “single shot” realizations of a superradiance experiment and for the determination of shot to shot fluctuations as well. Using this formalism, one should be able – at least in principle – to predict the results of any superradiance experiment, however complicated the sample geometry or the energy level scheme is.

We have limited this review to the description of superradiance in “free space”, as opposed to the collective emission of atoms in a cavity restricting the number of available e.m. modes surrounding the atoms. A similar formalism can be applied to describe this latter kind of superradiance. If the cavity damping time is short enough, it can indeed be shown that the collective emission in the cavity obeys an equation quite similar to the mean-field superradiance equations described in this paper [9, 71]. We have also limited this essay to the case where superradiance is initiated by the fluctuation of the spontaneous emission field. This is realistic at short wavelengths. At long wavelengths ($\lambda \geq 100 \mu\text{m}$) and at room temperature ($T = 300 \text{ K}$), the situation is however different: the fluctuation of the blackbody radiation field overcomes those of the vacuum field and superradiance is rather triggered by the thermal radiation background [4]. The effect of this triggering is to shorten somewhat the delay of the emission [71]. The nature of the emission fluctuations is on the other hand not modified: this comes from the fact that the statistics of the thermal radiation intensity is Gaussian, i.e. of the same nature as the statistics of the initial atomic polarization representing in the semi-classical equations the zero point fluctuations of the vacuum field. For this reason, most of the results recalled in this paper can be generalized without change to the description of blackbody induced superradiance experiments.

It might also be interesting to consider the case in which the superradiant emission is triggered by an externally applied field, adding its effects to the spontaneous and blackbody induced effects. When this field is large enough, its effect is to shorten the emission delay and to lock the polarization and phase of the emitted pulse to its own phase and polarization [71]. These effects can in turn be used in order to experimentally determine the initial tipping angle of a superradiant system [65], or else to measure very weak electromagnetic signals [59, 71]. The formalism described in this paper can very easily be extended to analyse such a triggering superradiance experiment.

Other situations can of course be considered, which we have not discussed in this paper: competition of superradiance with other dephasing processes such as Doppler effect or collision have been mentioned, without being described in detail.

One can also consider a generalization of the pumping scheme of fig. 2, in which the pump field and the subsequent superradiant field are non-resonant with the $f \rightarrow e$ and $e \rightarrow g$ transitions respectively: we would deal then with a superradiant-Raman process which has been considered in ref. [95].

All these situations could be described with the help of the general formalism outlined in this essay.

References

- [1] R.H. Dicke, Phys. Rev. 93 (1954) 99.
- [2] R.H. Dicke, Quantum Electronics Vol. I, eds. Grivet and Bloembergen (Columbia University Press, N.Y., 1964).
- [3] G.S. Agarwal, Phys. Rev. 178 (1969) 2025; A2 (1970) 2038; A4 (1971) 1778; A7 (1973) 1195;
see also refs. [84] and [85].
- [4] G.S. Agarwal, Quantum Optics 70, Springer Tracts in Modern Physics (Springer Verlag, 1974).
- [5] F.T. Arrechi and E. Courtens, Phys. Rev. A2 (1970) 1730.
- [6] L. Allen and J.H. Eberly, Optical Resonance and Two Level Atoms (Wiley, 1975).
- [7] A.V. Andreev, Sov. J. Quantum Electron. 8 (1978) 476.
- [8] F.T. Arecchi, E. Courtens, R. Gilmore and H. Thommas, Fundamental and Applied Laser Physics, eds. Feld, Javan, Kurnit (Wiley, New York, 1973) p. 835.
- [9] R. Bonifacio, P. Schwendimann and F. Haake, Phys. Rev. A4 (1971) 302; A4 (1971) 854.
- [10] R. Bonifacio, F.A. Hopf, P. Meystre and M.O. Scully, Phys. Rev. A12 (1975) 2568.
- [11] R. Bonifacio and L.A. Lugiato, Phys. Rev. A11 (1975) 1507; A12 (1975) 578.
- [12] R. Bonifacio, L.A. Lugiato and A.A. Crescentini, Phys. Rev. A13 (1975) 1648.
- [13] V. De Giorgio and F. Chielmetti, Phys. Rev. A4 (1971) 2415;
V. De Giorgio, Optics Comm. 2 (1971) 262.
- [14] N.E. Rehler and J.H. Eberly, Phys. Rev. A3 (1971) 1735.
- [15] C.R. Stroud Jr., J.H. Eberly, W.L. Lama and L. Mandel, Phys. Rev. A5 (1972) 1094.
- [16] V. Ernst, Z. Physik, 218 (1969) 111;
V. Ernst and P. Stehle, Phys. Rev. 176 (1968) 1456.
- [17] J.C. McGillivray and M.S. Feld, Phys. Rev. A14 (1976) 1169;
J.P. Herman, J.C. McGillivray, N. Skribanowitz and M.S. Feld, Laser Spectroscopy, eds. R.G. Brewer and A. Mooradian (1974).
- [18] F. Friedberg and S.R. Hartmann, Phys. Lett. 37A (1971) 285; 38A (1972) 227.
- [19] F. Friedberg, S.R. Hartmann and J.T. Manassah, Phys. Lett. 40A (1972) 365.
- [20] R. Friedberg, S.R. Hartmann and J.T. Manassah, Phys. Reports 7C (1973) 101;
F. Friedberg and S.R. Hartmann, Optics Comm. 10 (1974) 298.
- [21] F. Friedberg and S.R. Hartmann, Phys. Rev. A10 (1974) 1728.
- [22] F. Friedberg and S.R. Hartmann, Phys. Rev. A13 (1976) 495;
F. Friedberg and B. Coffey, Phys. Rev. A13 (1976) 1645.
- [23] B. Coffey and R. Friedberg, Phys. Rev. A17 (1978) 1033.
- [24] M. Gross, Thèse d'Etat, Université Paris VI (1980) (unpublished).
- [25] P. Pillet, Thèse d'Etat, Université Paris-Sud (1982) (unpublished).
- [26] F.A. Hopf and P. Meystre, Phys. Rev. A12 (1975) 2534;
F.A. Hopf, P. Meystre and P.W. McLaughlin, Phys. Rev. A13 (1976) 777.
- [27] F.A. Hopf, Phys. Rev. A20 (1979) 2064.
- [28] F. Haake and R.J. Glauber, Phys. Rev. A5 (1972) 1457.
- [29] R.J. Glauber and F. Haake, Phys. Rev. A13 (1976) 357;
R.J. Glauber and F. Haake, Phys. Lett. 68A (1978) 29.
- [30] F. Haake, H. King, G. Schröder, J. Haus and R.J. Glauber, Phys. Rev. A20 (1979) 2047;
see also F. Haake, H. King, G. Schröder, J. Haus, R.J. Glauber and F. Hopf, Phys. Rev. Lett. 26 (1979) 1740.
- [31] F. Haake, J.W. Haus, H. King, G. Schröder and R.J. Glauber, Phys. Rev. A23 (1981) 1322;
see also F. Haake, J. Haus, H. King, G. Schröder and R.J. Glauber, Phys. Rev. Lett. 45 (1981) 558.
- [32] R. Jodoin and L. Mandel, Phys. Rev. A9 (1974) 873.
- [33] C.T. Lee, Phys. Rev. A12 (1975) 575; A13 (1976) 1657; A14 (1976) 1926; A15 (1977) 2019; A16 (1977) 301.
- [34] F.P. Mattar, H.M. Gibbs, S.L. McCall and M.S. Feld, Phys. Rev. Lett. 46 (1981) 1123.
- [35] R.H. Picard and C.R. Willis, Phys. Rev. A8 (1973) 1536.
- [36] A.M. Ponte Goncalves and A. Tallet, Phys. Rev. A4 (1971) 1319;
G. Oliver and A. Tallet, Phys. Rev. A7 (1973) 1063;
E. Ressayre and A. Tallet, Phys. Rev. A11 (1975) 981.
- [37] E. Ressayre and A. Tallet, Phys. Rev. A12 (1975) 1725.
- [38] E. Ressayre and A. Tallet, Phys. Rev. Lett. 37 (1976) 424; Phys. Rev. A15 (1977) 2410.
- [39] E. Ressayre and A. Tallet, Phys. Rev. A18 (1978) 2196.
- [40] D. Polder, M.F.H. Schuurmans and P.H.F. Vrechen, Phys. Rev. A19 (1979) 1192;
M.F.H. Schuurmans and D. Polder, Proc. Fourth Intern. Conf. on Laser Spectroscopy, Rottach-Egern (Springer Verlag, Berlin-Heidelberg-New York, 1979).
- [41] M.F.H. Schuurmans, Opt. Comm. 34 (1980) 185.
- [42] P. Prakash and N. Chandra, Phys. Rev. A21 (1980) 1297.

- [43] R. Saunders, S.S. Hassan and R.K. Bullough, J. Phys. A9 (1976) 1725.
- [44] G.S. Agarwal, Phys. Lett. 45A (1973) 15.
- [45] G.S. Agarwal and S.S. Trivedi, Opt. Comm. 18 (1976) 417.
- [46] G.S. Agarwal, F. Haake and G. Schröder, Opt. Comm. 34 (1980) 283.
- [47] E. Abraham and R.K. Bullough, Opt. Comm. 34 (1980) 345.
- [48] A. Crubellier, Phys. Rev. A15 (1977) 2430;
A. Crubellier and M.G. Schweighofer, Phys. Rev. A18 (1978) 1797.
- [49] A. Crubellier, S. Liberman and P. Pillet, Opt. Comm. 33 (1980) 143.
- [50] K. Ikeda, Phys. Lett. 63A (1977) 248;
K. Ikeda, J. Okada and M. Matsuoka, J. Phys. Soc. Japan 48 (1980) 1636; 48 (1980) 1646;
T. Baba and K. Ikeda, J. Phys. Soc. Japan 50 (1981) 217.
- [51] P. Prakash and N. Chandra, Phys. Rev. Lett. 42 (1979) 37.
- [52] Ph. Cahuzac, H. Sontag and P.E. Toschek, Opt. Comm. 31 (1979) 37.
- [53] S. Liberman and P. Pillet, Phys. Rev. Lett. 41 (1978) 1237;
see also A. Grubelier, C. Brechignac, Ph. Cahuzac and P. Pillet, Proc. Fourth Intern. Conf. on Laser Spectroscopy, Rottach-Egern (Springer Verlag, 1979).
- [54] A. Crubellier, S. Liberman, P. Pillet and M.G. Schweighofer, J. Phys. B14 (1981) L-177.
- [55] A. Crubellier, S. Liberman, D. Mayou, P. Pillet and M.G. Schweighofer, Optics Lett. 7 (1982) 16.
- [56] A. Flussberg, T. Mosberg and S.R. Hartmann, Phys. Lett. 58A (1976) 373.
- [57] M. Gross, C. Fabre, P. Pillet and S. Haroche, Phys. Rev. Lett. 36 (1976) 1035.
- [58] M. Gross, J.M. Raimond and S. Haroche, Phys. Rev. Lett. 40 (1978) 1711.
- [59] N.W. Carlson, D.J. Jackson, A.L. Schawlow, M. Gross and S. Haroche, Opt. Comm. 32 (1980) 350.
- [60] F. Gounand, M. Hugon, R.P. Fournier and J. Berlande, J. Phys. B12 (1979) 547.
- [61] J. Okada, K. Ikeda and M. Matsuoka, Opt. Comm. 27 (1978) 321.
- [62] J. Marek, J. Phys. B12 (1979) L-229;
J. Marek and Marek and M. Ryschka, J. Phys. B13 (1980) L-491.
- [63] Q.H.F. Vrehen, H.M.J. Hikspoors and H.M. Gibbs, Phys. Rev. Lett. 38 (1977) 764.
- [64] H.M. Gibbs, Q.H.F. Vrehen and H.M.J. Hikspoors, Phys. Rev. Lett. 39 (1977) 547.
- [65] Q.H.F. Vrehen and M.F.H. Schuurmans, Phys. Rev. Lett. 42 (1979) 224.
- [66] Q.H.F. Vrehen and J.J. der Wedewe, Phys. Rev. A24 (1981) 2857;
see also Q.H.F. Vrehen, Proc. Fourth Intern. Conf. on Laser Spectroscopy, Rottach-Egern (Springer Verlag, 1979).
- [67] N. Skribanowitz, F.P. Herman, J.C. McGillivray and M.S. Feld, Phys. Rev. Lett. 30 (1973) 309;
see also ref. [17].
- [68] A.T. Rosenberger and T.A. De Temple, Phys. Rev. A24 (1981) 868.
- [69] M. Gross, C. Fabre, P. Goy, S. Haroche and J.M. Raimond, Phys. Rev. Lett. 43 (1979).
- [70] L. Moi, C. Fabre, P. Goy, M. Gross, S. Haroche, P. Encrenaz, G. Beaudoin and B. Lazareff, Opt. Comm. 33 (1980) 47.
- [71] L. Moi, P. Goy, M. Gross, J.M. Raimond, C. Fabre and S. Haroche, Phys. Rev. A (1983) to be published;
P. Goy, L. Moi, M. Gross, J.M. Raimond, C. Fabre and S. Haroche, Phys. Rev. A (1983) to be published.
- [72] Q.H.F. Vrehen and H.M. Gibbs, in: Topics in Current Physics 27, ed. R. Bonifacio (Springer Verlag, 1982).
- [73] A.V. Andreev, V.I. Emel'yanov and Yu.A. LI'Inskil, Sov. Usp. 23 (1980) 493.
- [74] M.S. Feld and J.C. McGillivray, in: Coherent Nonlinear Optics. Recent Advances, eds. M.S. Feld and V.S. Letokhov (Springer Verlag, 1980).
- [75] C. Cohen-Tannoudji, Ecole d'Eté des Houches (1975), in: Frontiers in Laser Spectroscopy, eds. R. Balian, S. Haroche and S. Liberman (North-Holland, Amsterdam, 1977).
- [76] V. Weisskopf and E. Wigner, Z. Phys. 63 (1930) 54.
- [77] E.A. Power and S. Zienau, Phil. Trans. Roy. Soc. 251 (1959) 427.
- [78] J.D. Jackson, Classical Electrodynamics (John Wiley, New York, London, 1962).
- [79] A. Icsevgi and W.E. Lamb Jr., Phys. Rev. 185 (1969) 517.
- [80] D.C. Burnham and R.Y. Chiao, Phys. Rev. 188 (1969) 667.
- [81] F.P. Mattar and M.C. Newstein, Comput. Phys. Commun. 20 (1980) 139;
F.P. Mattar, Appl. Phys. 17 (1978) 53.
- [82] M. Gross, to be published.
- [83] P.D. Drummond and J.H. Eberly, Phys. Rev. A25 (1982) 3446.
- [84] G.S. Agarwal, Phys. Rev. A4 (1971) 1791.
- [85] G.S. Agarwal, Phys. Rev. A3 (1971) 1783.
- [86] C. Leonardi and A. Vaglica, Phys. Lett. 74A (1979) 309.
- [87] F.P. Mattar and C.M. Bowden, Proc. 12th Simulation and Modeling Conf. (Pittsburgh, May 1981).
- [88] M.F.H. Schuurmans, Q.H.F. Vrehen, D. Polder and H.M. Gibbs, in: Advances in Atomic and Molecular Physics (1981).
- [89] P. Pillet, Thèse de 3ème cycle, Université Paris VI (1977) (unpublished).
- [90] J.C. McGillivray and M.S. Feld, Phys. Rev. A23 (1981) 1334.

- [91] C. Cohen-Tannoudji, Annales de Phys. 7 (1962) 423 and 469.
- [92] S. Haroche, in: High Resolution Laser Spectroscopy, ed. K. Shimoda (Springer Verlag, 1976).
- [93] J.M. Raimond, Thèse de 3ème cycle, Université Pierre et Marie Curie (1979) (unpublished).
- [94] A. Crubellier, S. Liberman, P. Pillet and M.G. Schweighoffer, to be published.
- [95] A. Grubellier, S. Liberman, D. Mayou and P. Pillet, to be published.
- [96] H. Haken, Encyclopedia of Physics, XXV 12c (Springer, Berlin, 1970).
- [97] P.W. Miloni and P.L. Knight, Phys. Rev. A10 (1974) 1096.
- [98] M.J. Stephen, J. Chem. Phys. 40 (1964) 669.